NILDA MARTINS

DEVELOPMENT OF PLASMA ASSISTED PYROLYSIS OF POLYMER DERIVED CERAMIC COATINGS ON SINTERED STEEL

Tese de Doutorado apresentada ao Programa de Pós-Graduação em Ciência e Engenharia de Materiais, como requisito parcial para a obtenção do grau de Doutor em Ciência e Engenharia de Materiais.

Orientador: Dr. Aloisio Nelmo Klein
Coorientador: Dr. rer. nat. Günter Motz

FLORIANÓPOLIS
Março, de 2017

Nilda Martins

DEVELOPMENT OF PLASMA ASSISTED PYROLYSIS OF POLYMER DERIVED CERAMIC COATINGS ON SINTERED STEEL

Esta Tese foi julgada adequada para obtenção do Título de "Doutor em Ciência e Engenharia de Materiais" e aprovada em sua forma final pelo Programa de Pós-Graduação em Ciência e Engenharia de Materiais.

Florianópolis, 03 de Março de 2017.

_____
Prof. Dr. Guilherme M. Barra
Coordenador do Curso

Banca Examinadora:

_____   _____

Prof. Dr. Ing. Aloísio Nelmo Klein   Prof. Dr. Antonio Eduardo
Universidade Federal de Santa   Martinelli
Catarina (UFSC)   Universidade Federal do Rio
Orientador   Grande do Norte (UFRG).

_____   _____

Dr$_a$. Tatiana Bendo   Prof. Dr. Lírio Schaeffer
Universidade Federal de Santa   Universidade Federal do Rio
Catarina (UFSC)   Grande do Sul (UFRGS)

_____   _____

Prof. Dr. João Cardoso de Lima   Prof. Dr. João Batista R. Neto
Universidade Federal de Santa   Universidade Federal de Santa
Catarina (UFSC)   Catarina (UFSC)

I dedicated this thesis to
my parents, Elza and João, and family.
For their endless love, support and encouragement.

ACKNOWLEDGMENTS

The completion of my Ph.D. has been a long journey and I could not have succeeded without the invaluable support of several. I am filled with a great sense of gratitude towards so many who have made this journey possible. So, I want to thank all of you who have collaborated, in some way, with this process of "maturity and discovery".

It is with immense gratitude that I acknowledge the support, supervision, patience and help of my Advisor Aloisio Nelmo Klein. He has my admiration and respect for the professional, and the person, he is.

I would like to thank Dr. Ren Gunter Motz for the opportunity to work in his research group in Bayreuth and for all the help.

I would also like to thank all the members of our Bragecrim project, in Brazil and Germany, for all the contributions. Specially for those which helped me with sample process and characterization. As well to the trainee students who helped our group, specially the one who helped me with great part of the experiments presented in this thesis.

I wish to thank the professors in my thesis committee.

I want to thank the PGMAT Coordination for the support at all the times I needed.

It gives me great pleasure in acknowledging prof. João Cardoso de Lima for having helped me doing the Rietveld Refinement. I also wish to thank Deise R. Consoni, Patricia B. Prates, e Tatiana Bendo, and employees of LCM e LCME, for the characterization performed. In the same way, I must thank all the LabMat staff members, who were always prompt to help. Being part of this LabMat group was very important in my academic career, since in this group I found support in different ways.

I am grateful to prof. Dr. João Batista R. Neto, prof. Dr_a Sonia M. H. Probst, Dr_a Cristiano Binder and Ms. Nicolás Ignacio Araya for the discussions about my topic.

Thank you very much to all who helped me with the discussions, processing and characterizations.

I want to thank the collaborators of the project Amanhecer, of HU, who helped me during the process of writing this thesis.

I want to thank my friends who helped, in some way with this research. Since they are so many I will not mention their names, but I am sure they can recognize themselves. Thank you for the talks, encouragement and love!

I would like to thank Edegar for being my teacher and friend, and give

me always a support during the ph.D, and specially while writing this thesis.

For those friends I have made in Germany, in the research laboratory and outside the lab. I would like to thank all that even far away we keep connected, not only by the internet, but also by the heart.

I also want to thank my friends from my room office, where we shared nice talks, smiles and knowledge.

And, as I said, in the LabMat in found support in different forms. Then, I cannot finish my acknowledgement without being very grateful for those who shared time with me in the "coffee time" or in the "psychological coffee", as I used to call it. I found not only technical support but also motivation, kindness and patience from all of them, as well very inspiring remarks, such as: "If your plasma does not shine, do not create an arc in mine." A heartfelt thanks to all of you.

Finally, I must express my very profound gratitude to my parents, sisters, brothers and family, for providing me with unfailing support and continuous encouragement throughout my years of study.

I could not have finished my thesis without this support. Thank you!

"There is a driving force more powerful than
steam, electricity and nuclear power:
the willpower."

Albert Einstein

ABSTRACT

The use of precursors loaded with fillers to process ceramic coatings rises the possibility to tailor the microstructure and coating properties for a wide range application, like thermal barrier coatings, environmental barrier coating or for wear applications. Thus, the present research aims to develop and to employ the novel process of plasma assisted pyrolysis (PAP) for developing ceramic composites coating on sintered steel substrate. The coatings are based on polymer derived ceramic, being the precursor a polyorganosilazane. During the development of the PDC based coating different fillers were used. The active fillers $TiSi_2$ and TiB_2 were used in order to compensate the shrinkage of the precursor and to generate in situ formation of phases as nitrides and carbides. Initially it was necessary to investigate the influence of PAP both on the pyrolysis behavior of the pure precursor and on the polymer precursor loaded with filler particles, in comparison to conventional pyrolysis. For such investigations, cylindrical bulk specimens were used (diameter of 13 mm and thickness between of 2-4 mm). It was demonstrated that the ceramic yield as well as the elemental composition of the polyorganosilazane are not adversely influenced by PAP process. The bulk samples based on precursor and $TiSi_2$ under conventional pyrolysis, under N_2 atmosphere, showed no significant conversion of the fillers into nitrides. In contrast, the use of PAP led not only to an enhances filler conversion but also to a densification of the composite. The resulting microstructure is dominated by $Ti(C,N)$ as well as a mixture of α- and β- Si_3N_4 phases embedded in an amorphous SiCN matrix. In the same way the coatings, on sintered substrates, based on polyorganosilazane and TiB_2, processed under conventional pyrolysis showed almost no filler conversion up to temperature of 1150 °C. The final coating was based mainly on TiB_2 and the formed SiCN network. While in the specimens after PAP process mainly Ti (C, N) and $C_{0.858}$ $(BN)_{0.571}$ were formed, and no residual TiB_2 was detect. The diffusion phenomenon between coating and sintered substrate was also drastically affected under plasma conditions. Considerable amount of iron could be detected in the coating, after the plasma assisted pyrolysis. Such difference between conventional and plasma assisted pyrolysis process is attributed to the high reactivity of the plasma environment, in which reactive species, as atomic nitrogen, are available to react with the sample. It could be demonstrated that plasma assisted pyrolysis is a very suitable way to process polymer derived ceramic composite materials

with a tailored microstructure.

RESUMO

O uso de precursores carregados com fillers possibilita projetar a microestrutura e as propriedades de revestimentos cerâmicos para diferentes aplicações, como revestimentos de barreira térmica, revestimento de barreira ambiental ou para aplicações tribológicas. O objetivo deste trabalho foi desenvolver e empregar o novo processo de pirólise assistida por plasma (PAP) para o desenvolvimento de revestimentos compósitos cerâmicos sobre substratos de aço sinterizado. Os revestimentos são baseados em cerâmica derivada de polímero, sendo o precursor um poliorganossilazano. Durante o desenvolvimento do revestimento utilizaram-se diferentes *fillers*. As cargas ativas, como $TiSi_2$ e TiB_2, foram utilizadas para compensar a retração do precursor e para gerar a formação *in situ* de fases como nitretos e carbonetos. Inicialmente foi necessário investigar a influência da PAP sobre o comportamento do precursor puro e no comportamento do precursor carregado com partículas de *fillers*, em comparação com a pirólise convencional. Para tais investigações, foram utilizados amostras cilíndricas (diâmetro de 13 mm e espessura entre 2 e 4 mm). Foi demonstrado que o rendimento cerâmico, assim como a composição elementar do poliorganossilazano, não são influenciados negativamente pelo processo PAP. As amostras baseada no precursor e $TiSi_2$ sob pirólise convencional, atmosfera de N_2, não mostrou nenhuma conversão significativa dos *fillers* em nitretos. No entanto, a utilização da PAP promoveu tanto ao aumento na conversão do *filler*, assim como uma maior densificação do compósito. A microestrutura resultante é dominada por Ti (C, N), e uma mistura de fases α- e β-Si_3N_4 incorporadas numa matriz amorfa de SiCN. Do mesmo modo, os revestimentos sobre os substratos sinterizados, compostos por poliorganossilazano e TiB_2, processados em pirólises convencionais, mostraram quase nenhuma conversão do *filler* até na temperatura de 1150 ° C. O revestimento final baseou-se principalmente em TiB_2 e na fase SiCN. Enquanto, as amostras após o processo de PAP formaram principalmente fases como Ti (C, N) e $C_{0.858}$ (BN) $_{0.571}$, e não foi detectado TiB_2 residual. O fenômeno de difusão entre o revestimento e o substrato sinterizado também foi drasticamente afetado no ambiente de plasma. Uma quantidade considerada de ferro pode ser detectada no revestimento, após a pirólise assistida por plasma. Essas diferenças entre o processo de pirólise convencional e assistido por plasma é atribuída à alta reatividade do ambiente de plasma, no qual as espécies reativas, como o nitrogênio atômico, estão disponíveis para reagir com a amostra.

Pode ser demonstrado que a pirólise assistida por plasma é uma maneira muito adequada para processar materiais compósitos cerâmicos derivados de polímeros com uma microestrutura projetada.

Palavras-chave: plasma, pirólise, cerâmica derivada de polímeros, fillers ativos, materiais sinterizados, revestimentos.

LIST OF FIGURES

LIST OF TABLES

LIST OF SYMBOLS AND ABREVIATIONS

PAP - Plasma assisted pyrolysis
PDCs - Polymer derived ceramics
PDC - Polymer derived ceramic
AFCOP - Active filler controlled polymer pyrolysis process
DCP - Dicumylperoxide
HTT1800 –Liquid polycarbosilazane precursor
HTTS - solid polycarbosilazane precursor
Ton - Plasma switched on time
Toff - off pulse period
CP - Conventional pyrolysis
SEM - Scanning electronic microscopy
FEG-SEM - Field emission scanning electron microscopy
EDS - Energy dispersive x-ray spectroscopy
XRD - X-ray Diffraction
R_{WP} - weighted R-profile
GOF - Good of fitness
GDOES - Glow discharge optical emission spectroscopy
TGA - Thermogravimetric analysis
BSE - Backscattered electrons
PAP-A - PAP in anode configuration
PAP-C - PAP in cathode configuration

TABLE OF CONTENTS

1.   INTRODUCTION AND OBJECTIVES

Ceramic materials have applications in different fields, due to their excellent combination of properties, like automotive area, electronic industry, aerospace, etc, where high temperatures or resistance to oxidation, corrosion and wear are necessary,. However, the application of ceramics has been somewhat limited due to the conventional processing routes, whereas the powders are compacted and, usually, high temperatures are needed for the ceramics sintering process. Besides it, the traditional powder routes offer limitations in terms of component shaping.

In the current advanced stage of technological development, net shaped components processing techniques, with tailored properties and reduced processing time, temperatures and energy consumption are required. Based on that, the route of polymer derived ceramics (PDCs) has been an alternative to the conventional processing of ceramics. It uses precursors, also called preceramic polymers, which are inorganic/organometallic systems. They commonly contain silicon and upon pyrolysis ceramic materials are formed, as nitrides, carbides and oxides, or their ternary and quaternary systems providing tailored properties for different applications.

In this approach, some advantages have been essential for the expansion of this area:

- Lower processing temperature (pyrolysis temperature);
- Possible use of conventional polymer processing techniques to make complex shaped components;
- Better control of impurities and
- Potential for developing amorphous or crystalline ceramic products with tailored microstructures.

However, PDCs undergo a tremendous shrinkage during pyrolysis. The conversion of the precursor into a corresponding ceramic is associated with high volume shrinkage (up to 50 %) due to the mass lost by release of gaseous products as well as an increase in density. To overcome this drawback most of the PDCs are based on filler loaded precursors, where inert, also called passive, (SiC, BN, ZrO_2, Al_2O_3 etc) and/or active (Ti, Cr, Fe, Al, Nb, Hf, $TiSi_2$, $CrSi_2$ etc) fillers are used to compensate the shrinkage, and the inherent problems associated. While inert fillers decrease the fraction of polymer and, consequently, the volume shrinkage, active fillers react with the decomposition products

of the precursor as well as with gaseous chemical species present in the pyrolysis atmosphere, forming new phases. The formation of those respective phases compensate the precursor shrinkage. The use of precursors loaded with fillers to process ceramics coatings rises the possibility of having dense and thicker coatings, and it is possible to tailor the coating properties for a wide range application, like thermal barrier coatings, environmental barrier coatings or for wear applications (COLOMBO et al., 2010).

Even though the use of filler has been useful to process PDCs, normally the fillers exhibit insufficient reactions to the respective phases in nitrogen atmosphere up to 1200 °C. A more reactive environment is needed to improve the reaction rate of the fillers during pyrolysis. Thus, in the present research it is proposed to process the pyrolysis in a plasma reactor, where higher reactive chemical species are generated by dissociation of gaseous molecules, such as the generation of atomic nitrogen by dissociation of N_2, well known in plasma assisted nitriding. It is expected that in plasma assisted pyrolysis the conversion rate of the fillers into the desired hard phases (such as nitrides, carbonitrides or carbides) is increased, resulting in an increase in volume expansion to compensate the normal shrinkage of the sample during pyrolysis process.

Besides it, in spite of considerable research development in the field of powder metallurgy, it is still possible to expand the application field of sintered materials by the use of PDC coatings. Thus, the present research aim at develop the process of plasma-assisted pyrolysis and to produce PDC coatings on sintered steel components, considering the experience of LabMat (Materials Laboratory/UFSC) in the area of powder metallurgy and in plasma assisted processing techniques.
This work is part of a cooperation between the LabMAT (UFSC/Brazil) and the Ceramic Materials Engineering Institute (CME), University of Bayreuth, Germany, in the BRAGECRIM project entitled "Development of wear resistant and self-lubricating coatings on sintered steels from polymer-derived ceramics".

OBJECTIVES

The main goal of the present research is to develop the plasma assisted pyrolysis process of polymer derived ceramic composites coating on sintered steel substrates.

In order to achieve the general objective, the following specific objectives have been defined:

- To process PDC coatings on sintered steel.
- To study the influence of a reactive plasma atmosphere on polymer derived ceramic process and to compare, the microstructure and formed phases, with the conventional pyrolysis.
- To assess the influence of the plasma reactor configuration, cathode and anode, on the filler conversion rate and on the precursor conversion.
- To assess the influence of pyrolysis process parameters (temperature and plasma parameters) on the filler conversion.
- To assess the influence of plasma assisted pyrolysis process on the conversion of different active fillers.

2. LITERATURE REVIEW

2.1. POLYMER DERIVED CERAMICS

Polymer derived ceramics have been developed since the early 1960 (RIEDEL et al., 2006) and there are several reports and reviews on literature about this subject (KROKE et al., 2000), (COLOMBO et al., 2010) (GREIL, 2000). The polymeric precursors (also known as preceramic polymers) are inorganic/organometallic systems that provide ceramics with tailored chemical composition and specific microstructure (amorphous or nanocrystalline) by proper thermal treatment. They commonly contain silicon and are used to obtain ceramics such as SiC, Si_xN_y, SiCN, SiCO and BN.

Preceramic polymers have received special attention due to several advantages they offer compared to traditional methods of ceramic processing. Some of the main advantages of the preparation of ceramic materials using preceramic polymer pyrolysis, over other conventional techniques like powder processing, include the following points:

Lower processing temperatures: Ceramic products manufactured by powder processing routes are sintered in high temperature, usually between 1000 and 2500 °C while the PDC are manufactured in lower temperature (500 to 1500 °C); ease in processing complex shape by the ability to use polymeric processing techniques such as pressing, casting, injection molding, extrusion, dip-coating, fiber drawing, etc. Furthermore, the PDC route provides better control of impurities and the potential for developing amorphous or crystalline ceramic products with tailored microstructures (RANGARAJAN; ASWATH, 2011) (GREIL, 2000).

PDCs have applications in different areas, such as high temperature resistant materials (energy materials, automotive, aerospace, etc), hard materials, chemical engineering (food and biotechnology, etc), functional materials in electrical and micro components materials, etc (RIEDEL et al., 2006) (COLOMBO et al., 2010) due to their tailored physical-chemical properties, as well as their ability to be shaped by different processing methods. However, while significant effort has been made to create bulk and near-net shape parts, one of the most promising areas for the application of PDC has been in low-dimensional products, such as joints, fibers, and coatings.

Precursors based coatings are an alternative and relatively low-cost possibility to process ceramic-like coatings that combine the processing ease of polymer derived ceramics (PDCs) and the favorable

properties of the resulting silicon-containing ceramics like thermal stability, thermal shock resistance, high hardness values or abrasion and corrosion resistance. The properties can be tailored for a wide range of applications like thermal barrier coatings, environmental barrier coatings or for wear applications (GREIL, 1995a), (BARROSO; KRENKEL; MOTZ, 2015) (GÜNTHNER et al., 2009) (JACOBSON; OPILA; LEE, 2001), (GÜNTHNER et al., 2011).

Besides it, the process of film deposition needs temperature variation from room until high temperature. This sometimes can induce phase transformations, softening or even geometric and dimensional distortions into the substrate. Thus, the development of coating process with low temperature is very attractive (CGEE, 2010).

2.1.1 Processing and pyrolysis of preceramic polymers coatings

Over the past few decades, a variety of preceramic organosilicon polymers have been developed as precursors to ceramics with a wide range of compositions in the Si, B, C, N, O system (RIEDEL, MERA, *et al.*, 2006). The processing of those PDC based coating can be divided into four steps: (i) Synthesis of the polymeric precursor, (ii) shaping (iii) cross-linking of the precursors into a high molecular weight compound forming an infusible network and (iv) pyrolysis of the cross-linked polymer into an amorphous or crystalline ceramic (MERA et al., 2015) (GÜNTHNER, WANG, *et al.*, 2012). Figure 1 shows the temperature range from the shaping to crystallization.

Figure 1: Production process of polymer derived ceramic coating.
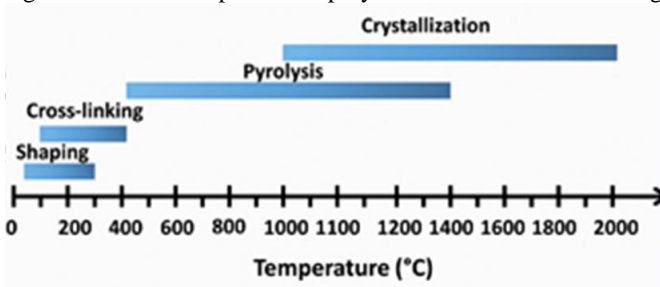
Source: (COLOMBO et al., 2010)

(i) Synthesis

The type of the preceramic polymers and molecular structure (functional and substituent groups) are defined during the first step, the

synthesis that usually is done by commercial companies. Thus, the synthesis has major importance in the PDC area, since it influences the ceramic composition, the phases distribution, as well as the microstructure of the final ceramic (COLOMBO, MERA, *et al.*, 2010).

A general formula of an organosilicon polymer used as a precursor for the synthesis of ceramic is shown in Figure 2.

Figure 2: General oversimplified representation of the molecular structure of preceramic organosilicon.
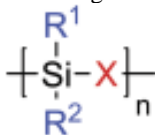
Source: (COLOMBO, MERA, et al., 2010)

Two important parameters to design the preceramic compound on the molecular level are the group (X) of the polymer backbone and the substituents R^1 and R^2 attached to silicon. The variation of the group X results in different classes of Si-based polymer as shown in Figure 3. Changing the functional groups R^1 and R^2 it is possible to tailor properties such as thermal stability, solubility of polymer, optical, electronic and rheological properties. Usually these groups are hydrogen, aliphatic or aromatic organic side groups. The presence of organic side groups allows the control of the amount of carbon in the ceramic, and this is a key of final properties ceramic component (COLOMBO, MERA, *et al.*, 2010).

Although there are different types of polymeric precursors, they should have some specific properties in order to be effective as PDC coating, such as:

- the polymeric precursor should have a sufficiently high molecular weight in order to avoid the volatilization of low-molecular components;
- appropriate rheological properties and solubility for the shaping process;
- presence of functional groups for the cross-linking step and
- they should also have considerable ceramic yield (COLOMBO, MERA, *et al.*, 2010).

In some cases, ceramic yield as high as 85% has been reported

(SHAH; RAJ, 2002). Accordingly, the PDC coatings are based mainly on silicon containing precursors like polysiloxanes (TORREY; BORDIA, 2008), polycarbosilanes (MUCALO; MILESTONE, 1994), and polysilazane (KROKE et al., 2000), (GÜNTHNER et al., 2009).

The polysilazanes and polycarbosilazanes based coating are very promising and interesting because they are oxygen free. Thus, the derived ceramic can be used for metal corrosion and oxidation protection for corrosive environments (in marine or automobile components), harsh environments at elevated temperatures in industrial application (WANG et al., 2011). As already mentioned, considerable attention has been directed to the use of these polymers as precursors to high performance ceramics such as Si_3N_4 and Si_3N_4/SiC.

Figure 3: Main classes of Si-polymer as precursors for ceramics.
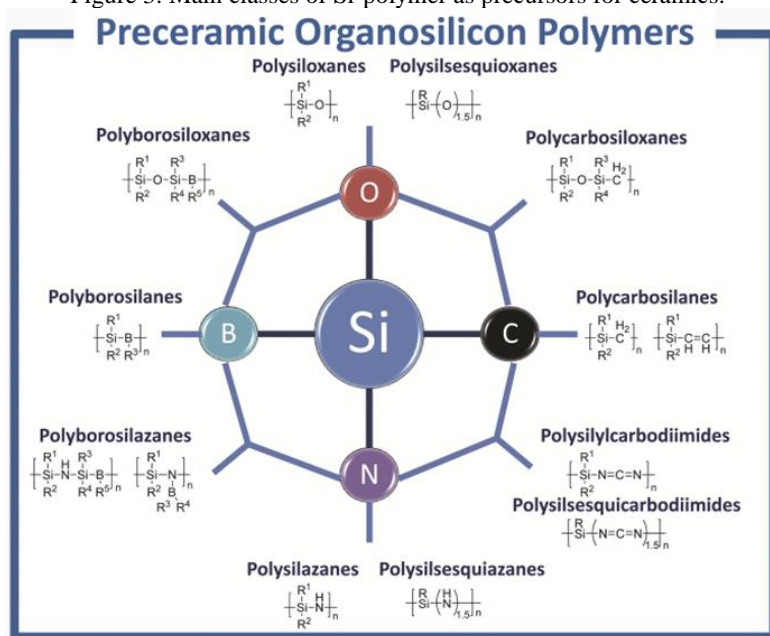
Source: (COLOMBO, MERA, et al., 2010)

The polysilazane are polymers that consist of silicon and nitrogen in their backbone. The lateral groups can be hydrogen and in some cases carbon. Thus, it is possible consider either inorganic polysilazanes without carbon (perhydropolysilazanes) or organic polysilazanes that tipically have carbon-containing groups, such as methyl or vinyl (such as organopolysilazanes or polycarbosilazanes).

These polymers are characterized by a direct and strong bonding between silicon and carbon that prevent carbon from volatilizing in the form of small hydrocarbon molecules during pyrolysis in controlled inert environments (RIEDEL et al., 2006), (COLOMBO et al., 2010).

The first publication talking about the synthesis of poly(organosilazanes) by the ammonolysis of organosilicon chlorides was in 1964 by Kruger and Rochow (KRUGER, C. R.; ROCHOW, 1964). Currently, the synthesis of polysilazanes can still be made by ammonolysis reactions of chlorosilanes with ammonia or by aminolysis with amines (KROKE, LI, *et al.*, 2000). It is important to point out that the greatest difficulty in this method is the separation of the polymeric reaction product NH_4Cl or N_3NRCl (COLOMBO et al., 2010). More information about these subject can be found in the literature (R. RIEDEL, 2006), (ALDINGER; WEINMANN; BILL, 1998).

Furthermore, there exist already some oligomeric and polymeric silazanes commercially available. Thus, a research increase in this area has occurred, and many researchers have been studying the correlation between the microstructure and the properties of the polymer derived ceramics with the molecular structure of the starting precursor polymeric.

One of the advantages of coatings based on poly(carbo)silazanes as precursors is that they have optimum bonding to metal substrates without complicated application procedure (SCHÜTZ et al., 2012). The reactivity of the polysilazanes with oxide surfaces leads to direct chemical bonding between the coatings and the substrates and therefore to a very good adhesion. A pull-off strength > 38 N/mm^2 was determined by adhesion pull tests according to ASTM D4541 (GÜNTHNER et al., 2009).

(ii) Shaping

The choice of the techniques to process coatings based on PDCs greatly depends on the physical and chemical properties of the selected precursors such as solubility, rheology, infusibility, the behaviour of cross-linking and pyrolysis. A preceramic polymer can be liquid or solid; if solid, they can be dissolved in several organic solvents or can be molten at low temperature (usually < 150 °C). Thus, liquid, meltable solid or soluble polymers can be applied by spraying, spinning or dipping onto substrates (COLOMBO, MERA, *et al.*, 2010) (KROKE, LI, *et al.*, 2000).

(iii) Cross-linking

The next step is the cross-linking, where the precursor is

transformed into a thermoset capable of retaining it's shaping and to avoid the evaporation of oligomers during pyrolysis. The cross-linking occurs by a sequence of reactions as for example condensation, dehydrogenation, dehydrocoupling, hydrosylilation and transamination. In the presence of an adequate catalyst, precursors could be cured at temperatures as low as 100 - 200°C. Polysilazanes can be cured either thermally or chemically using radical initiators like peroxides or catalyst (KROKE et al., 2000).

For example, coating based on liquid oligosilazanes, such as HTT1800, are generally cross-linked with dicumylperoxide and with Pt catalysts (FLORES et al., 2013). Further information about this step can be found in the cited authors.

 (iv) Pyrolysis

After cross-linking, the preceramic component has to be converted into a ceramic by the pyrolysis. This conversion involves complex processes, which are difficult to investigate, due to the poorly defined structure of the preceramic materials as well as to the amorphous nature of the resulting ceramic. The pyrolysis step consists of heating the sample (in inert or reactive atmosphere) at temperatures between 400 to 1600 °C.

Initially, the organic-inorganic transition (400 -800 °C) occurs forming an amorphous structure; The rearrangement and radical reactions result in cleavage of chemical bonding and release of gaseous decomposition products, for example organic functional groups as methyl, vinyl, phenyl, etc., and Si-H, Si-OH, or Si-NH$_x$. During this step an open-pore channel net-work is formed, and it can diminish (transient porosity) with further heating up to 800 - 1000 °C. PDCs are intrinsically fairly complex systems, as they undergo profound modifications, when exposed to temperatures higher than 1000°C. Depending on the polymer, heating up to 1000 – 1800 °C, a crystallization process takes place. This process is linked to the redistribution of the chemical bonds, phase separation, and finally nucleation and growth of nanocrystals (KARAKUSCU, 2010). Figure 4 shows the possible steps from the conversion of monomer to ceramic.

Figure 4: Process of polymer derived ceramic.
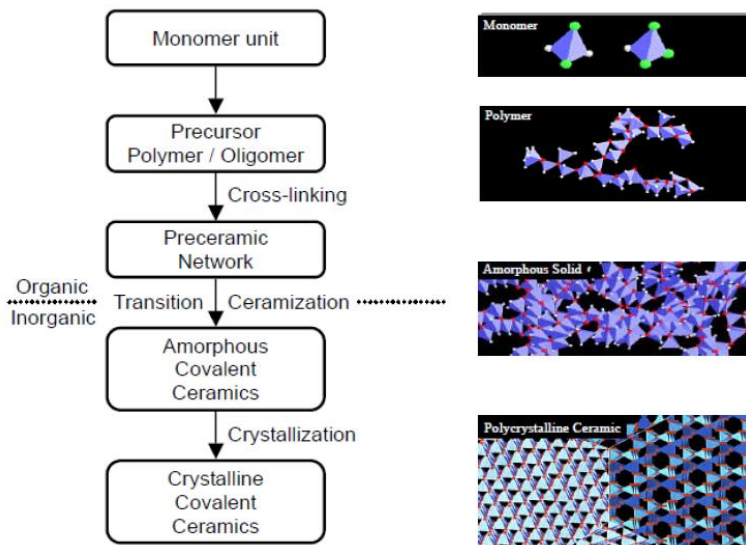
Source: (KARAKUSCU, 2010)

During the polymer conversion to an amorphous ceramic, a high volume shrinkage of about 50 vol.% and density increase accompanied by cracks and pore formation occur (GREIL, 1995b), (GREIL, 2012). The density differences between the polymer precursor ($\rho \sim 1$ g/cm^3) and the final ceramic product ($\rho \sim 2$ to 3 g/cm^3) is typically a factor of 2 to 3 (ERNY et al., 1993). This is the biggest difficulty to produce bulk components from polymeric precursors by pyrolysis process (GREIL, 2000). However, these drawbacks can be overcome with the addition of fillers of various nature (polymeric, metallic, ceramic), dimension and shape. By adding passive fillers like SiC, BN, Si_3N_4, ZrO_2, Al_2O_3 and/or active fillers, commonly transition metals or intermetallic like Ti, Cr, Fe, Al, Nb, Hf, $TiSi_2$, $CrSi_2$, TiB_2, the volume change during polymer to ceramic conversion can be significantly reduced.

While inert fillers decrease the fraction of polymer and hence the volume shrinkage, reactive fillers compensate the polymer shrinkage by expansion of the filler through reaction with the pyrolysis atmosphere, gaseous pyrolysis products or with the formed SiCN network. A combination of reactive and inert fillers can also be used to stabilize a homogeneous distribution of the additives both in the suspension and in the resulting coating (COLOMBO, MERA et al., 2010),(SEIFERT et al., 2014).

Figure 5 represents, in the left side, the polymer without filler and the inherent problems after pyrolysis; while in the right, the polymer/filler interaction after pyrolysis.

Figure 5: Scheme of polymer without filler and the polymer/filler interaction after pyrolysis.
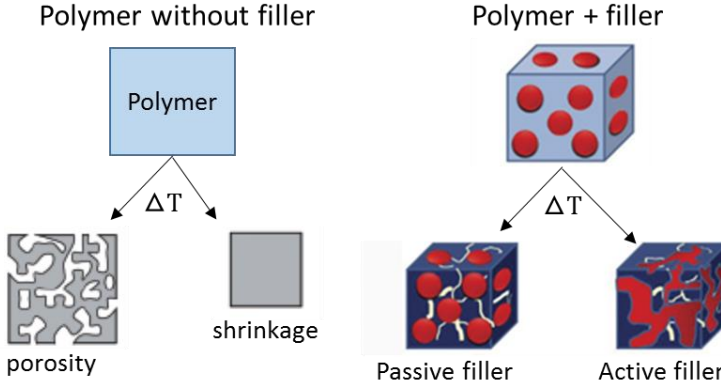
Source: Adapted from (RIEDEL et. al, 2006 and COLOMBO et. al, 2010).

The use of active filler is based in the process of active filler controlled polymer pyrolysis process (AFCOP) developed by Greil (GREIL, 1995b), where the active filler reacts during pyrolysis and form carbides, nitrides, oxides or mixtures thereof, and then reducing drastically the shrinkage and consequently the inherent problems as porosity, cracks and coating delamination (GREIL, 2003).

The AFCOP makes it possible to calculate (Eq. 1) the appropriate volumetric fraction of active filler necessary to fully compensate the shrinkage of the component (GREIL, 2000).

$$V_f = \frac{(\tau_p - 1) - P}{\left(\frac{\tau_p - 1}{V_{fc}}\right) - (\tau_f - 1)} \qquad \text{(Eq. 01)}$$

Where V_f is the filler volume fraction, V_{fc} is the critical filler volume fraction which corresponds to the maximum packing density of the filler powder, τ_p is the specific volume change of the precursor, τ_f is the specific specific volume change of the filler, and P is the residual porosity .

The equation 1 assumes complete reaction of the fillers, thus the real filler amount needed depends of the filler conversion degree

and can be much higher. For example, metal silicide or metal boride particles exhibit an increased volume expansion up to 1000 °C in a reactive atmosphere like air, however these fillers exhibit insufficient reactions to the respective nitrides in nitrogen atmosphere up to 1200 °C. In this case, the amount of filler necessary to reduce porosity may be increased (GREIL, 2012).

Due to shrinkage, the coatings of precursors are porous and this often leads to the formation of defects, cracks or even delamination of the coatings. However, by incorporation of fillers it is possible to reduce some of these problems and to tailor the mechanical, physical or chemical properties (SCHÜTZ et al., 2012).

Furthermore, the addition of filler makes it possible to increase the critical coating thickness. If the thickness exceeds this critical value, cracking and delamination of the coatings occur during pyrolysis. For unfilled PDC-based coatings, the critical thickness value lies in the range of a few micrometers (GÜNTHNER, GLATZEL, *et al.*, 2011), while for composite coatings (using active or passive fillers), the critical coating thickness can be clearly increased. For example, by the addition of $TiSi_2$ particles Torrey and Bordia (2008) for instance, developed ceramic composite coatings on steel, as a barrier to oxidation and carburization with a coating thickness of 18 µm and 10 vol% porosity. Barroso, et al (2015) applied onto steel substrate a thermal barrier coating, 50µm, based on a polysilazane bond-coat followed by a top coating based on (organo)silazane (Durazane 1800) with the combination of passive (YSZ) and active (ZrSi2) fillers. SCHÜTZ et al. (2012) developed precursor-based composite coatings with a noteworthy thickness up to 100 µm to be applied against oxidation. The barrier coating system consisting of a PHPS-derived bond coat and a composite PDC-based top coat applied on mild and stainless steel substrates. The best composite top coating could be achieved with HTT1800 as polysilazane, ZrO_2 as passive filler and two adequate glass powders as sealing agents. After cyclic oxidation tests on coated samples up to 700 °C the thick coating system was still undamaged and no oxidation occurred on the mild steel substrates. (GÜNTHNER et al., 2011) (WANG et al., 2011). The use of filler is also helpful to adapt the thermal expansion coefficient between the composite coating system and the substrate, as in the last example.

The use of active filler in the processing of coating also enables the in situ formation of carbides, nitrides, oxides or mixture thereof, and then reducing drastically the already mentioned shrinkage and consequently the inherent problems (GREIL, 2003). Therefore the

suitable system (polymer precursors, fillers and pyrolysis atmosphere) choice is of fundamental importance to manufacturing tailored coating material.

Usually the selection of the suitable filler is based on the molar volume changes of the filler in the specific expected reaction (GREIL, 1998). Another considerable point is the formed phase stability (SEIBOLD; GREIL, 1993), predicted by thermodynamic, since it will define the final material properties and future applications. Although these two factors are of major importance and may serve as important criteria to evaluate suitable fillers, final material obtained is still limited by the kinetics during process.

For example, TiB_2 is considered a potential active fillers due to the relatively high expansion coefficient calculated (GREIL; SEIBOLD, 1992),(ALLAHVERDI; CANNON; DANFORTH, 2000) under nitrogen atmosphere. However in the system composed of polysiloxane polymer and SiC-TiB_2 fillers, the TiB_2 remained practically unreacted upon the completion of the process at 1000 °C, as may predicted by the stability of TiB_2(YU; DANFORTH; LEUNG, 1995). In the same way $TiSi_2$ shows no reaction below 1000 °C in nitrogen atmosphere(ROGER; MAILLÉ; DOURGES, 2014).

Even though many efforts have been made to control the microstructure and shrinkage of PDC, this factor is still a key aspect to develop precursor loaded materials application. This research is a contribution in this field, in order to enhance the filler conversion during pyrolysis of PDC, resulting in an increased volume expansion of the fillers, decreasing the porosity, and generating in-situ phases like nitrides, carbonitrides and carbide phases.

2.2. PLASMA ASSISTED PYROLYSIS AND PLASMA BASICS ASPECTS.

The PAP process was based in the already well known application of the DC plasma technology to powder metallurgy (KLEIN et al., 2013) (BENDO et al., 2016).

One way to generate a DC plasma, for the pyrolysis purpose, is applying a potential difference between two electrodes, anode and cathode, inside a chamber containing a gas mixture. The generated electric field promotes the electron acceleration and, consequently, the collisions with neutrals species (atoms/molecules), promoting the ionization and excitation of the gas. When a specific number, great

enough, of the ionized/excited species are reached, the plasma is generated. Plasma commonly used in materials process has an ionization degree in the order of 10^{-4} to 10^{-5}(Chapman, B. 1980).

According to current-voltage used, different discharge regimes can be established, namely Corona, Townsend-, sub-normal, Normal, Abnormal and Arc regimes. Among these regimes, the abnormal glow discharge has a special interest for materials processing, mainly due to two facts: in this regime the cathode is completely covered by the glow region and the current increases with the applied voltage, allowing the control level of ionization and excitation gas (CHAPMAN, B. 1980), (KLEIN et al., 2013).

When a steady-state glow discharge is formed the potential distribution between the electrodes follows the Scheme of Figure 6, where VP is the potential of the plasma (~10 V), 0 V is the zero potential and V is the potential difference between anode and cathode.

Figure 6 corresponds to the usual kind of glow discharge used where the sample to be treated acts as the cathode of the discharge. In this case, the anode is grounded. In Figure 6 are also indicated three mean regions of fundamental importance in the DC plasma: cathodic sheath, anodic sheath and glow region (equipotential region), where the main plasma phenomena occur.

Figure 6: Potencial distribution between the discharge electrodes when the glow discharge is operating and the regions.
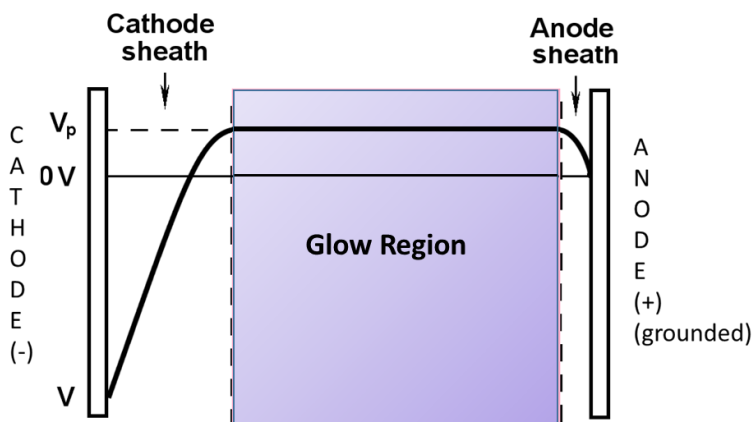
Source: Adapted from (KLEIN et al., 2013)

The reactions occurring in the glow region, also called

luminescent region, are responsible for the formation of active gas species, which are of great importance in plasma treatment. The reactions include ionization (generating atomic and molecular ions), excitation (generating exited atoms or molecules), dissociation (generating atomic species and radicals from molecules), recombination (the opposite of ionization) and relaxation (when the electron decays spontaneous to a lower level, emitting a photon). The typical plasma luminescence is due to the spontaneous relaxation of some excited species.

All these reactions are important in plasma processing materials because they generate species, such as electrons, ions, radicals and atoms from dissociation of molecules, which promotes the high plasma reactivity. It is important to mention that these reactive species are not present in the gas flow under normal conditions, or are present only in very low quantity. This fact is the basis to understand why the reactions are favored and accelerated in the plasma conditions.

Based on the main reactions occurring in each region and the setting used, some different possibilities to carry out the process of materials can be used (KLEIN et al., 2013). Further discussion covers the main reaction occurring when the samples (parts to be treated) are placed in the anode and cathode configuration.

The anodic sheath is characterized by a small potential fall, shown in Figure 6, consequently a minor surface bombardment occurs. Due to the low intensity electric field the anode is bombarded mainly with slow energetic electrons (2 – 8 eV) (CHAPMAN, 1980) from the luminescent region, and fast secondary electrons from the cathodic sheath. These electrons have a higher average kinetic energy that can be equivalent to the sheath voltage. The bombardment with ions also occurs, although the intensity of the ions bombarding the anode is much lower compared to the bombardment of the cathode. Usually ions with energy <10 eV reach the anode (BUDTZ-JØRGENSEN; BØTTIGER; KRINGHØJ, 2001). However, according to Budtz-Jorgensen, Bottiger and Kringhoj (2001) when a pulsed voltage sources is used, the ion bombardment on the anode can become important, since during the off pulse period (Toff), high energy ions also bombard the anode.

The cathodic sheath is characterized by the presence of a strong electric field, contributing to the acceleration of ions previously formed in luminescent region. These ions can collide with neutral atoms of the gas generating fast neutrals by symmetrical charge exchange and ions with lower kinetic energy (slow). These energetic species, mainly ions and fast neutral atoms, are then accelerated towards the cathode. During

materials treatment under nitrogen gas flowing, the dissociation of molecular nitrogen is one of the most important reactions, since it provides atomic nitrogen to the plasma environment, that further can diffuse to the sample (KLEIN et al., 2013). The energy distribution of these ions, atomic neutral and neutrals bombarding the sample depends on the voltage applied to the cathode, mean free path between atoms and molecules gas related to the pressure, and cathode sheath thick.

The bombardment of such species against the sample surface can cause various phenomena, illustrated in Figure 7 and listed in the sequence. More details and information about the phenomena in each region can be found elsewhere (CHAPMAN, 1980) (BRUNATTO et al., 2016).

Figure 7: Typical Plasma-surface physical interaction.
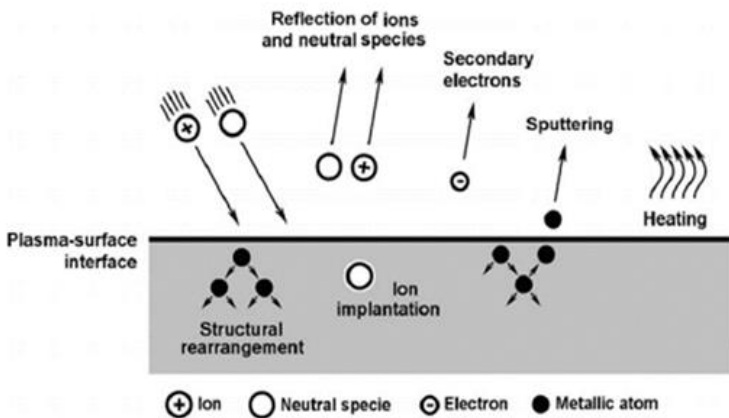
Source: (KLEIN et al., 2013)

- Sample/cathode heating, as a result of the momentum transfer when the high kinetics energy species bombard its surface.
- Emission of secondary electrons, from sample and cathode surface, that are accelerated by the potential fall of the cathode sheath into the glow region, acquiring high energy and playing an important role in the discharge maintenance.
- Sputtering: atoms of the cathode material surface are ejected as a result of the high energy plasma species bombardment. It has been estimated that as much as 90% of the sputtered atoms are

back diffused to the cathode (MASON; PICHILINGI, 1994).

- Ion implantation in the crystal structure. This phenomenon occurs when high pulsed voltage is used, due to the presence of fast species with higher energy.
- Increase of surface defects (like vacancies, interstitial, and/or substitutional atoms) in the first atomic layers of the sample.
- Composition changes and chemical reactions as a result from the use of reactive gas species in the plasma.

Based on previous aspects, the main goal to use a DC glow discharge is to generate a highly reactive atmosphere by means of excited species enriched medium. In the case of pyrolysis process, the main goal and the big difference compared with the "traditional process" using a nitrogen atmosphere, is the generation of atomic nitrogen in the atmosphere. The presence of such species can promote many plasma surface interactions and enhance, or accelerate, reactions on the part to be treated.

3. DEVELOPMENT METHODOLOGY AND JUSTIFICATION

As already mentioned, the objective of this thesis is part of a BRAGECRIM project entitled 'Development of wear resistant and self-lubricating coatings on sintered steels from polymer-derived ceramics", o project developed by a partnership between the Ceramic Materials Engineering Institute/University of Bayreuth and LabMat/UFSC. The adopted methodology of the thesis, within this project, is described in the sequence.

One of the great challenges of this work was to unite the development of PDC coatings on sintered steels simultaneously to the development of the plasma assisted pyrolysis process. Since both goals are novel and require the study of many parameters, many steps were necessary to achieve the desired goals and knowledge about the process. The methodology used to develop PDC coatings on sintered steel using plasma atmosphere during the pyrolysis process was divided into three main phases, as follows and summarized in the scheme of Figure 8.

Figure 8: Scheme of the methodology used in this research.
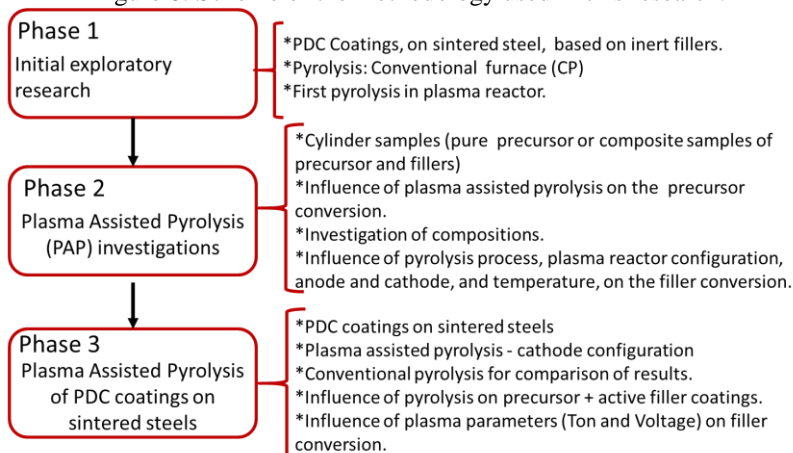
Source: Elaborated by the author

3.1. PHASE 1: INITIAL EXPLORATORY RESEARCH

At this stage, the development of PDC coatings on sintered steels started using inert fillers, based on previous work of the research group (GÜNTHNER et al., 2011), and the pyrolysis was performed in a conventional furnace in order to obtain information about the behavior

of the coating on sintered steels as substrate. After the preliminary results in a conventional furnace, the first experiments of pyrolysis in a hybrid plasma reactor were performed, i.e, plasma assisted pyrolysis.

3.2. PHASE 2: PLASMA ASSISTED PYROLYSIS (PAP) INVESTIGATIONS.

Analyzing the results obtained in the previous step was chosen to initiate the second stage using cylindrical bodies processed with only the precursor or the PDC loaded filler, and no more coatings. This decision was taken to gain knowledge on PDC composite behavior in the presence of plasma atmosphere without the substrate influence.

3.2.1 Influence of PAP on the pyrolysis behavior of HTTS

The pyrolysis behavior of the pure polyorganosilazane precursor (called HTTS) is well investigated under nitrogen atmosphere in a conventional furnace (FLORES et al., 2013). To verify the influence of the plasma atmosphere on the pure precursor were performed pyrolysis in anode and cathode configuration, as well as conventional pyrolysis to compare the obtained results, at 1000 °C.

3.2.2 Composition investigations

Different compositions were investigated, including types of fillers and filler to precursor ratio. The goals of this stage were to investigate the volume and mass change and phase transformations of different compositions, under plasma atmosphere.

3.2.3 Influence of PAP configuration and temperature

Among the compositions studied in the last step (3.2.2) it was selected a potential composition based on $TiSi_2$. Then it was performed conventional pyrolysis (normal furnace) and plasma assisted pyrolysis in both reactor configurations, sample acting as cathode or anode, in order to comprise the conversion behavior of the filler with respect to the chemical species of plasma atmosphere interacting with the sample. The pyrolysis of the selected sample, precursor with $TiSi_2$, was also investigated under different temperatures and holding times, in order to follow the reactions and to verify the influence of temperature on the formed phases.

3.3. PHASE 3: PLASMA ASSISTED PYROLYSIS OF PDC COATINGS ON SINTERED STEELS.

Having further understanding about the behavior of the PDC composite after PAP and the influence of some process parameters, the research was conducted with PDC coatings on sintered steel substrates.

Based on the results obtained in both anode and cathode reactor configuration, from this point the pyrolysis was always performed on the cathode configuration, aiming higher filler conversion and formation of new phases.

The activities at this stage include:

3.3.1 Coating composition

Compositions based on SiC, Ti, B, $TiSi_2$, Si_3N_4 and TiB_2 were applied on the sintered steels. The formed phases were analyzed as well as the coating thickness.

3.3.2 TiB_2 particle as active filler

To continue developing the PAP process it was chosen to use the TiB_2, one of the potential active fillers in accordance with both results and literature(GREIL; SEIBOLD, 1992). The basis for choosing this filler to process PDC coating on sintered steel was mainly due to the formed phases, TiC, Ti(C,N), and TiN, which are phases with improved properties.

In order to follow the filler conversion, under plasma atmosphere, pyrolysis was performed under different temperatures. So that to demonstrate the improved conversion of TiB_2, and formation of new phases during the plasma assisted pyrolysis process, experiments were also carried out in a conventional tube furnace.

3.3.3 Influence of plasma process parameters

The influence of the plasma switched on time (Ton) (pulse length) and Voltage (V) on the filler conversion of PDC coating on sintered steels was investigated.

Modifying the plasma switched on time changes the interaction average time between the atomic nitrogen, and other energetic species, with the surface coating under bombardment

The modification of plasma voltage implies in the energy

variation of the nitrogen ions bombarding the cathode. This energy (E) is also related to energy loss due to collisions between these species with neutral gas in the cathode sheath. Thus, it is necessary to find the optimized parameters between number of collisions (N), related to the thickness of the cathode sheath and mean free path, and Voltage. The equation 2 describes this relation, where C_1 is a constant of proportionality (CHAPMAN, 1980).

$$E = C_1 \left(\frac{V}{N}\right)$$ (Eq. 02)

It is known from literature that increasing the energy of the ions bombarding the surface enhances the kinetic energy transferred to the atoms from the surface and consequently possible increase in mobility and surface diffusion (MALISKA et al., 2003) of the ions/atomic nitrogen to the coating surface.

Then, the goal is to evaluate the influence of these two parameters on the kinetics of filler conversion, especially in the formed phases.

4. EXPERIMENTAL PROCEDURE AND CHARACTERIZATION

4.1. EXPERIMENTAL PROCEDURE – SINTERED SUBSTRATE PROCESSING

4.1.1 Raw materials

The steel substrate composition is Fe1.5%Mo 2.0 %Ni 0.6% C (wt%) . The raw materials used were the pre-alloyed iron molybdenum and the elementary nickel and carbon powders. The suppliers and particle size of the raw materials, in accordance with the data sheet from the supplier, are shown in Table 1.In order to assist during the pressing step 0.8wt% of amide wax (Acrawax C – Lonza) was added to the initial composition. The particle size distribution of the AstaloyMo, from the data sheet of the supplier, is shown in Table 2.

Table 1: Raw materials information.

Powder	Comercial Name	Supplier	Particle Size-D50 (µm)
Fe1.5wt%Mo	AstaloyMo	Höganäs	-
C	Micrograf 99511UJ	Nacional de Grafite	9.88
Ni	Pure Nickel	Epson Atmix corporation	6.06

Source: Elaborated by the author

Table 2: Particle size distribution of AstaloyMo powder.

Particle Size (µm)	Distribution (%)
> 250	0
150 - 250	6,9
106 - 150	20,4
75 – 106	22,0
45 – 75	25,8
< 45	24,6

Source: Elaborated by the author (data from supplier)

4.1.2 Mixing, compacting and sintering

The steel substrates were processed following the traditional steps of the powder metallurgy: selection and mixing of powders, die compaction of the mixture and the sintering (GERMAN, R.M. 1998).

In the first step, the powders and amide wax were precisely

weighted and homogenized by mixing in a Y-type mixer during 45 minutes at 35 RPM. After it, the powder mixtures were uniaxially pressed (600 MPa) by a double-action press in a floating die. The samples were processed in a cylindrical geometry with dimensions of 25 mm diameter and approximately 5 mm thickness. These specimens were then sintered in a resistive tubular furnace (Fortlab) with controlled atmosphere (95% argon and 5% hydrogen), flow of $6,6x10^{-5}$ m^3s^{-1}, heating rate of 5 °C/min, with a debinding step at 550 °C during 30 minutes (to eliminate the amide wax) and final sintering step at 1150 °C during 60 minutes.

4.2. EXPERIMENTAL PROCEDURE – PDC

Since this work involves different compositions and parameters of pyrolysis, in order to facilitate the reading, the experimental procedure is presented as following: First, it is shown the raw material (precursor) used, the procedure to process the coating and the bulk sample and the general parameters of the pyrolysis process for conventional (CP) and plasma assisted pyrolysis (PAP). In the sequence are presented the fillers and the specifics parameters of the pyrolysis process for each phase (phase 1, phase 2 and phase 3).

4.2.1 Raw materials

The criteria for the selection of the precursor were workability, high ceramic yield, compatibility with the sintered steel and the fillers, temperature stability of the formed ceramics up to 1300 °C, commercial availability and low price. Previous work from the partner of the University of Bayreuth has identified the liquid polysilazane HTT1800 as a potential precursor to develop the coatings. The HTT1800 is synthesized by co-ammonolysis of dichloromethylvinylsilane and dichloromethylsilane. It can be cross-linked by heating from 180 to 200 °C or by adding a free radical initiator at lower temperatures. The HTT1800 chemical structure, before cross-linking, consists of 20% methyl/vinyl and 80% of methyl/hydride silazanes units, as shown in Figure 9. The ceramic yield is approximately 80% (1200 °C, N_2) by using 3 wt.% of the radical initiator dicumylperoxide (DCP 98%, Sigma Aldrich, USA). HTT1800 is commercially available at Kion® HTT1800 (AZ Electronic).

Figure 9: Chemical structure of the precursor HTT1800.
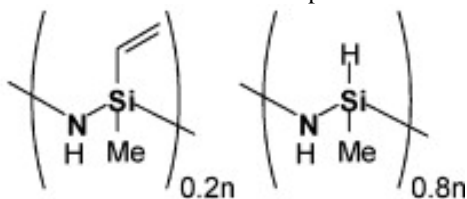
Source: (FLORES et al., 2013)

For this work, the self-synthesized solid and meltable polyorganosilazane HTTS was used to prepare the bulk samples. The HTTS polymer results from a controlled cross-linking of the commercially available liquid precursor Kion® HTT1800 (AZ Electronic Materials, Germany) to a meltable solid as described elsewhere (FLORES et al., 2013)(MOTZ et al., 2012). Final cross-linking of the HTTS polymer into a thermoset starts at a temperature of 110 °C via hydrosilylation between vinyl and Si-H groups and polymerization of the vinyl groups (ZIEGLER et al., 1999), by adding 3 wt.% of the radical initiator dicumylperoxide (DCP 98%, Sigma Aldrich,USA). After milling and sieving of the synthesized HTTS powder particles smaller than 63 μm were obtained.

The fillers used in this work are described in the sequence, separated by phases of the project.

4.2.2 Suspensions development and coating application into sintered substrates

The suspension and the coating application of this work were prepared following the step shown in Figure 10.

Figure 10: Scheme of the coating processing steps.
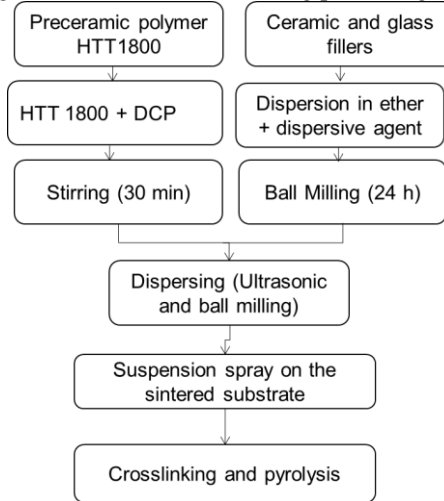
Source: Elaborated by the author

First, suspensions of each filler in di-n-butylether (50 wt.%) (Alfa Aesar GmbH & Co KG, Germany) using 5 wt.% Disperbyk 2070 (BYK-Chemie GmbH, Germany) as dispersant agent were prepared. The precursor HTT1800 was stirred with 3 wt.% of dicumylperoxide (Sigma Aldrich). In the sequence, the HTT1800 and fillers suspensions were mixed to obtain the desired compositions. The suspensions were homogenized by ultrasonic and ball milling. In the ball milling step zirconia balls (1 mm diameter) were added to help the dispersion. The final suspension, with the desired coating composition (based on the calculations reported by Greil et al. (1995)), was then applied on the sintered steel substrate by spray technique. The spray process was done in a paint booth, as shown in Figure 11, using a spray gun (Krautzberger Mignon 3) manually positioned around 10 cm from the sample to be coated. It was applied a pressure of 1.75 bar, measured with a manometer (Wika model).

Figure 11: Spray coating booth.

Source: Archive of CME

4.2.3   Processing of the cylindrical bulk sample.

The first step to process the cylindrical bulk sample is to prepare a suspension with the desired amount of filler and precursors, in order to mix and homogenize the components. The selected ratio of precursor and fillers is also based on the calculations reported by Greil et al. (GREIL, 1995b) to obtain zero shrinkage of the composite ceramics.

Each filler is suspended into 50% vol. solvent (pentane or isopropanol) solution at first with dispersing agent (BYK2070 -Altana AG, Germany) at 10 wt%. The HTTS is also dissolved in 50 % vol. solvent. Next, the fillers and precursor are mixed in a bottle and homogenized by ultrasonic and magnetic stirring. After mixing for 6 hours, a stable suspension was obtained.

In the sequence, the solvent was removed using a rotary evaporator working at low pressure (1.5 x 10^3 Pa) and a temperature of 40 °C. The solid products were dried, crushed and sieved into particles smaller than 32 µm and uni-axially pressed under 200 MPa to obtain solid tablets with diameter of 13 mm and thickness between 2 and 4 mm. During the pressing step, the samples were heated to 160 °C during 1h for complete cross-linking of the precursor. The next step was the pyrolysis, described in the sequence. A summary of those steps, to process the bulk, sample is presented in Figure 12.

Figure 12: Scheme of the bulk processing steps.
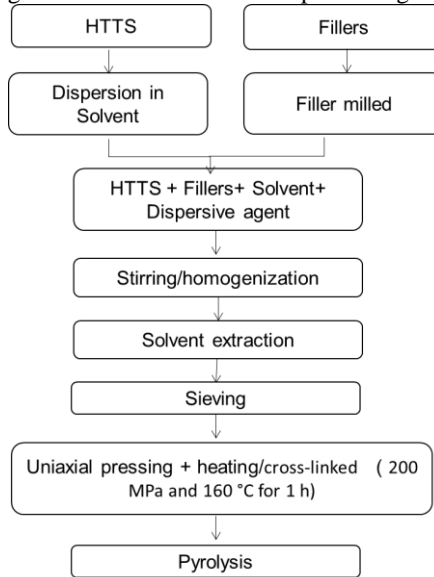
Source: Elaborated by the author

4.2.4 Pyrolysis

Conventional pyrolysis was carried out in a Al_2O_3 tube furnace (Thermal Technology, USA or Fortlab) under flowing nitrogen atmosphere (purity 5.0). The thermal treatment of coatings performed in air were carried out in a chamber furnace (Nabertherm® LH 60/14, Nabertherm, Germany).

All the PAP experiments were performed in a hybrid plasma reactor, containing a grounded anode and a cathode connected to the negative voltage output besides a resistive heating system inside a grounded vacuum chamber.

To generate the abnormal glow discharge a square waveform DC pulsed power source (SDS Plasma, Brazil) with a potential difference between the electrodes (AISI 304) of 500 V was used (except in the phase three, where the voltage was changed, as mentioned below). Pulsed voltage is used to avoid the shift from abnormal glow to arc discharge regime leading to an instability of the generated plasma. Additionally, the energy input into the furnace could be decreased resulting in a more uniform temperature distribution. The pulse length (Ton) was set to 100 µs (except in phase three, where the Ton was

systematically varied) in combination with pulse repetition time of 250 μs (Ton + Toff) leading to a plasma duty cycle (Ton / (Ton + Toff)) of 40%.

All of the treatments were carried out under reduced nitrogen pressure of 200 Pa (purity 5.0) controlled with a capacitance manometer (626C Baratron MKS, USA). The gas flow was set to 4.17×10^{-6} m^3/s and was monitored by an 825MKS mass-flow controller. By using this experimental setup an abnormal glow discharge with a current of 0.2 A was measured at the cathode side.

To investigate the reactor configuration influence, the PDC samples were placed in two different positions, anode and cathode, in relation to the electrodes during the PAP process. The mean difference between both configurations is how the species bombard the sample. As already mentioned, sample as cathode will have much more ions and atomic species impinging the sample, and as anode much more electrons. This promotes different reactions in the PDC samples, especially in the conversion phenomenon of the reactive fillers used in the PDC composite. A scheme of both configurations of the plasma reactor is shown schematically in Figure 13.

The anode and cathode support, made with stainless steel AISI 304, have dimensions of 12x19x2.5 cm and 14.6x16.7x5 cm, respectively. And the distance between them were approximately of 5 cm. Thermocouples of type K (Inconel sheath) were used for monitoring the temperature inside the plasma chamber; the thermocouple is coupled to a sample, called reference, localized next to the sample being pyrolyzed as showed in Figure 13

Figure 13 Schematic representation of the anode (A) and cathode(B) configuration.
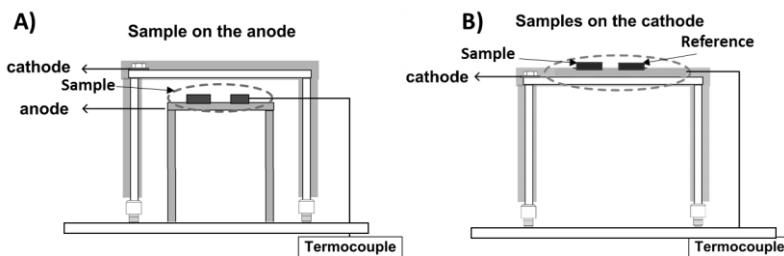
Source: Elaborated by the author

Since different parameters (temperature, holding time, atmosphere, etc) were used, a summary of the pyrolysis parameters is

presented in each phase description as follows.

4.2.5 Raw materials and Pyrolysis Parameters – Phase 1

In the first phase of this research, three different compositions, C1, C2 and C3, were developed as shown in Table 3. Those filled polysilazane coatings applied on the sintered substrate were based on the well investigated coating from previous research (GÜNTHNER et al., 2011).

The passive fillers used in this step were ceramics and glasses. Boron nitride (BN) (Henze BNP GmbH, Germany), silicon nitride (Si_3N_4) (H. C. Starck GmbH, Germany) and zirconium dioxide (ZrO2) (Alfa Aesar, USA) with an average particle size (D_{50}) of 0.6, 0.7 and 1 µm respectively, were tested as passive fillers. Two glass powders, 8470 (borosilicateglass) and G018-311 (barium silicate glass), whose coefficient of thermal expansions (α around $10x10^{-6}$/K) close to that of the steel substrates (α around $9x10^{-6}$/K) were also used. The average particle size of the glass powders were 3.3 and 3.1 µm respectively. With those fillers and the HTT1800 precursor it was processed coating onto the sintered substrate, as described in the section (4.2.2).

Table 3: Coating Compositions.

Name Composition	System	Composition (Vol%)
C1	HTT1800- G018311 - G8470 - ZrO2	10 - 32.5 - 32.5 -25
C2	HTT1800 - G018311- ZrO2 - Si_3N_4 - BN	20 - 20 - 25 - 25-10
C3	HTT1800 - ZrO_2 - Si_3N_4 - BN	20 - 20 - 40 - 20

Source: Elaborated by the author

Table 4 shows the pyrolysis parameters used for each sample. The holding time of the pyrolysis in this step, both CP and PAP, were 1h.

At PAP process the anode was grounded and the cathode was negatively biased with 500 V through a DC pulsed power source. The pulse lenght (Ton) of the power source was fixed at 100 µs and the measured current was 0,2 A. The gas atmosphere was 100% N_2, with the flow $4.17 \times 10^{-6} m^3 \cdot s^{-1}$ and the pressure system was fixed at 200 Pa (1.5Torr). The heating rate was 3 K/min for all the experiments.

Conventional pyrolysis (CP) was performed at atmospheric pressure ($1.01x10^5$ Pa) under flowing nitrogen ($6.5x10^{-6}$ m^3s^{-1}) with the same heating rate of °C/min or under no controlled atmosphere (air) in the chamber furnace.

Table 4: Pyrolysis parameters- Phase 1.

Composition name	Pyrolysis Process	Pyrolysis Temperature (°C)	Atmosphere
C1, C2	CP	700	Air
C2	CP	1000	N_2
C2	CP	900	N_2
C2	PAP – A*	900	N_2
C3	CP	1000	N_2
HTT 1800	PAP – A*	900	N_2

*A= anode configuration.

Source: Elaborated by the author

4.2.6   Raw materials and Pyrolysis Parameters – Phase 2

The passive fillers used in this step were Si_3N_4 (H. C. Starck GmbH, Germany) and silicon carbide (SiC), Grade S UF25, with particles $D_{99} < 0.8$ µm (H.C. Starck GmbH, Germany).

As active filler, titanium (Ti) particles (Alfa Aesar, USA), with particle size $D_{99} < 0.8$ µm and boron (Alfa Aesar) particle size $D_{99} < 38$ µm were tested. Another studied active filler was the $TiSi_2$ powder (ABCR, Germany, purity 99.5%) with a average particle size 45 µm. $TiSi_2$ was milled in a planetary ball mill (Pulverisette 5, Fritsch,Germany) in order to reduce the particle size to a D_{50} of 10 µm. The powder was milled with a speed of 350 rpm for 6 h in a Si_3N_4 crucible using Si_3N_4 balls with a diameter of 5 mm using isopropanol as solvent. The powder/ball weight ratio was 1:170.

Based on those fillers and the HTTS as precursor, bulk samples were processed, as described in the section (4.2.3), with the compositions shown in Table 5.

The pyrolysis behavior of HTTS at temperatures up to 1000 °C in a conventional furnace under nitrogen atmosphere is well investigated (KROKE et al., 2000), (TRASS et al., 2000) (TRASSL et al., 2002). Samples based on HTTS (without filler) were also processed in order to verify the influence of PAP process on the HTTS conversion. The pyrolysis of HTTS specimens was carried out at 1000 °C for 2 h in the plasma reactor in both anode and cathode configuration as well as in a Al_2O_3 tube furnace.

Table 5: Bulk sample Compositions- Phase 2.

Name Composition	System	Composition (Vol%)
C4	HTTS-Ti-Si$_3$N$_4$	34 - 26 – 40
C5	HTTS-Ti-SiC	55 - 14 – 31
C6	HTTS-B-TiSi$_2$	55 - 10 – 35
C7	HTTS- TiSi$_2$	40 – 60
C8	HTTS- TiSi$_2$	30-70
	HTTS	100

Source: Elaborated by the author

The samples composed of compositions C4, C5, C6 and C7 were pyrolyzed under PAP process, at anode configuration, 1000 °C, 2h. While the specimens composed of TiSi$_2$ –HTTS, composition C8, was performed at 900, 1000 and 1150°C, for 2h in a conventional furnace and in the plasma reactor, in anode and cathode configuration. In order to follow the reactions at 1150°C the annealing time was set to 5h additionally. As in the last phase, during PAP process, 500 V, Ton of 100 μs and 100% N$_2$ atmosphere were used. The heating rate was 3 K/min for all the experiments. Conventional pyrolysis was performed at atmospheric pressure (1.01×10^5 Pa) under flowing nitrogen (1.5×10^{-5} m^{3}s^{-1}) and heating rate of 3 °C/min.

The pyrolysis parameters process performed on this phase are summarized in Table 6.

Table 6: Pyrolysis parameters- Phase 2.

Composition name	Pyrolysis Process	Pyrolysis Temperature (°C)	Holding Time (h)
HTTS	PAP- A* PAP- C** CP	1000	2
C4, C5, C6, C7, C8	PAP – A CP	1000 900,1000, 1150	2 2
C8	PAP – A	900,1000, 1150	2 (2 and 5 for 1150 °C)
C8	PAP – C	900,1000, 1150	2 (2 and 5 for 1150 °C)

*A= anode configuration **C= cathode configuration
Source: Elaborated by the author

4.2.7 Raw materials and Pyrolysis Parameters – Phase 3

In the third phase of the project, coatings on the sintered steel substrate were developed. The procedure to prepare the coating and the application onto the substrate was already described in section (4.2.2).

The filler used in this section includes the passive Si_3N_4 and the active $TiSi_2$ used in the last phase, as well as titanium diboride (TiB_2)(H.C. Starck -Grade F), particle Size D_{50} between 2.5 to 3.5 µm and D_{90} 4 to 7µm as active filler. The compositions are shown in Table 7.

Table 7: Coating Compositions- Phase 3.

Name Composition	System	Composition (Vol%)
C9	HTT1800-TiSi$_2$	30 - 70
C10	HTT1800-TiSi$_2$-Si$_3$N$_4$	30 - 60 - 10
C11	HTTS-TiB$_2$	30 - 70

Source: Elaborated by the author

This phase can be divided in two parts. In the first, all the experiments performed under PAP using the same voltage and Ton as in phases 1 and 2. In the second part, the voltages and Ton were changed in order to verify the influence of these parameters on the PDC pyrolysis. The other parameters, as gas flow, pressure and heating rate, were kept constant for all the phases. The holding time was 2h. The conventional pyrolysis were performed under flowing nitrogen and heating rate of 3 °C/min, as in phases 1 and 2. The pyrolysis process parameters performed on this phase are summarized in Table 8.

Table 8: Pyrolysis parameters- Phase 3.

Name	Pyrolysis Process	Pyrolysis Temperature (°C)	Ton (µs)	Voltage (V)
C9	PAP- C	1150	100	500
C10	PAP – C	1150	100	500
C11	PAP- C	900, 1000, 1075, 1150	100	500
C11	CP	1000, 1150	-	-
C11	PAP – C	1000	70, 100, 130, 150	500
C11	PAP – C	1000	100	400, 500, 600

Source: Elaborated by the author

4.3.   CHARACTERIZATION METHODS

The sintered steel substrate and the polymer derived ceramic composites (coating and bulk sample) were analyzed using a variety of methods. Density, porosity, microstructure, phase composition, hardness and micro hardness, were evaluated using the techniques summarized in this section.

The sintered steel substrates were characterized by microstructural analyzes using an optical microscopy (Olympus BX60) and scanning electronic microscopy (SEM- JEOL JSM-6390LV) in both secondary electron and backscattered electron modes. The densities of the substrates were determined by geometrical methods. The Brinell hardness measurements were carried out with a durometer (EMCO-Test, M4C25063), using a 2.5 mm indentation sphere and 31.25 N of applied load during 5 seconds and the microhardness measured by a Leco microdurometer (LM100AT), using an applied load of 100 gf for 10 seconds. Image analysis (software Leica, Las X) was used to perform the quantitative analysis of the porosity. The images were obtained from unetched samples using a camera coupled to an optical microscope (Leica – DM4000 M), 200x magnification, in gray scale. Five samples were analyzed, and for each sample a number of 10 images were acquired, following the methodology described in details elsewhere (PAVANATI et al., 2007)

The microstructure of the pyrolyzed composite materials and the HTTS was analyzed by scanning electron microscopy. Using a JEOL JSM-6390LV (LCME) and TESCAN Vega 3 LMU (LABMAT), or Zeiss 1540ESB SEM (Germany) in both secondary electron and backscattered electron modes. Field emission scanning electron microscopy (FEG-SEM), JEOL JSM-6701F (LCME) was used to evaluate the surface of the coatings. Quantitative energy dispersive x-ray spectroscopy (EDS), coupled with SEM, was used to study the composition and the elemental distribution of the samples after pyrolysis. Voltages between 5 and 20 kV were used.

The crystalline phases of the $TiSi_2$ and HTTS bulk sample were detected by X-ray powder diffraction analysis (D8 ADVANCE, Bruker AXS, Karlsruhe, Germany) using monochromated CuK_α radiation. Phase composition and lattice parameters were determined via quantitative Rietveld analysis by using the evaluation software TOPAS (V4.2, Bruker AXS, Karlsruhe, Germany) and PDF-4+ 2012 structural database for crystallographic information.

X-ray Diffraction (XRD) (Philips X'Pert) was used to study crystalline phases and the formation of new phases of the samples (except the samples mentioned above) after pyrolysis. A Cu-Ka radiation source (λ = 1.5418 Å) and monochromator was used and scans were carried out between 3° to 115 °, with a step size of 0.02° degree, angular step time of 1 s, applied voltage of 40 kV, 30 mA of current. Lattice parameters and phase composition were determined via quantitative Rietveld analysis, using the program DBWS-9807 and DMPLOT to compare the theoretical spectrum with the refined ones. In order to obtain the crystallographic information, necessary to the structural refinement by the Rietveld Method, the Inorganic Crystal Structure Database (ICSD) and the PDF-2 data base from International Centre for Diffraction Data (ICDD) were used.

The Rietveld method consists of minimizing the difference between the experimental and calculated diffraction pattern by the least squares method. During refinement, parameters, called global and specific for each constituent phase and sometimes instrumental parameters, that physically affect the XRD patterns, can be considered, calculated and compensated (ERIC J. MITTEMEIJER; SCARDI, 2004).

To perform the refinement the same sequence of parameters adjustment for the entire sample was used. The parameters adjusted in this work were:

  a) Background (Baseline): Correct data gathered in the XRD pattern and interpolation between these points. The background also provides information about the presence of amorphous phases in the sample.

  b) Scale factor: is related to the amount of each phase.

  c) Cell parameters: The cell parameters of each phase can be fitted by Bragg's Law.

  d) Peak profile: The width and position of the peaks are related to the characteristics of crystallite size and cell, respectively. Analytical equations, as Gaussianand the Lorentzian, are used to correct these effects.

  e) Factor of structure: Involves the adjustment of the atomic positions, the isotropic or anisotropic temperature factors and the occupation number.

  f) Factors of temperature: correct deficiencies related to the radiation, absorption and surface roughness.

g) Preferential orientation: some phase tends to place parallel to a particular crystallographic direction, this factor is then corrected.

The quality of refinement is verified by statistical indicators, R_P, R_{WP} (weighted R-profile), and GOF (Good of fitness). The good of fitness compares the final values of R_{WP} with the expected value of the error (R_{EXP}), (GOF = R_{WP}/R_{EXP}). The R_{EXP} is derived from statistical data. The refinement is considered acceptable when the value of R_{WP} is between to 2-10 % and the GOF is close to 1.0; In fact those value being smaller, better is the refinement. However, is always important to consider the visual analysis between the calculated and experimental XRD pattern (KNIESS; CARDOSO DE LIMA; PRATES, 2005) (TOBY, 2006).

Thus, in order to better access the results of the refinement, the values for the weighted R-profile and the goodness of fit are always given in addition to the calculated values.

The glow discharge optical emission spectroscopy (GDOES) was used to make a qualitative profile of the chemical elements presents in the pyrolyzed coating, from its surface to a depth of micrometers. The characterization was performed only in a qualitative form due to the lack of standards to quantify each element. The measurement parameters used are described in Table 9.

Table 9: GDOES measurement parameters.

Flushing Time	Pre integration Time	Pressure	Power	Anode size
200s	150s	630 Pa	30 W	4 mm

Source: Elaborated by the author

To follow the weight changes during nitridation, the fillers powder were analyzed with thermogravimetric analysis (TGA, L91, Linseis, Germany) up to 1200 °C with a heating rate of 5 °C/min under nitrogen atmosphere (purity 5.0).

The densities of the green bulk samples were measured by the geometric method (cylindrical samples) and theoretical density, calculated with the mixing rule. The porosity of the green sample was determined by subtracting the bulk density from the theoretical density.

The density of the pyrolyzed PDC bulk samples was measured using a He-pycnometer (AccuPycII 1340, Micromeretics, Germany) or by the geometric method (cylindrical samples). After pyrolysis the

porosity was estimated by image analysis, evaluating the binary images of the SEM pictures.

It is important to mention that the partner research group at Germany performed some of those characterizations.

5.   RESULTS AND DISCUSSION

5.1.   SINTERED SUBSTRATE CHARACTERIZATION

In this session, a brief characterization of the sintered substrate after sintering (before pyrolysis) is presented. More details can be found elsewhere (JUSTUS, 2016) (GONÇALVES, 2016).

This common route of processing powders leads to the presence of residual porosity, as it can be observed in the unetched microstructures in Figure 14, where the dark regions represent pores. The sintered substrate presented an average density of $7.01\pm0.03 g/cm^3$ and a porosity, measured by image analysis (Figure 15), of 8.96 ± 1.9 %. Those values are typical for sintered steels produced by mechanical pressing (the conventional PM route) and are in accordance with results obtained by Chawla and Deng (2005). For similar composition (Fe–0.85Mo, pre-alloy powder, 2.0 wt.% Ni, and 0.6 wt.% graphite) they found the porosity measured by image analysis yielded values of around 12% and the density of 7.0 g/cm^3.

Figure 14: Optical Micrograph (transversal section) of the unetched sintered steel after sintering at 1150 °C, 60 min.
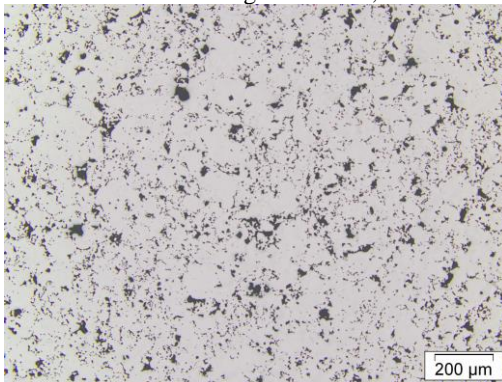
Source: Elaborated by the author

Figure 15: Images of sintered substrate after image analysis, where the dark region was counted as pores.
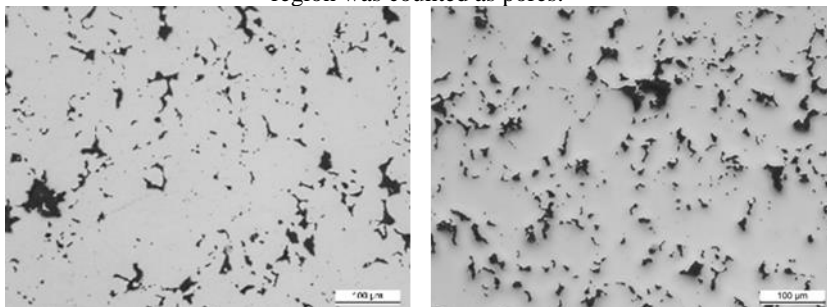
Source: Elaborated by the author

After etching with 2% Nital the samples revealed a heterogeneous microstructure (Figure 16), composed of a mix of perlite (P), bainite (B), austenite (A) and martensitic (M), as indicated in the SEM image of Figure 17. The presence of different phases is a result of concentration gradients of the alloying elements due to the diffusion rates at the used sintering temperature, time and cooling rate.

Figure 16: Optical micrograph (transversal section) of the etched sintered steel after sintering at 1150 °C, 60 min.
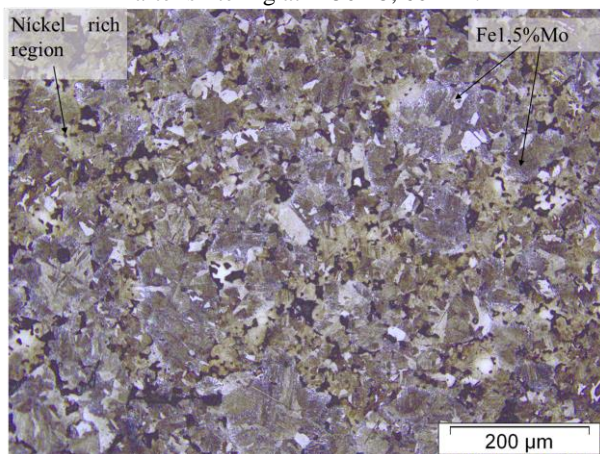
Source: Elaborated by the author

Figure 17: SEM micrographs (transversal section) of the etched sintered steel after sintering at 1150 °C, 60 min. SE signal.
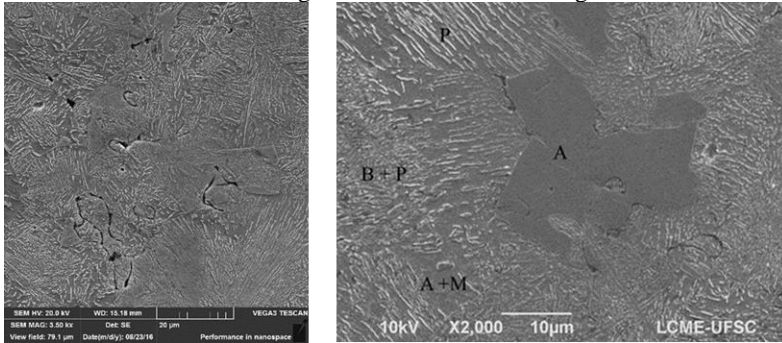
Source: Elaborated by the author

The measured microhardness of the phases vary in the range of 200 – 393 HV. Those results of microhardness data are in accordance with morphological observations for bainite, perlite and austenite phases; However the values are rather low for the martensite phase, indicating that could have been a mix of phases martensite–austenite (HÖGANÄS, 1999). As expected, the hardness of the bulk sintered substrate (165.3 ± 9.8 HB) was lower than the microhardness of constituent phases, due to the residual porosity which decreases the matrix continuity.

5.2.   PHASE 1: INITIAL EXPLORATORY RESEARCH

The first filled polysilazane coatings applied on to the sintered substrate were based on ceramic (BN, Si_3N_4, ZrO_2) and glass (Schott 8470, G018-311) fillers, based on the well investigated coating from previous research (GÜNTHNER et al., 2011).

Figure 18 shows the SEM micrograph of the sintered substrate coated with HTT1800/ZrO_2/Glasses (Composition C1) after conventional pyrolysis at 700 °C, holding time of 1 h, and air atmosphere. In order to facilitate the reading and comprehension, as many compositions were used, the compositions named C1, C2 and C3 are listed again in Table 10.

It is noted a visual evidence of adhesion between coating and substrate and the substrate morphology is well covered by the coating. At the interface an interlayer is observed, by the color differences. However, this layer and the diffusion phenomena at the interface

substrate/coating were not investigated, since the main objective was to have information about how the coatings based on polysilazane and fillers would cover the sintered substrate. So, it was observed that it is possible to apply this composition on the sintered substrate.

Figure 18: SEM micrograph (BSE signal) of the sintered substrate coated with HTT1800/ ZrO2/Glasses (C1). Conventional pyrolysis at 700 °, 1 h, air.
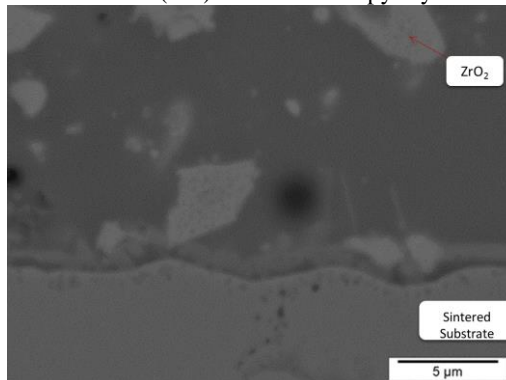
Source: Elaborated by the author

Table 10: Coating Compositions- Phase 1.

Name Composition	System	Composition (Vol%)
C1	HTT1800 - G018311 - G8470 - ZrO2	10 - 32.5 - 32.5 -25
C2	HTT1800 - G018311- ZrO2 - Si_3N_4 - BN	20 - 20 - 25 - 25-10
C3	HTT1800 - ZrO_2 - Si_3N_4 - BN	20 - 20 - 40 - 20

Source: Elaborated by the author

The next step was to change the composition, by the elimination of the glasses and filler modification, in order to have coatings with tribological application in the sequence of the project.

The SEM micrograph of the substrate coated with composition C2, after pyrolysis at CP at 700 °C, is shown inFigure 19 in two magnification. The coating composition C2 has the glass G018.311 and ZrO_2, Si_3N_4 and BN as passive fillers. The coating thickness is around 50 μm and shown cracks and even holes; however, it seems that the biggest hole seen in the microstructure image was generated during the metallography preparation. The coating shows resistance to handling; However, the adhesion between coating and substrate was not measured.

Figure 19: SEM micrograph of the substrate coated with
HTT1800/glass/ZrO$_2$/Si$_3$N$_4$/hBN, after CP at700 °C, 1h, Air.
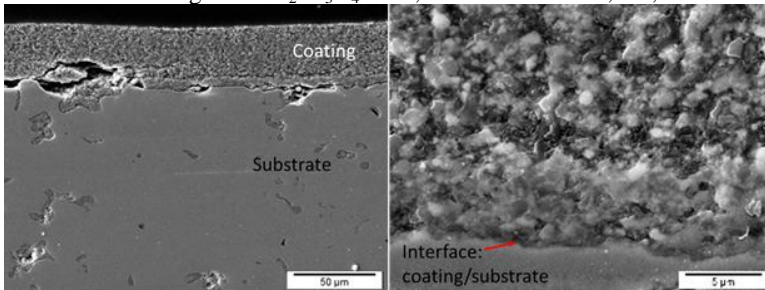
Source: Elaborated by the author

Based on that, it were investigated the pyrolysis temperature
and atmosphere. Figure 20 shows the micrograph of the substrate coated
with composition C2 (transversal section) after conventional pyrolysis,
at 1000 °C, under nitrogen atmosphere and 1h holding time. In the right
side the coating is shown with high magnification.

It is noted that there is no "gap" between the metal substrate and
the coating and the coating shows resistance to handling. It is also
observed that the coating is covering the substrate pores, which could
help physically the interfacial adhesion. The coating has an average
thickness of 40μm, without the presence of cracks, but still with a high
number of pores.

Figure 20: SEM micrograph of the substrate coated with composition C2 after
conventional pyrolysis at1000 °C, 1h, N$_2$atmosphere.
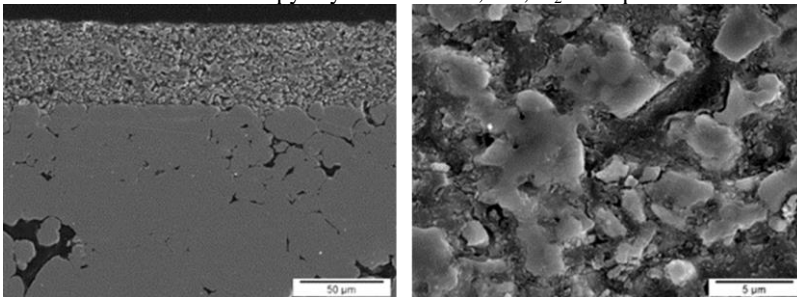
Source: Elaborated by the author

The next step was to eliminate the glass and to optimize the
amount of fillers. Then, it was developed the composition C3, based on
HTT 1800, ZrO$_2$, Si$_3$N$_4$ and BN. This composition was investigated

under temperatures between 700 ° C- 1000 °C, at nitrogen atmosphere. The SEM micrograph, Figure 21, after pyrolysis at 1000°C, shows porosity and apparently evidence of low adhesion to the coating/substrate interface. The cracks presented in the image look to be from the metallography preparation, since it was noted cracks only in few regions.

Figure 21: SEM micrograph of the substrate coated with composition C3 after conventional pyrolysis at1000 °C, 1h, N_2. In the Right, higher magnification.
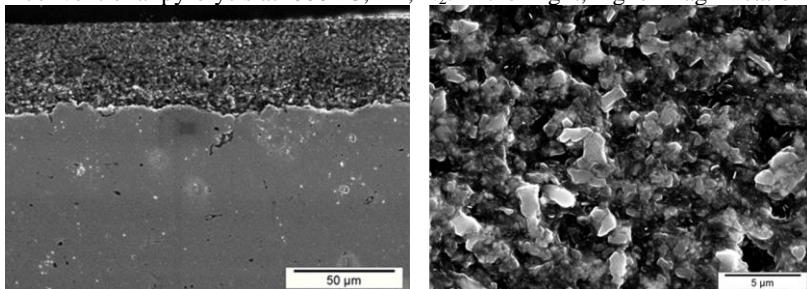
Source: Elaborated by the author

After the previous preliminary results under conventional furnace, the research of plasma assisted pyrolysis was initiated. The precursor HTT1800, with 3% DCP, was applied onto sintered substrates and pyrolyzed at 900°C, 1h holding time, at anode configuration. The SEM micrograph, from the top view, is shown in Figure 22. The EDS analysis performed in the region indicated by 1 and 2, in the left, confirm that the region 1, is mainly iron, carbon and some oxygen, probably due to the handling. Region 2 is composed by C, N, Si, O and Fe from the substrate. This region (dark color) is the formed SiCN ceramic. In the right side image, it is possible to identify better the regions (indicated by arrows) in which the formed ceramic based on SiCN delaminated and, as expected, the formed cracks due to the high shrinkage of the precursor.

Figure 22: SEM micrograph of the substrate coated (top view) with HTT 1800. PAP, anode configuration, at 900 °C, 1 h,. Signal Left: BSE, Right: SE
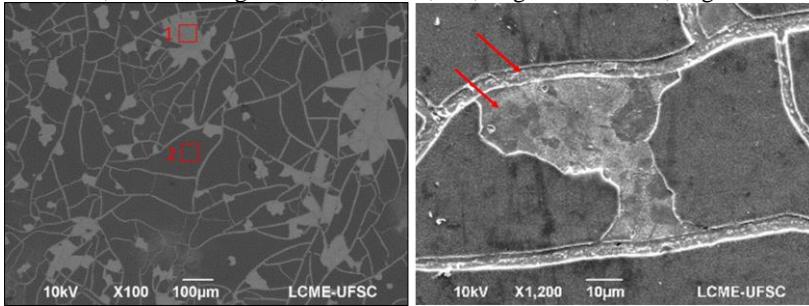
Source: Elaborated by the author

The SEM micrograph of the sintered substrate coated with composition C2 performed by PAP, at 900 °C, under 100% plasma nitrogen, using anode configuration, is shown in Figure 23. It is possible to find regions without cracks and delamination, and other with such problems, as indicated in the right side of the image.

Figure 23: SEM micrograph (cross-section) of the substrate coated with C2 after PAP, anode configuration, plasma nitrogen, at 900 °C, 1h.
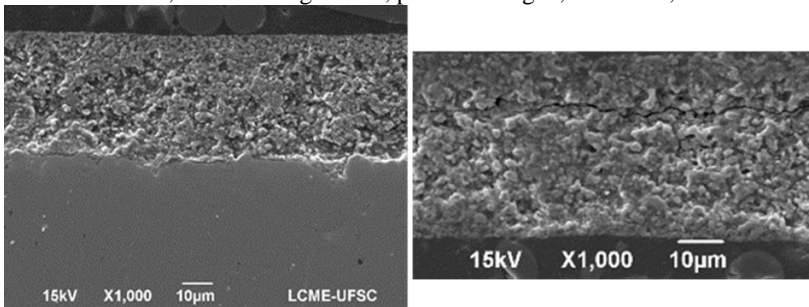
Source: Elaborated by the author

The SEM micrograph image, with high magnification, of the sample C2 after PAP and CP, at 900 °C are shown in Figure 24.

Figure 24: SEM micrograph of the substrate coated with C2 after PAP –anode-
(left) and CP(right), 900 °C.
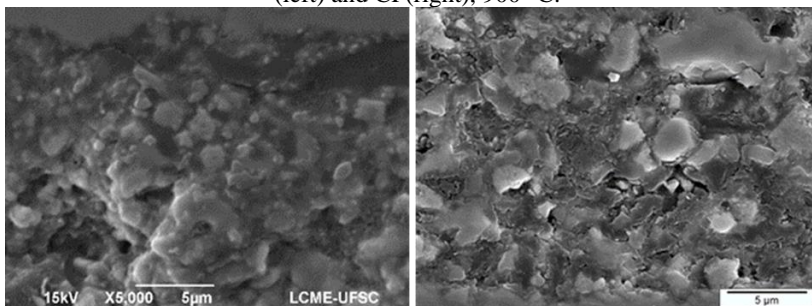
Source: Elaborated by the author

Comparing both samples, by visual analysis, the sample after PAP process formed a denser coating, with less porosity, than the sample after CP. Even comparing the coating after PAP at 900 °C, with the sample after CP at 1000 °C (Figure 20), the sample after PAP seems to be denser.

This is an indication that the PAP process can promote PDC coating with better properties, even when passive fillers are used.

5.3. PHASE 2: PLASMA ASSISTED PYROLYSIS INVESTIGATIONS.

Although the first results, from phase 1, indicated that the PAP could promote coating with superior properties, the coating compositions analyzed until that point shows a lot of porosity and many cracks due to the polymer to ceramic conversion. In order to compensate the shrinkage of the precursor during pyrolysis, and to reduce porosity and cracks, active fillers were investigated.

The results shown in this chapter were obtained with cylindrical bodies processed with only the pure HTTS and compositions of active filler loaded HTTS, and no more coatings. These type of specimens allow the understanding of the composite ceramic behavior, as explained in the methodology. The results include the influence of PAP process on the conversion of HTTS, composition investigation and the influence of PAP configuration and Temperature on the filler conversion.

5.3.1 Influence of PAP - Pyrolysis behaviour of HTTS

In order to verify the atmosphere influence on the pure precursor it were performed pyrolysis in the plasma reactor, in anode and cathode configuration, and by conventional pyrolysis, at 1000 °C, 2h.

It were performed pyrolysis in CP and PAP at anode and cathode with the same parameters (Temperature, holding time, heating rate). However, when the pyrolysis was performed at cathode configuration the sample "exploded" during treatment as shown in Figure 25. The arrows indicate the small pieces of the samples after pyrolysis. One possible explanation for this is due to the high reactivity promoted by the cathode configuration. When the sample composed with HTTS is placed on the cathode, is subjected to collisions mainly with energetic ions and fast neutrals. These bombardments promote a surface heating, that lead an increasing in the reaction kinetics preferentially at the surface, and this phenomenon could trap gaseous products inside the sample. Furthermore, the collision interactions with the gaseous products from the HTTS (CH_4, NH_3 and H_2 and oligomeric Si species (FLORES et al., 2013)) could have produced an even more reactive atmosphere, increasing, consequently, both surface heating and release of gases.

Figure 25: Picture of the sample broken during the PAP at cathode configuration.
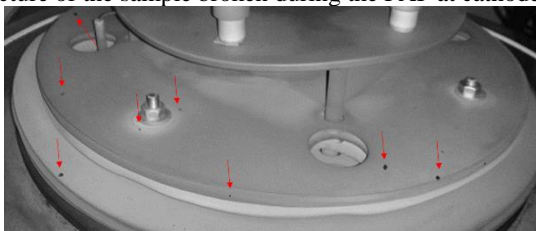
Elaborated by the author

In the region between 500 °C - 600 °C, where more gaseous products may be released, according to the TGA analysis (Figure 26), it was detected an increasing of arcs during these experiments at cathode. Based on that, it was changed the heating rate of the pyrolysis to avoid the breakdown of the sample. Thus, the heating rate applied in cathode configuration was reduced from 3 to 1.5 °C/min at the temperature range of 400 to 500 °C and to 0.5 °C/min from 500 to 700 °C. With these heating rates, the pyrolysis at cathode configuration could be

performed and the samples were intact at the end.

Aiming at having some information about the mass loss of the HTTS under plasma conditions it was performed one pyrolysis cycle at cathode configuration (PAP-C), 1000 °C, stopping the pyrolysis five times and measuring the mass of the sample. The obtained curve is shown in Figure 26, where there is also the TGA from HTTS under nitrogen atmosphere. Analyzing the curves it is noted that around 450 °C the mass change after PAP is about 5wt %, while in the TGA measurement is around only 1 wt %. This can be attributed to the high reactivity of plasma atmosphere, favoring the increases reaction kinetics, and usual phenomena such as outgassing tend to occur at lower temperatures than usual. However, in the range between 500 °C – 600 °C the curves are similar, and at 650°C both curves show the same value of mass change, around -17 wt%.

The main mass loss occurs in the range of 200 – 700 °C, when the polymer change to amorphous SiCN ceramic, promoting the evaporation of the CH_4, NH_3 and H_2 and oligomeric Si species(FLORES et al., 2013).

The measured mass loss after the PAP-C, stopping the pyrolysis, was about 18 wt%, lower than the value measured by TGA (23%).

However, when the sample was pyrolyzed in one step (without stopping the pyrolysis for weighing) the total mass change was around 20 wt%. Close to the results obtained after conventional pyrolysis (22%) and TGA (23 wt%). The lower mass change obtained (18 %) after the cycle with stops can be attributed to oxygen incorporation; since each time the cycle was stopped, to measure the sample weight, oxygen could be introduced to the reactor and to the sample due to handling.

The mass loss of HTTS pyrolyzed in anode configuration was about 23 wt%.

Figure 26: TGA of the HTTS and Mass change of the sample under PAP, at cathode configuration.
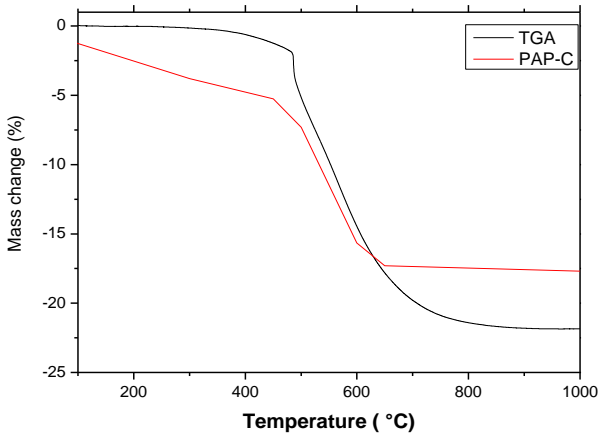
Source: Elaborated by the author and adapted from (FLORES et al., 2013)

The results of elemental analysis of HTTS after thermal treatment at 1000 ºC, for 2 h, under different conditions are shown in Table 11.

Table 11: Ceramic yield and elemental composition of HTTS after CP and PAP in anode (PAP-A) and cathode (PAP-C) configuration at 1000 °C.

Pyrolysis	Ceramic yield (%)	Elemental composition HTTS (at.%)				
		Si	C	N	O	H
CP	79.2	35.4	29.3	31.5	3.7	< 0.1
PAP-A	78.1	35.3	29.1	31.9	3.8	0.1
PAP-C	80.3	32.8	31.1	27.4	8.7	< 0.1

Source: Seifert et al, 2016

The results indicated that the ceramic yield is unaffected by the treatment, as the results are around 80% yield, in accordance with literature (SEIFERT et al., 2014). The chemical composition (measured by analytical methods) of the sample after CP (conventional pyrolysis process) and PAP-A (Plasma Assisted Pyrolysis – sample on anode) are identical, while the chemical composition after PAP-C (plasma Assisted Pyrolysis sample on cathode) is still comparable, featuring however

small differences. For example, the treatment at PAP-C shows an increased amount of oxygen, while nitrogen and silicon amount declines. This difference can be resulted from the incorporation of oxygen while handling.

These results indicated that there is no depolymerization effects or decomposition of the precursor during pyrolysis at abnormal glow discharge conditions.

The XRD patterns of the HTTS after CP and PAP, at 1000 °C under nitrogen flow, are shown in Figure 27.

Figure 27: XRD patterns of the HTTS after conventional pyrolysis (CP) and in Plasma atmosphere with anode (PAP-A) and cathode (PAP-C) configuration, 1000 °C.
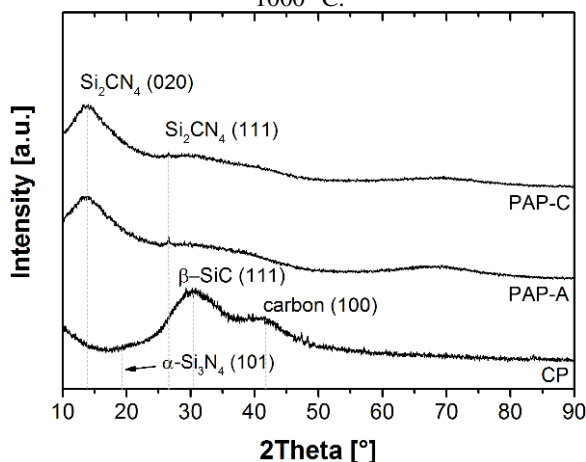
Source: Seifert et al, 2016

The diffraction patterns of the sample after CP shows only broad peaks, suggesting that the sample is amorphous with a small rearrangement, characteristic of the formed PDC. Mocaer et al. (1993) investigated an organosilazane containing methyl and secondary amino groups. They suggest that some local atomic rearrangements occur in the solid which, however, remains amorphous up to about 1200°C. They detected the characteristic peak of β-SiC and carbon formed at temperatures between 1100 °C and 1300 °C at the same 2θ range. The weak second peak can be attributed to a graphitic structure which is formed during pyrolysis of carbon rich polyorganosilazanes (STÖRMER; KLEEBE; ZIEGLER, 2007). Monthioux and Delverdier (MONTHIOUX; DELVERDIER, 1996) studied the crystallization

behavior of various PDCs. They reported a local crystallization within the ternary Si–C–N systems was observed at 1100 °C, where the nucleation of the excess free carbon phase is always the first crystallization event to occur, followed by the nucleation of SiC.

The XRD-patterns of the samples after PAP showed one broad peak in the range of 10° to 20° 2θ and a second flat peak in the range from 25° to 30° 2θ, characteristic of Si_2CN_4 nanocrystallites firstly reported by Riedel et al (1997). This phase occurred after pyrolysis of polyorganosilylcarbodiimides in inert atmosphere at temperatures up to 1000 °C. The Si_2CN_4 structure consists of layers of condensed SiN_4 tetrahedrons and results from the decomposition of SiC_2N_4 environments in the temperature range from 920 to 1000 °C.

In general, precursor systems like HTTS are composed of mixed SiC_xN_y (x + y = 4) tetrahedral units as well as SiC_4-units and a free carbon phase after pyrolysis at 1000 °C in inert atmosphere (STÖRMER; KLEEBE; ZIEGLER, 2007). Thereby the amount of the free carbon phase and the mixed tetrahedral units strongly depend on the molecular architecture of the used precursor. In the same way, the ceramics decomposition and crystallization correlate to the chemical composition, architecture and chemical homogeneity of the amorphous SiCN network.

During the PAP process the sample is also treated with reactive species, as ions and electrons, which should influence the cross-linking and pyrolysis behavior of the precursor. The XRD measurements revealed the formation of Si_2CN_4 nano-crystallites for the samples treated in anode and cathode configuration. An explanation of this phenomenon is given by the temporal variation of the plasma potential caused by the use of a pulsed voltage source. The literature relies on the fact that when the cathode voltage is suddenly changed from 500 V to ground (0 V) there is an abrupt collapse of the plasma, and the charged species cannot redistribute themselves instantaneously. In this case, during Ton the sample surface in cathode configuration is bombarded mainly with fast neutrals and high-energy ions. During Toff electrons are redirected to the sample/cathode due to an abrupt change of the boundary conditions of the discharge. Whereas in anode configuration, during Ton, the sample is bombarded mainly with fast secondary electrons from the cathode with an average energy that can be equivalent to the sheath voltage, slow energetic electrons from the luminescent region (2 to 8 eV) and ions with energy <10 eV. However during Toff it is believed that in the first microseconds of the off pulse high-energy ion bombardment of the discharge anode is also possible

(BUDTZ-JØRGENSEN; BØTTIGER; KRINGHØJ, 2001)(CHAPMAN, 1980).

Based on that it is possible that during PAP the structural rearrangement processes within the amorphous SiCN network are strongly influenced by the nitrogen ions interacting with the sample leading to a shift towards formation of nitrogen rich phases in comparison to conventional pyrolysis. However, it is not possible to disregard the effect of the electrons. Specially because, as reported in the literature, the treatment of carbon rich polyorganosilazanes and polycarbosilazanes with high energetic electron irradiation leads to an increase in the degree of crosslinking (SUGIMOTO et al., 1995)(OKAMURA; SEGUCHI, 1992)(KOKOTT; MOTZ, 2007). Therefore, the results show that further investigations are necessary to clarify the influence of PAP on the pyrolysis processes of organosilazanes in detail.

5.3.2 Composition Investigations

First, different compositions, including type of fillers and amount between filler and precursors were investigated. The choice of Ti, TiB_2, $TiSi_2$ and B as active fillers was based on the literature and previous results. These indicates that those fillers are potential active filler due to the fact that they can react with the nitrogen atmosphere and/or with the products from precursor gases decomposition; or even, they can react with the ceramic amorphous phase SiCN, minimizing the shrinkage and forming phases as TiN, TiC, Ti (C,N) or Si_3N_4.

The TGA measurement of these fillers, under nitrogen, are shown in Figure 28.

Figure 28: TGA for the active fillers: B, Ti, $TiSi_2$ and TiB_2.
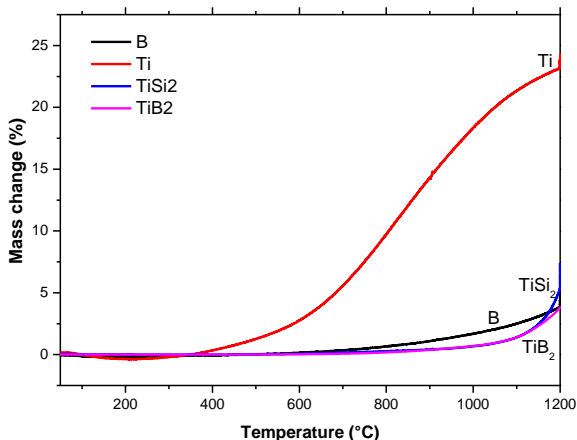
Source: Elaborated by the author

Observing the mass gain during the TGA measurement it is possible to have information about the filler conversion under nitrogen atmosphere. The term filler conversion in this work is used to refer the ability of the filler to form phases, accompanied by the volume expansion, in order to reduce porosity and compensate the shrinkage of the samples and coatings. Among the investigated fillers Ti has the highest mass gain (around 23 wt%) under nitrogen atmosphere. The chemical reaction of Ti starts at low temperature, around 400 °C, resulting in higher conversion. The expected nitriding of elemental Ti occurs by the reaction Ti+N →TiN.

In the first approach Ti, B and $TiSi_2$ were used as the active filler and SiC and Si_3N_4 as passive fillers. The investigated compositions are shown in Table 12. It was also shown the results of the pure HTTS in order to compare some of them.

Table 12: Coating Compositions- Phase 2

Name Composition	System	Composition (Vol%)
C4	HTTS-Ti-Si_3N_4	34 - 26 - 40
C5	HTTS-Ti-SiC	55 - 14 - 31
C6	HTTS-B-$TiSi_2$	55 - 10 - 35
C7	HTTS- $TiSi_2$	40 - 60
	HTTS	100

Source: Elaborated by the author

The volume and mass change of the samples after pyrolysis, at 1000 °C, 2h, after PAP at anode configuration, is shown in Figure 29.

Figure 29: Volume and Mass change for the investigated compositions and HTTS after PAP-A, at 1000 °C.
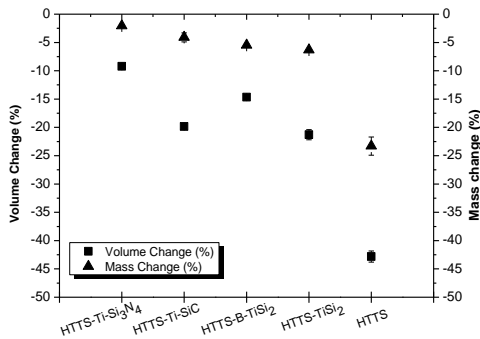
Source: Elaborated by the author

The precursor has shrinkage of about 45 vol %, and 23 wt% mass change. The shrinkage of the filled HTTS, after PAP-A, varied between around 10 to 20 vol% and the mass change between 2 to 5 wt%. Since these differences are related to the amount of filler and precursor, and to the expansion of the active filler as well as to the plasma atmosphere acting specifically at the sample surface, only this information of volume and mass change is not appropriate to select the composition coating for further PAP investigation. Thus, the formed phases were investigated by XRD.

Among the compositions investigated, the composite based on HTTS/TiSi$_2$ (C7) shows a great conversion potential under plasma atmosphere. The XRD patterns of the coating based on HTTS/TiSi$_2$ after CP and PAP at anode configuration, at 1000 °C, 2h, are shown in Figure 30.

Figure 30:XRD patterns of the coating based on HTTS/TiSi$_2$(C7) after CP and PAP at anode configuration (PAP-A). 1000 °C, N$_2$, 2h.
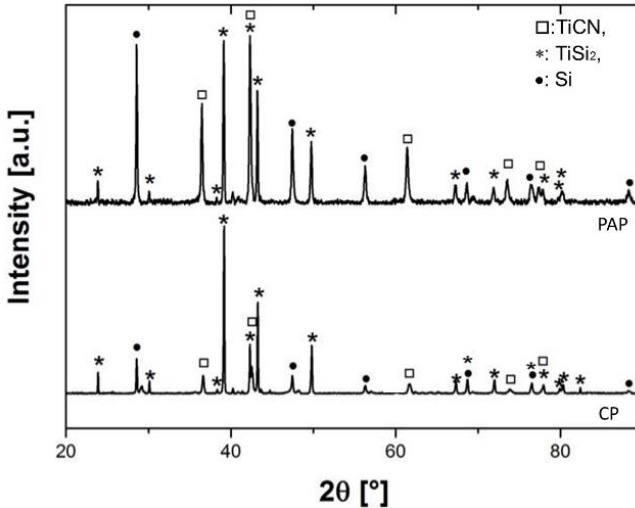
Source: Seifert et al, 2016

Although the detected phase are the same in both process, it is noted that the peaks of Si and TiC$_x$N$_y$ are much more evident after PAP process, a strong evidence that the filler conversion is higher during PAP. Further investigation was done with this composition.

5.3.3 Influence of pyrolysis process, PAP configuration and Temperature

After choosing a potential composition based on HTTS/TiSi$_2$ the filler amount was optimized to reduce the porosity. Therefore the composition C7 was optimized, and the composition investigated from this point on has the composition of 70 vol% TiSi$_2$ and 30 vol.% HTTS (Composition C8). It was performed conventional pyrolysis and plasma assisted pyrolysis. The PAP were performed in both reactor configuration, sample acting as cathode and as anode, in order to c]omprehend the conversion behavior of the filler in dependency on the specimens interacting with the sample surface. The pyrolysis temperature were 900°C, 1000 °C and 1150 °C.

Figure 31 shows the SEM micrograph of the sample after conventional pyrolysis (CP) and after PAP in anode configuration (PAP-A), at 1150 °C for 2 h.

Figure 31: SEM micrograph of the HTTS/TiSi$_2$sample conventionally pyrolyzed at 1150 ℃ for 2 h (CP) and after PAP-A at 1150 ℃ for 2 h
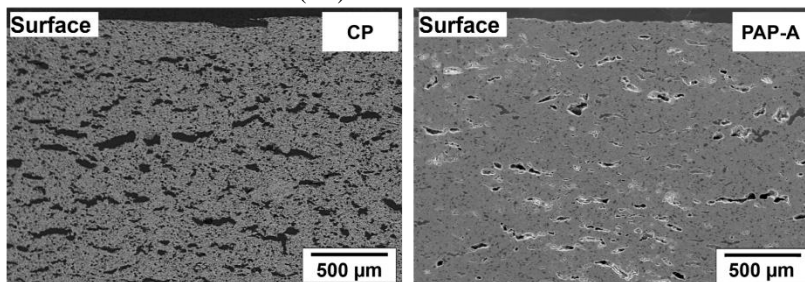
Source: Seifert et al, 2016

The SEM images reveal the formation of mainly elongated pores with a diameter of up to 200 μm after both processes. However, the sample pyrolyzed in anode configuration shows less porosity. Using the binary images of the SEM pictures the porosity was estimated in 27.7 % during CP, and 21 % for the samples treated under PAP-A. In contrast, the samples treated in cathode configuration (Figure 32) reveal an almost dense and homogenous microstructure and it seems that only closed porosity is formed. At cathode configuration even the pyrolysis at 900 ℃ (Figure 32) is sufficient to enhance the densification of the samples compared to CP or PAP-A. The porosity value estimated by image analysis is smaller than 2 %.

Figure 32: SEM micrograph of a TiSi$_2$/HTTS (70/30 vol.%) sample after PAP at 900 °C and 1150 ℃ for 2 h in cathode configuration
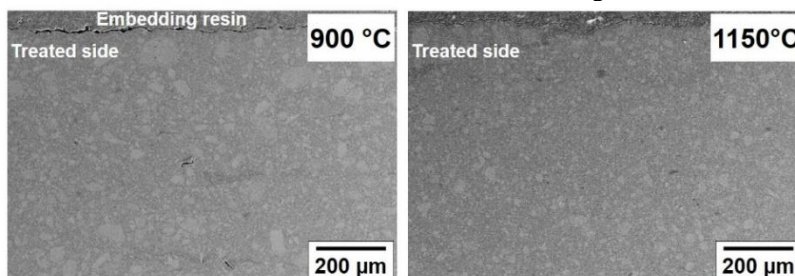
Source: Seifert et al, 2016

The porosity values can be correlated with the densities of the composite materials determined with He-pycnometry (closed porosity is neglected). While the densities of samples resulting from conventional

pyrolysis and PAP-A at 1150 °C for 2 h revealed values of $\rho_{CP} = 2.5$ g/cm³ and $\rho_{PAP-A} = 2.4 \pm 0.1$ g/cm³, respectively, the density of the samples treated in cathode configuration is higher, in the range of 2.9 ± 0.1 g/cm³.

Figure 33 shows the SEM micrographs of the samples which were pyrolyzed in a conventional furnace (A) and after PAP in cathode configuration (B), at 1150 °C for 2 h. The microstructure of the CP sample exhibits a network of interconnected $TiSi_2$ filler particles with a core-shell structure. Preliminary results on Niobium particle loaded PSZ showed, that these structures are formed during solid–solid reactions of the amorphous SiCN matrix and the active filler at temperatures exceeding 1000 °C(SEIFERT et al., 2014).

EDS analysis of certain spots (marked with arrows in Figure 33a, in the left) in combination with the XRD results (shown in the sequence) prooved, that the shell is composed of titanium carbonitride phases and elemental Si, while unreacted $TiSi_2$ forms at the particle core. Also a remarkable amount of porosity is visible which is formed due to the shrinkage of the precursor during pyrolysis and the insufficient conversion of the active filler particles.

In contrast, the microstructure of the sample after PAP-C (Figure 33 b) appears blurred with no distinct reaction zone, core-shell structure or porosity. The dark spots (indicated as Si) are corresponding mainly to elemental Si, as shown by the EDS analysis in Figure 34.

Figure 33: SEM micrograph of the samples after CP(a) and PAP (b), at 1150 ºC for 2 h
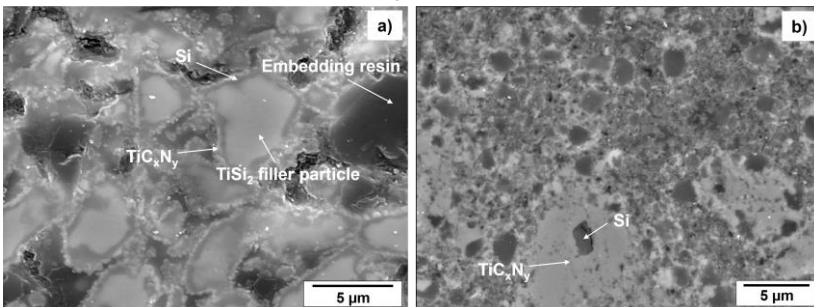
Source: Seifert et al, 2016

Figure 34: EDS analysis of the sample (dark spots) after PAP – C at 1150°C.
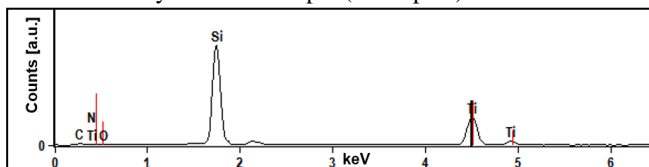
Source: Elaborated by the author

In order to investigate the elemental distribution after PAP at cathode configuration, element maps were derived using EDS analysis (Figure 35). Beside smaller regions which consist mainly of elemental Si, the homogenous distribution of the elements is an indication of a transformation of the filler particles under the reactive plasma conditions. The surface of the samples reveal a dense layer of about 1 μm in thickness. The elemental maps shows that this layer is enriched with silicon and nitrogen. This is supposed to be an effect of the sputtering, where atoms sputtered from the surface substrate/coating can react with activated nitrogen atoms in the plasma atmosphere forming nitrides (RIE, 1999). Due to condensation and dissociation of the formed nitrides at the sample surface a diffusion front is formed which enables nitrogen diffusion inside of the treated material. In addition, Rie and Lampe (RIE; LAMPE, 1985) demonstrated in their work that beside ion bombardment and reactive sputtering during nitriding of titanium and titanium alloys with low energy nitrogen ions also chemisorption of the nitrogen on the surface has a significant influence on the nitride layer formation. The adsorbed particle can be sputtered off, stay bonded to the surface or dissociate further. Besides it the nitrogen chemisorption is enhanced by the ion bombardment (LUGMAIR et al., 2004) due to the fact that the presence of reactive species on the surface can provide enough energy for the chemisorption of nitrogen process (LAMPE; EISENBERG; LAUDIEN, 1993).

Rolinski and Karpinkwki (apud LAMPE; EISENBERG; LAUDIEN, 1993)have proposed a model to describe the plasma nitriding where the layer formation mechanism depends on the Gibbs energy. They stated that on the one hand chemisorption of nitrogen becomes an important mechanism for metals like titanium with a high negative Gibbs energy(-528 KJ/mol at 1150 °C (XIONG et al., 2010)). On the other hand, metals with smaller or positive Gibbs energy like silicon, ion bombardment and reactive sputtering have a significant influence on the nitride layer formation. Eisenberg (apud LAMPE;

EISENBERG; LAUDIEN, 1993) shows that activation of nitrogen promotes an accelerated layer formation and when, in addition, there is sputtering of titanium from the work piece surface condensed titanium nitrides are found on the surface. Based on the facts it is supposed that a thin layer of silicon nitride is formed at the samples surface, which can enhance the nitrogen diffusion inside of the composite material and therefore increase the filler conversion.

Figure 35: Elemental distribution of Ti, Si and N within the plasma treated surface after PAP-C at 1150 ºC for 2 h in cathode configuration
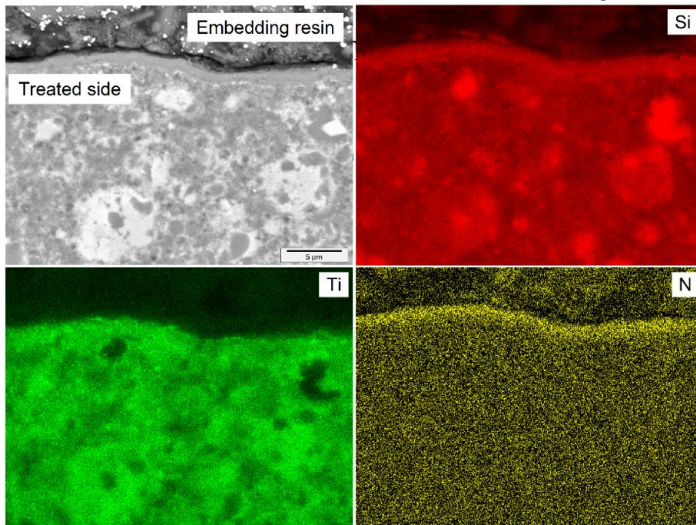
Source: Seifert et al, 2016

The X-ray patterns of the samples obtained after conventional pyrolysis at different temperatures under nitrogen atmosphere is show in Figure 36. Up to a pyrolysis temperature of 900 °C in the conventional furnace only $TiSi_2$ could be detected with XRD suggesting neither reactions of the $TiSi_2$ filler particles with the amorphous SiCN matrix nor with nitrogen from the pyrolysis atmosphere. This correlates with observations reported in the literature (TORREY; BORDIA, 2008) where $TiSi_2$ exhibits insufficient reactions with nitrogen below temperatures of 1000 °C. Increasing the pyrolysis temperature to 1000 °C enhanced formation of carbonitride phase and an increased amount of elemental Si accompanied by a reduction of the $TiSi_2$ phase. The formation of a cubic TiC_xN_y phase, with lattice parameter of a = 4.25 Å, close to the composition $TiC_{0.4}N_{0.6}$ could be detected. After CP at 1150

°C, for 2 h, there are the same phases, Si, TiC_xN_y and $TiSi_2$. The amount of unreacted $TiSi_2$ determined with quantitative Rietveld refinement, at 1150 °C, is about 60 wt.%.

Figure 36: XRD pattern of the $TiSi_2$/HTTS samples, after CP in different temperatures for 2h (●Si, □ TiC_xN_y *$TiSi_2$)
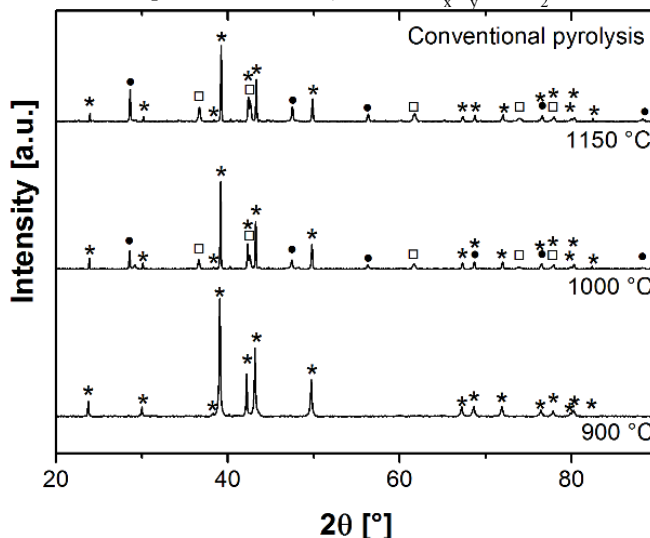
Source: Seifert et al, 2016

The XRD pattern of the samples after PAP-A (on anode), is show in Figure 37.

After treatment in anode configuration at 900 °C the formation of TiC_xN_y, with a lattice parameter of a = 4.27 Å beside elemental Si could be detected. As well as for conventional pyrolysis, the diffraction patterns show that an increase in the pyrolysis temperature to 1000 °C leads to an enhances formation of carbonitride phase and an increased amount of elemental Si accompanied by a reduction of the $TiSi_2$ phase. This correlates with the fact that Si is the main reaction product assuming partial conversion of the $TiSi_2$ phase during nitriding reaction, by the equation 3 (SAMBASIVAN; PETUSKEY, 1994). The TiC_xN_y phase formed during PAP-A is close to a composition of $TiC_{0.33}N_{0.67}$ (CÓRDOBA et al., 2005).

$$TiSi_2 + N \rightarrow TiN + 2Si$$ (Eq. 03)

Figure 37:XRD pattern of the TiSi$_2$/HTTS samples, after PAP (anode) in different temperatures for 2h (●Si, □ TiC$_x$N$_y$, *TiSi$_2$)
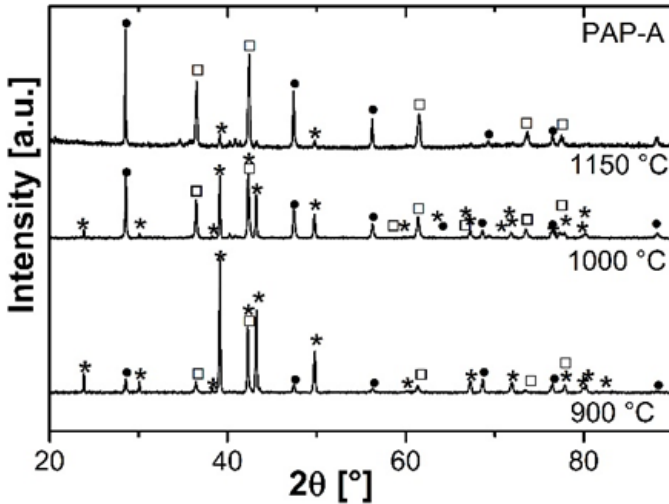
Source: Seifert et al, 2016

After pyrolysis at 1150 °C, PAP-A, 2 h, the amount of residual filler phase, TiSi$_2$, is about only 6.7 wt.% (R$_{wp}$=12.1, GOF=3). Amounts of 47.4 and 36.4 wt.% were determined for elemental Si and Ti(C,N) respectively. An increase of the annealing time from 2 to 5 h at 1150 °C resulted in the same phase composition for both treatments. After annealing for 5 h no differences in the ratios of the peak intensities or in the peak positions could be detected.

In anode configuration, mainly high energetic electrons interact with the specimen surface while nitrogen ions with a very low energy reach the sample. However, as already mentioned, it is also possible that high energy ions, in a small amount and lower energy compared to the cathode, are also reaching the sample at anode during the Toff. Due to this fact the filler conversion and/or the pyrolysis behavior of the precursor ought to be seen as a treatment under reduced nitrogen pressure at PAP-A, however promoting higher filler particles conversion due to the presence of such reactive species.

It is assumed that the formation of the Ti(C,N) during PAP-A and CP can be attributed to both, the reaction of TiSi$_2$ filler particles with nitrogen coming from the pyrolysis atmosphere and with fine distributed carbon within the SiCN matrix .

The diffraction patterns of the samples treated at 900 °C, 1000

°C and 1150°C at PAP-Cathode, are show in Figure 38.

The XRD pattern at 900 °C are comparable to those obtained from PAP-A. Some differences could be observed at 1000 °C in comparison to the X-ray pattern of PAP-A. The ratio of the intensities of TiSi$_2$ and elemental Si of the pattern of PAP-C reveals that the amount of residual TiSi$_2$ at the specimen surface is increased while the Si amount declines. It were detected the same phases as the sample after PAP at anode configuration, at 1000 °C, however additionally it were also formed the phases TiC and α-Ti. At higher temperatures, TiC is more likely to be formed by further reaction of α-Ti with free carbon originating from the amorphous ceramic network.

Figure 38:XRD pattern of the samples, after PAP (cathode) in different temperatures for 2h. (●Si, □ TiC$_x$N$_y$ *TiSi$_2$, ∇Ti$_5$Si$_3$, ♦Si$_3$N$_4$, ○TiC, α-Ti)
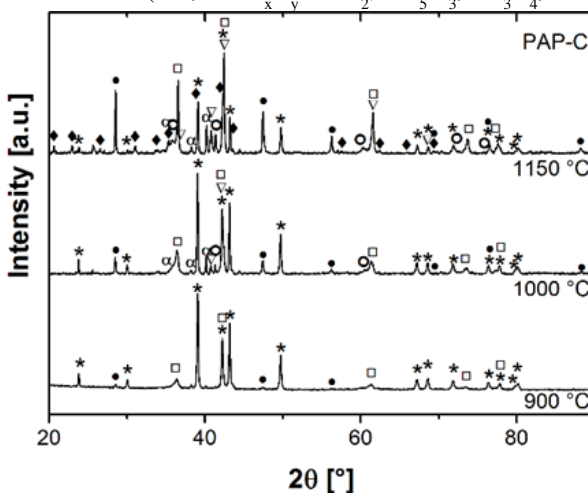
Source: Seifert et al, 2016

After treating the samples at 1150 °C, PAP-A, in the plasma atmosphere the formation of mixed α- and β-Si$_3$N$_4$ could be detected with an amount of 11.1 wt.% (R_{wp} = 13.3, GOF = 1.9). According to the literature nitriding of Si to α-Si$_3$N$_4$ starts at T > 1300 °C and of β-Si$_3$N$_4$ at T > 1350 °C. Also rapid nitriding of the Si grain-core starts at these temperatures leading to a mixture of α-Si$_3$N$_4$ and β-Si$_3$N$_4$(MACKENZIE et al., 1999).

Additionally, Rietveld refinement revealed an amount for TiC$_x$N$_{(x-1)}$ of 28.7 wt.%. The lattice parameter of this cubic phase is a = 4.26 Å. An increase in annealing time to 5 h resulted in an increase in

the amount of carbonitride phase to 29.9 wt.% as well as of the Si_3N_4 phases (17.9 wt.%) while the amount of $TiSi_2$ declined to 6.2 wt.%. The existence of α-Ti could not be proofed by XRD analysis. These results lead to the assumption that the filler conversion is not completed after plasma treatment for 2 h.

During treatment of the $TiSi_2$/HTTS specimens in cathode configuration atomic nitrogen coming from the glow region is accelerated towards the cathode and induce a bombardment of the sample surface. As it is reported in the literature ion bombardment with low average energies up to 100 eV lead to an increased defect density in metals (ELTOUKHY; GREENE, 1980), promoting the enhancement of the nitrogen diffusion. As a result, it is assumed the formation of a mixture of α-Si_3N_4 and β-Si_3N_4 already at a temperature of 1150 °C and the increased filler conversion (reaction of Ti and Si).

The following equations (Eq. 4 and Eq. 5) summarize the major reactions, which are likely to occur at the $TiSi_2$-SiCN interface during treatment in cathode configuration at temperatures up to 1150 °C.

$$2TiSi_2 + (4 + 2y)N \rightarrow 2TiN_y + Si_3N_4 + Si \qquad \text{(Eq. 04)}$$
$$TiN_y + C_x \rightarrow TiC_xN_y \qquad \text{(Eq. 05)}$$
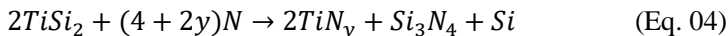
Table 13 summarize the formed phases at the different pyrolysis processes and temperatures. In summary, it can be noted that PAP in cathode configuration enhances the filler conversion by forming multiple nitride, carbonitride and silicide phases, correlating with the blurred appearance of the microstructure (Figure 33b). Based on the principles of active filler controlled pyrolysis (AFCOP)(GREIL, 1995a), the formed phases should compensate the shrinkage of the polymer and reduce the porosity. Thus, supporting the densification of the composite materials after PAP.

The difference between the samples pyrolyzed in both configuration it is assumed to be due to the specimens interacting with the sample surface. While in anode configuration high energetic electrons and nitrogen ions with a very low energy interact with the specimen surface, in cathode configuration atomic nitrogen coming from the glow region are accelerated towards the cathode and bombard the sample surface. This bombardment enhances the nitrogen diffusion and consequently higher filler conversion. It should also highlighted that the pyrolysis under these more reactive conditions, at cathode, leads to enhances reactions between the active filler and the atmosphere as

well as with the amorphous SiCN network.

Table 13: Detected phases after pyrolysis at different temperature and process

Temperature (°C)	Phases CP	Phases PAP -Anode	Phases PAP -Cathode
900	$TiSi_2$	$TiSi_2$, Si, TiC_xN_y	$TiSi_2$, Si, TiC_xN_y
1000	$TiSi_2$,Si, TiC_xN_y	$TiSi_2$, Si, TiC_xN_y	$TiSi_2$, Si, TiC_xN_y TiC, α-Ti
1150	$TiSi_2$,Si, TiC_xN_y	$TiSi_2$, Si, TiC_xN_y	$TiSi_2$, Si, TiC_xN_y TiC, α-Ti, Ti_5Si_3, Si_3N_4,

Source: Elaborated by the author

5.4. PHASE 3: PLASMA ASSISTED PYROLYSIS OF PDC COATINGS ON SINTERED STEELS.

After the previous step, with further understanding about the behavior of the PDC composite under PAP, specifically the influence of the reactor configuration, the research was conducted with PDC coatings on sintered steel substrates (95.9 %Fe + 1.5%Mo + 2.0%Ni + 0.6%C wt%). Based on the results obtained in both reactor configurations from this point on the pyrolysis were always performed with the sample as cathode, aiming the highest filler conversion and formation of new phases.

5.4.1 Coating composition

First, two different compositions were used, i.e., the composition C9 based on the active filler investigated in the last step ($TiSi_2$) and one composition based on both active and passive fillers ($TiSi_2/Si_3N_4$). The coating thickness influence after pyrolysis was investigated. In the sequence of the research the active filler TiB_2 was also investigated.

Table 14 shows the composition, the measured coating thickness and the pictures of the sample after pyrolysis at 1150 °C, at cathode configuration, 2 h holding time.

Table 14: Pictures of the sample after pyrolysis at 1150 °C, at cathode, 2 h.

Composition	Measured Coating Thickness (µm)		
	~ 50 - 60	~ 40 - 50	~ 10 - 20
C9 TiSi$_2$/HTT1800 70/30 Vol %			
C10 TiSi$_2$/Si$_3$N$_4$/HTT1800 60/10/30 Vol %			

Source: Elaborated by the author

For these two compositions, the maximum coating thickness after pyrolysis should be around 50 µm, for coating thicker than 50µm the coating delaminated, as shown by the pictures after pyrolysis. However, it is known that changing the coating system, type of filler, as well as the amount of them, this behavior can be completely different.

The XRD patterns of the samples are shown in Figure 39. Analyzing the XRD pattern it is observed that no crystalline residual TiSi$_2$ filler phase could be detected. The formed phases are based on the system Ti(C, N) and iron silicide. The coating with highest thickness revealed the formation of Fe$_3$Si, while the reduction of the coating thickness resulted in the formation of FeSi. It is also noted that the reduction of the thickness resulted in the formation of FeSi beside Ti(C,N) phases. The observed differences in the formed phases, in accordance with thickness, are an indicative that the diffusion phenomena between coating and steel substrate has great influence on the formed phases. This is also highlighted comparing XRD result from the sample with composition TiSi$_2$/HTTS without substrate (Figure 38) with the XRD result from Figure 39, where composition TiSi$_2$/HTT1800 was applyed on the sintered substrate. The formed phases ares different due to the elements diffusion between coating and substrate. The microstructure of the coating with composition C9 (TiSi$_2$ /HTT1800), thickness in the range of 40 – 50 µm, and the elemental distribution of iron, silicon, molybdenum and titanium are shown in Figure 40.

Figure 39: XRD pattern of the samples based on $TiSi_2/Si_3N_4/HTT1800$ and $TiSi_2/HTT1800$, after PAP (cathode) at 1150 °C, 2h.
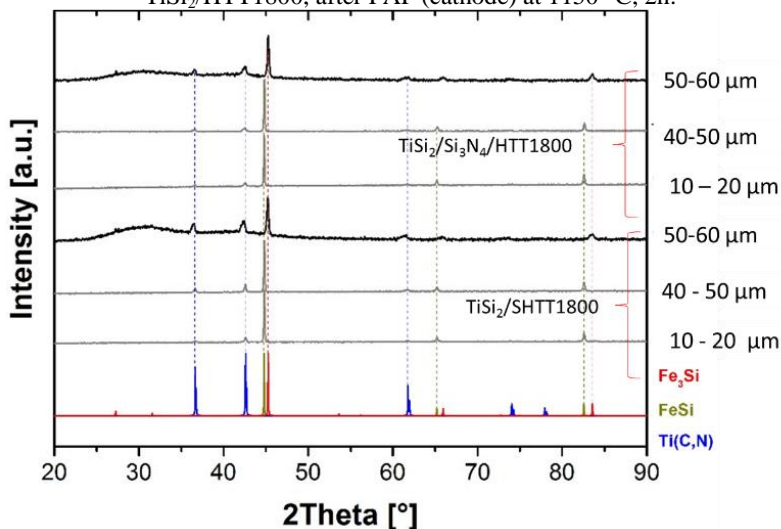
Source: Elaborated by the author

Figure 40: SEM micrograph of the $TiSi_2/HTT1800$ coating on sintered steel after PAP, at 1150 °C, 2h and the Elemental distribution of the Mo, Si, Fe and Ti.
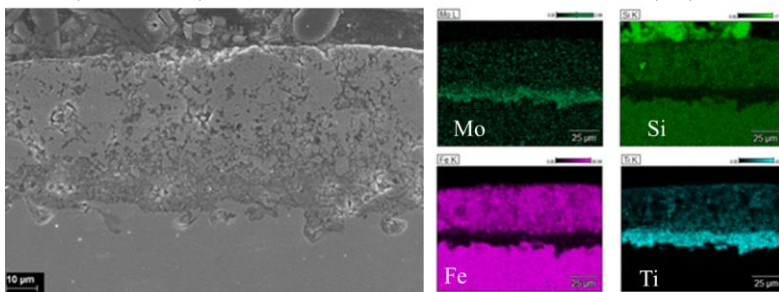
Source: Elaborated by the author

It is observed a dense, crack free and apparently well adherent coating on the sintered substrate. The elemental maps distribution shows that the $TiSi_2$ decomposed during reaction, confirming the results obtained by XRD. It is noted high iron diffusion into the coating and a distinct interlayer between the coating and the substrate. This interlayer is based on Ti and Mo, without the presence of Fe and Si, as shown in the elemental distribution. Further experiments and characterization

should be necessary to explain the formed interlayer.

Another investigated coating composition is based on TiB_2 as active filler. The composition, C11, is composed of 30 vol % HTT1800 and 70 vol% TiB_2. Figure 41 shows the SEM of the transversal section coating on the sintered substrate after PAP, at 1150 °C, 2h holding time.

Figure 41: SEM micrograph (right side BSE and left SE) of the TiB_2/HTT1800 coating after PAP, at 1150 °C, 2h.
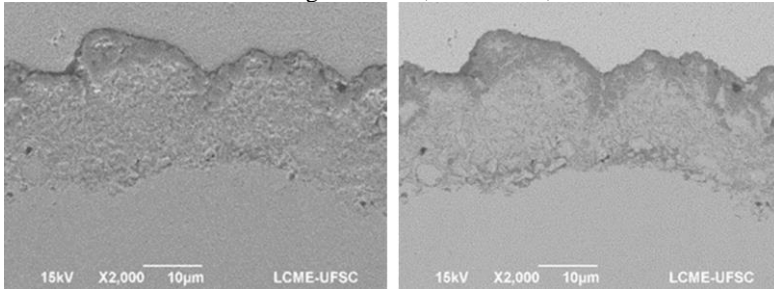
Source: Elaborated by the author

XRD was performed at this sample, and mainly phases based on TiC, TiC_xN_y, TiN and iron based phases were identified, as shown and described in the sequence.

Analyzing the formed phases of the different compositions investigated, it is concluded that the composition with TiB_2 particle as active filler shows the formation of desired phases, as well as a higher number of phases after PAP at 1150 °C. These are some indicatives that the TiB_2 is a potential active filler to continuous investigating the plasma assisted pyrolysis process. Therefore, the sequence of research was conducted with the composition TiB_2/HTT1800 (70/30 Vol %).

5.4.2 TiB_2 particle as active filler

In order to demonstrate the improved conversion of TiB_2 under plasma assisted pyrolysis, experiments were also carried out by conventional pyrolysis. The phase transformations and microstructural changes as a function of the pyrolysis conditions were evaluated. Microstructure and phase evolution of the coatings were also examined as a function of pyrolysis temperature.

Scanning electron microscope was used to investigate the microstructure of the coating systems.   Figure 42 shows SEM micrographs of the cross section of the sample after pyrolysis under nitrogen, at conventional furnace and after PAP. They were both

pyrolyzed at 1000°C, 2 h holding time. In both cases no delamination or cracks in the ceramic coating have been observed. Although it is possible to identify in both processes the unreacted filler particles, some small differences can be observed between the microstructures. The sample after PAP seems to be denser, while the sample after CP shows more porous. In spite of the similar coating microstructures, the substrate shows a pronounced difference close to the interface after PAP process. In the 5.4.4 a discussion about it is carried out.

It is also important to mention that the main difference between the coating thicknesses is due to the coating application process, which was manually done by spray.

Figure 42: SEM micrograph of the samples, cross section, after CP (left) and PAP (right), at 1000 °C, 2h.
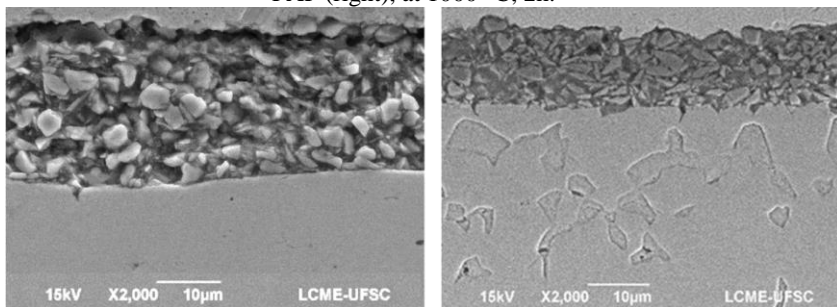
Source: Elaborated by the author

The EDS analysis are shown in Figure 43 for CP and in Figure 44 for PAP.

Figure 43: Maps distribution of the elements after CP, 1000 °C, 2h.
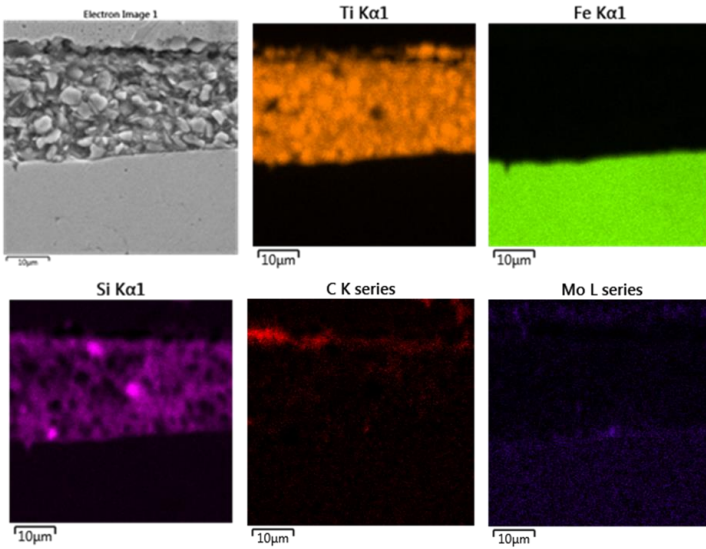
Source: Elaborated by the author

Figure 44: Maps distribution of the elements after PAP, 1000 °C, 2h.
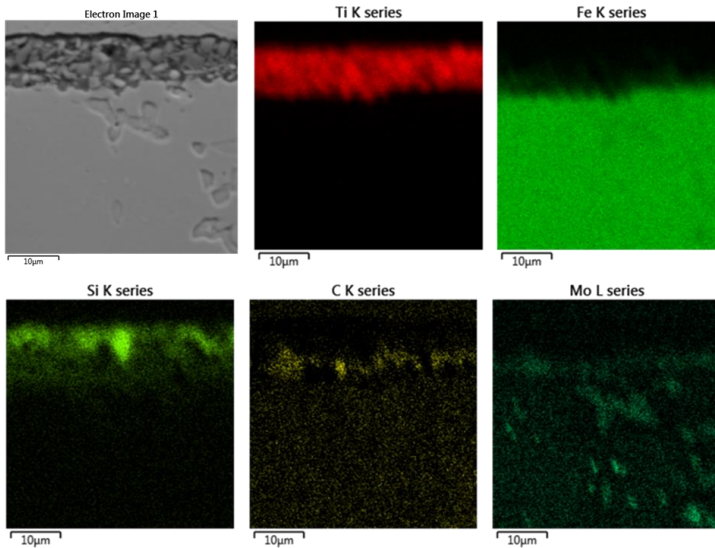
Source: Elaborated by the author

In both processes, CP and PAP, the EDS analysis evidence the presence of the TiB_2 particles, by the distribution of titanium. However, the titanium map distribution after CP shows that the presence of TiB_2 particles is more evident by smaller regions consisting mainly of Ti where the TiB_2 particles are clearer and well defined, while the titanium map after PAP process is more blurred, suggesting that the reactions to form new phases started. Another difference is noted in the Silicon map distribution. After CP, silicon is well distributed in the coating, while after PAP there is a concentration closer to the surface. It is also observed that after PAP process there is a concentration increase of carbon and molybdenum at the interface, and that iron shows a blurred boundary between coating and substrate. This indicates that iron is diffusing from substrate to the coating and that, at the interface, a diffusion layer is formed. The presence of diffusion between coating and substrate indicates a possible strong chemical bonding between the steel and the coating (TORREY; BORDIA, 2008). In comparison, the sample after the conventional process shows the Fe boundary between coating and substrate well delimited, and there is no molybdenum at the coating, suggesting that the diffusion between substrate and coating is smaller at this condition.

To follow the difference between both processes it was also analyzed the top view (surface) of the coatings. Field emission scanning electron microscopy (FEG-SEM) was performed on the surface of the coating after CP and PAP, at 1000 °C, 2 h holding time. These images are shown in Figure 45.

Figure 45: FEG-SEM image of the coating surface, top view, after CP (left) and PAP (right), at 1000 °C, 2h.
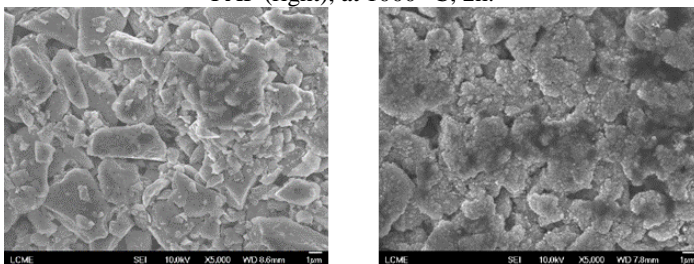
Source: Elaborated by the author

It is possible to note that the coating surface shows high roughness for both processes. After PAP the coating seems to begin a coalescence behavior.

In order to investigate the crystalline formed phases, at 1000 °C, according to the used pyrolysis process, XRD experiments were performed at the surface of the coatings. The X-ray patterns of the samples before pyrolysis, in order to compare, and after PAP and CP process at 1000 °C are shown in Figure 46.

Before pyrolysis, as expected, only the phase TiB_2 (ICSD – 78848) could be detected, since the polymer precursor phase is amorphous. It was also found Fe, indicating that the X-ray penetration depth is reaching the substrate; in this case, the deep penetration is greater than the coating thickness, around 12μm.

At 1000 °C, after conventional pyrolysis process is also observed only the presence of the cubic Fe (structure type ICSD– 43421) and hexagonal TiB_2 (ICSD – 78848) indicating that neither reactions of the TiB_2 active filler with the amorphous SiCN matrix nor with nitrogen from the pyrolysis atmosphere occur. This results are in accordance with Allahverdi at all (ALLAHVERDI; CANNON; DANFORTH, 2000), whereas they showed practically no reaction of TiB_2 –SiC filled blackglas resin, under nitrogen atmosphere, 1000 °C.

Figure 46: XRD pattern of the sample before pyrolysis, after CP and PAP, at 1000 ° C, 2 h.
($\circ TiB_2$,● TiC_xN_y, *$Ti_6C_{3.76}$, ♦Fe_2B, ◊Fe_3Si, △Fe).
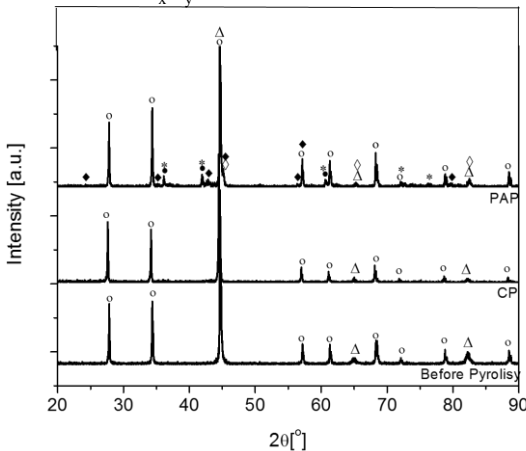
Source: Elaborated by the author

In contrast, the X-ray diffraction pattern of the sample after PAP process shows the presence of other phases, indicating the initial formation of Ti(C, N), Fe_xB_y and Fe_xSi. Since the elemental distribution

of iron shows an interface coating/substrate blurred, it is an indication that iron is reacting with the coating forming the Fe_xB_y and Fe_xSi phases at this diffusion zone. The tetragonal Fe_2B (ICSD – 42530) with a = 5.1003 Å and c = 4.2338 Å, and the cubic Fe_3Si (structure type ICSD – 43421) with the cell parameter of 2.8655 Å cell parameters were detected.

The presence of the phase Fe_3Si is an indicative that iron is reacting with the amorphous SiCN matrix by solid-state reaction. Francis et al.(FRANCIS et al., 2009) also showed in their work that the polysilazane (Ceraset, Kion) filled with 10 vol% iron powder allowed the formation of the Fe_3Si phase, by pyrolysis at 1100 °C under argon atmosphere.

It were also formed carbide phase identified as $Ti_6C_{3.76}$ (ICSD – 65938) and TiC_xN_y phase, close to the $TiC_{0.51}N_{0.12}$ (ICSD – 39942) composition. The calculated lattice parameter of the detected hexagonal $Ti_6C_{3.76}$ were a=3.0542 Å and c=14.8010 Å; and a=3.0751 Å, c=14.3576 Å for the TiC_xN_y phase (Rwp3.98, GOF=0.52).

The resulted relative phases after PAP at 1000 °C are shown in Table 15. The largest amount phases are from the unreacted TiB_2 (71.52 %) and Fe (15.02%) from the substrate. Considering that the peaks of such formed phases, as well as the amount calculated by Rietveld Refinement, are too small, it is assumed that the temperature of 1000 °C is when the reactions to form those phases begin. In order to strengthen this assumption it was also performed PAP at 900 °C. The x-ray diffraction (Figure 47) of the sample after PAP at 900°C shows only the TiB_2 peaks, which indicates that the reaction started after 900 °C. It is noted that there is no iron peaks in this sample, probably due to the coating thickness, that is around 50 µm. This means that the XRD diffraction is not reaching the substrate.

Table 15: Amount of relative phases after PAP at 1000 °C

Phase	Relative amount (% Mole)
$TiC_{0.51}N_{0.12}$	0.68
$Ti_6C_{3.76}$	1.72
Fe_3Si	6.24
Fe_2B	4.81
TiB_2	71.52
Fe	15.02

Source: Elaborated by the author

Figure 47: XRD pattern of the sample after PAP, at 900 °C, 2h. ○TiB2
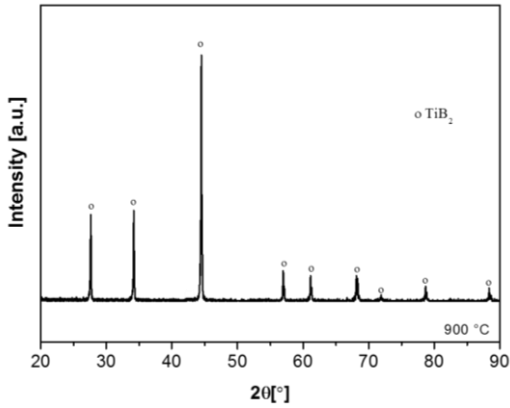
Source: Elaborated by the author

The accuracy of the obtained data by the Rietveld Refinement, confirming the Rwp 3.98 and GOF=0.52, can be verified by the simulation graphic. The measured (experimental) XRD pattern of the sample after PAP, 1000 °C, and the Rietveld simulation are shown in Figure 48

Figure 48:The XRD patterns (experimental) of the sample after PAP, 1000 °C, and the Rietveld simulation (simulated).
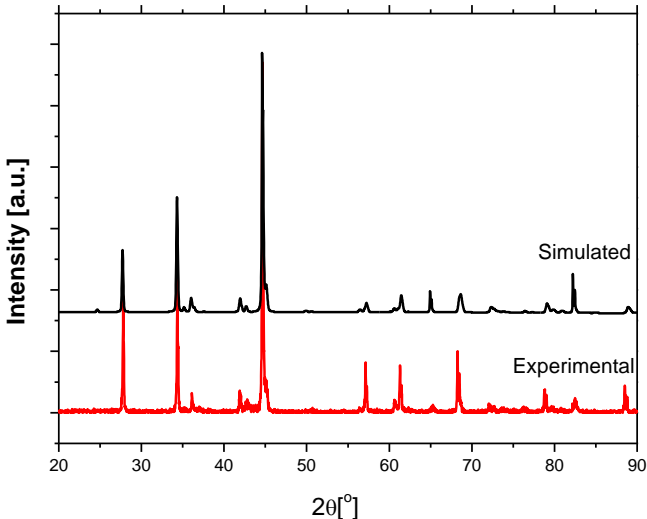
Source: Elaborated by the author

To evaluate the phase transformations and microstructural changes occurring during the pyrolysis process as a function of the processing temperatures the pyrolysis were carried out also at 1150 °C for both process.

The microstructure of the samples after CP and PAP process at 1150 °C are presented in Figure 49, where it is possible to see substantial difference between them.

After CP, even at 1150 °C it is still possible to verify the presence of the TiB_2 particles, indicating that most of TiB_2 remained unreacted. Whereas, after PAP process the microstructure of the sample is complex, with no distinct reaction zone or core-shell structure, suggesting that TiB_2 reacted, forming new phases with elements from the SiCN network, nitrogen from atmosphere as well as with iron diffused to the coating.

Figure 49: Micrograph of the samples after CP(left) and PAP(right), at 1150 °C.
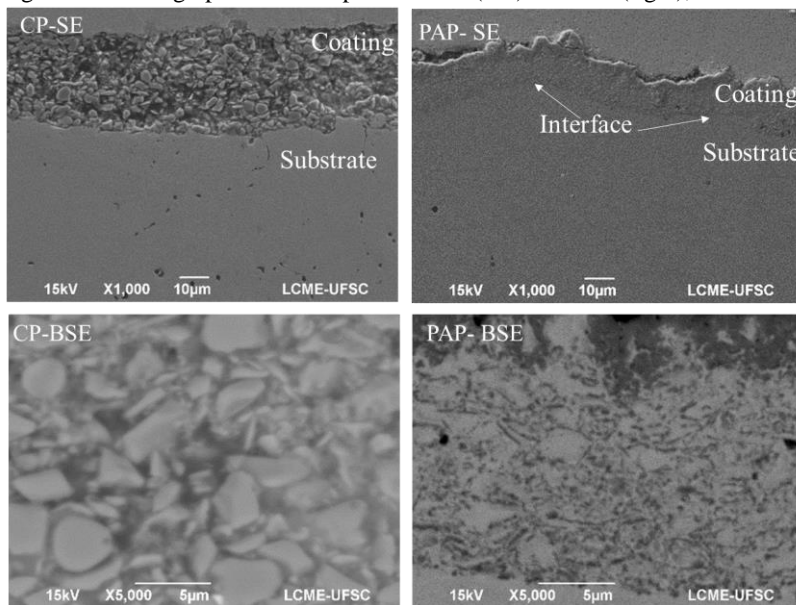
Source: Elaborated by the author

Elemental distribution of the sample after PAP and CP, at 1150 °C, is shown in the maps of the Figure 50 and Figure 51, respectively. The presence of TiB_2 particles after CP is visible in titanium map, by the orange dark regions where there are concentrations of it.

The distribution of titanium after PAP is an indication of a transformation of the filler particles. Moreover, the surface of the samples after PAP process reveals a dense layer of about 1 μm enriched with titanium and nitrogen,. Possibly, in this region is formed phases as TiN or Ti(C, N).

Figure 50: Elemental distribution after conventional process at 1150 °C.
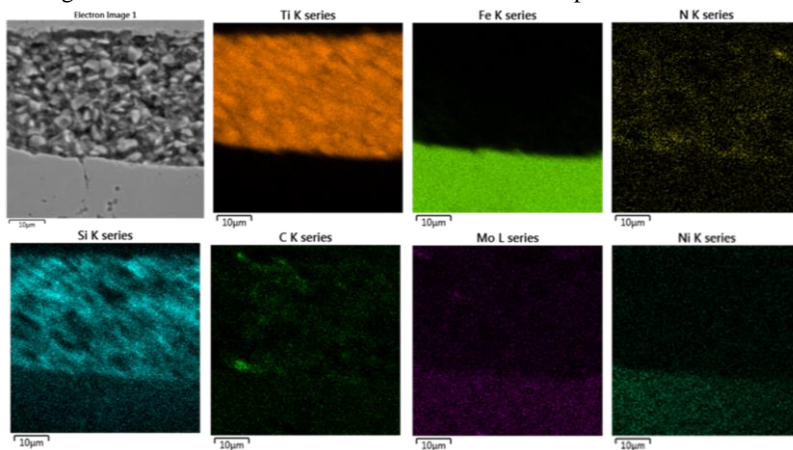
Source: Elaborated by the author

Figure 51: Elements distribution of the sample after PAP process at 1150 °C.
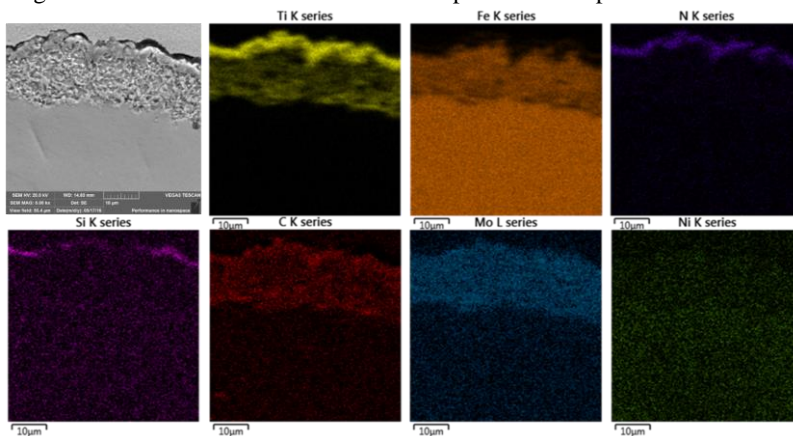
Source: Elaborated by the author

The maps of iron and molybdenum show a substantial

difference between two processes. At CP the maps show both elements only at the substrate. While, after PAP process, they are visible at the coating, indicating the diffusion elements from the substrate to the coating. The iron found in the coating after PAP is diffused from the substrate and a small amount could also be from the sputtering effect. This phenomenon is very common at plasma process, where iron ejected from cathode support reacts with nitrogen in the plasma atmosphere, forming iron nitrides, and diffused back to the sample on the cathode. These nitrides are unstable and decompose, releasing free nitrogen and iron to diffuse into the coating (LAMPE; EISENBERG; LAUDIEN, 1993).

The Silicon maps also indicate the differences between the processes. After CP the silicon is visible in the SICN network matrix coating, while after PAP the silicon is detected more concentrated close to the surface. As already mentioned, PDCs are intrinsically complex systems, which undergo great microstructural changes after pyrolysis with temperatures > 1000 °, and depending on the molecular structure can be amorphous up to 1000 °C- 1800°C (RIEDEL et al., 2006). In conventional pyrolysis the conversion of polyorganosilazane to a ceramic, up to 1000 °C, involves several reactions. At temperatures of 1100∘C rearrangement processes within the SiCN network result in the formation of amorphous Si_3N_4 and SiC. Increasing the temperature > 1400 °C a crystallization process occurs (SEIFERT et al., 2014). Thus, it is supposed that in the sample after conventional pyrolysis, up to 1150 °C, there is an amorphous SiCN network from the polymer precursor. The distribution of silicon after CP is an evidence of it. However, due to the fact that elements as C and N are difficult to be detected by EDS, and the measured XRD pattern does not show any broad halos, characteristic of amorphous materials (DE LIMA et al., 2013), it is not possible to prove it from our results. Should be necessary the use of other characterization, such as multinuclear MAS-NMR, to confirm it.

To highlight the difference between the CP and PAP, FEG-SEM images of the surface coating (top view) after pyrolysis under conventional pyrolysis (left) and after PAP process (right) at 1150 °C are shown in Figure 52.

Figure 52: FEG-SEM image of the top view, coating surface, after CP (left) and PAP (right), at 1150 °C, 2h.
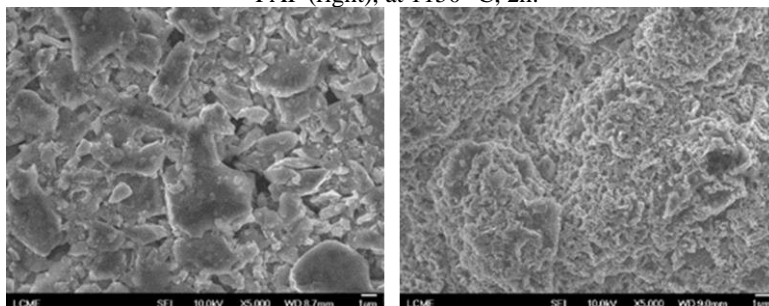
Source: Elaborated by the author

Comparing the top view image of both processes, even at 1150 °C, it is evident that the active filler TiB_2 unreacted under CP, while the microstructure after PAP is visibly different under these conditions. There is a kind of "growing" in the microstructure after PAP. Figure 53 shows in the left side the SEM with lower magnification (1000X) and in the right the FEG-SEM image with higher magnification (20.000 X) to evidence the "growing" mentioned, probably due to the expansion of the formed phases.

Figure 53: SEM(left) and FEG-SEM(right) image of the top view after PAP, at 1150 °C, 2h.
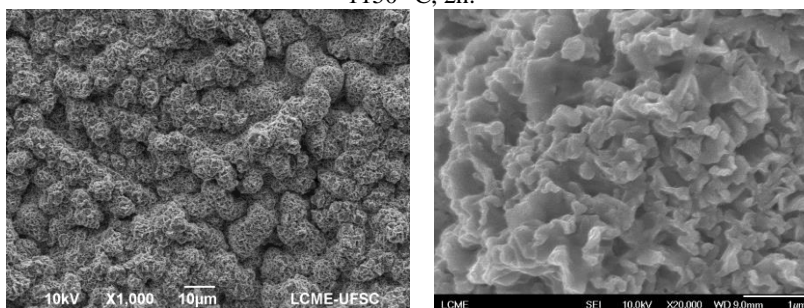
Source: Elaborated by the author

Figure 54 and Figure 55 show the Ti and N distribution in both processes, and Fe at PAP. At the sample surface after CP was not detected iron, as expected. After PAP titanium and nitrogen are evident at the surface, indicating the formation of Ti, N based phase, while in the CP it is possible do presume, by visual analysis, the particles of

TiB_2 in the region rich in titanium. The iron detected after PAP, is due to the sputtering effect, since there is some small agglomeration typical of plasma treatment.

Figure 54: Ti and N distribution of the sample, top view, after CP at 1150 °C.
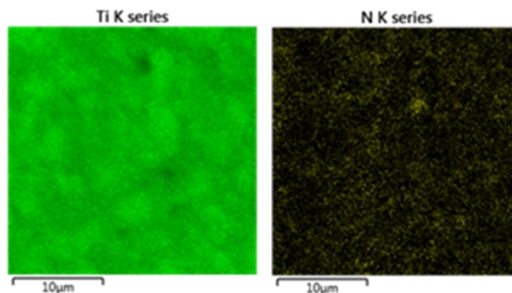
Source:Elaborated by the author

Figure 55: Ti, N and Fe distribution of the sample, top view, after PAP 1150 °C.
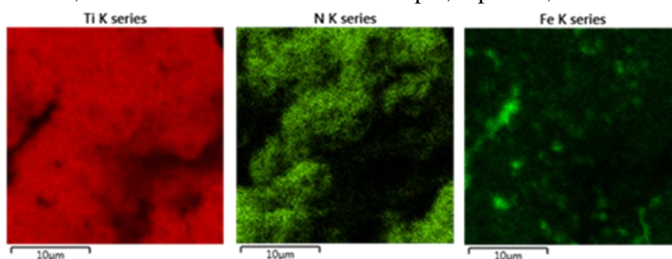
Source: Elaborated by the author

Evaluating the differences between the microstructure samples pyrolyzed at conventional and PAP processes, it is clear that the PAP promote more reaction and the formation of new phases, as discussed in the sequence. The X-ray diffraction pattern, Figure 56, shows the detected crystalline phases for both processes at 1150 °C, under nitrogen atmosphere. Since the sample after PAP process shows many small peaks, in order to distinguish better the peaks of each phase, it is shown an inset graph in the region between 43-47° for this sample.

In the XRD of the sample after conventional pyrolysis, the presence of the TiB_2 (91.64 %) and 8.36% of cubic TiN (ICSD – 064909) with calculated cell parameter of 4.2556 are observed. No evidence of crystalline phases based on boron was detected.

The XRD pattern after PAP shows the presence of multiple different phases, as carbonitride, nitride, silicide, intermetallic phases

and solid solutions, and no residual TiB_2, confirming the high reactivity of the plasma atmosphere. The major detected phases are TiC_xN_y (44.11 %) (ICSD – 39942) and $C_{0.858}(BN)_{0.571}$ (38.17 at%) (ICSD - 41583), followed by TiN (6.27 %)(ICSD – 064909). The carbonitride in this temperature has the composition close to $TiC_{0.7}N_{0.3}$, trigonal structure with lattice parameter of a=2.9988 Å and c=14.782 Å. The TiN has the lattice parameter of 4.2725Å. The Ti(C,N) is considered a solid solution in the TiC-TiN system, where, by a substitutional mechanism, N atoms replace C atoms (KWON; KANG, 2012). The formed TiCN structure depends on how the substitution takes place (LEVI; KAPLAN; BAMBERGER, 1998).

Figure 56: Phase composition of the sample after CP and PAP, at 1150 ° C. The inset graph shows the region between 43-47° for PAP.
($\circ TiB_2$,$\bullet$ TiC_xN_y, *TiN, $\Diamond Fe_3Si$, $\nabla Fe_{1.34}Si_{0.66}$, $\Phi FeB_{0.5}N_{0.5}$, $\blacklozenge FeN$, $\Delta Fe_3B_{0.25}Si_{0.25}$, $C_{0.858}(BN)_{0.571}$)
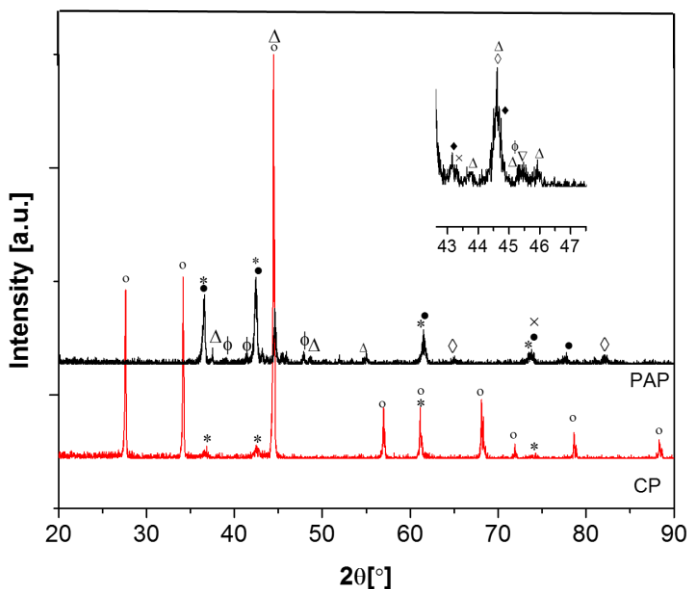
Source: Elaborated by the author

The calculated lattice parameter of $C_{0.858}(BN)_{0.571}$ solid solution was a=3.62 Å (KNITTLE et al., 1995). The remaining phases are most of them solid solutions or intermetallic phases based on iron. The

relative amount and cell parameters of the detected phase are presented in Table 16.

Table 16: Crystalline detected phases after PAP, at 1150°C.

Phase	Relative Amount (Mole %)	ICSD	Cell Parameters (Å)
Fe_3Si	5.72	43421	a=2.8685
$FeN_{0.0897}$	1.19	31912	a=2.8515 c=3.0884
$Fe_3B_{0.25}Si_{0.75}$	1.97	Prototype structure type ICSD – 38308	a=5.0935 b=6.7293 c=4.5205
$Fe_{1.34}Si_{0.66}$	1.0	87202	a= 2.8211
$Fe_3B_{0.5}N_{0.5}$	1.57	Prototype type FeB. ICSD – 30449	a=4.0463 b=5.4978 c=2.9292

Source: Elaborated by the author

The accuracy of the Riteveld Refinement is shown by the Rwp of 1.39, GOF=0.18 and also by Figure 57, where is presented the experimental XRD pattern of the sample after PAP, 1150 °C, and the Rietveld simulation.

Figure 57: The XRD patterns (experimental) of the sample after PAP, 1150 °C, and the Rietveld simulation.
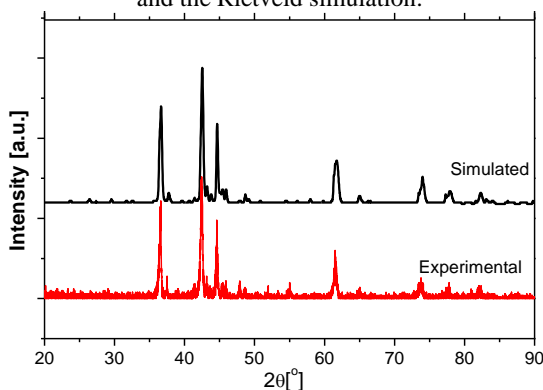
Source:Elaborated by the author

In order to give a general and summarized overview about the main reactions related to each phase, a summary of the main reactions that occur are listed below:

$$TiB_2 + \frac{3}{2}N_2 \rightarrow TiN + 2BN \qquad\qquad \text{(Eq. 06)}$$

$$TiB_2 + N \rightarrow TiN + 2B \qquad\qquad \text{(Eq. 07)}$$

$$TiB_2 + C \rightarrow TiC + 2B \qquad\qquad \text{(Eq. 08)}$$

$$TiB_2 + N_2 + \text{x}C \rightarrow TiC_xN + BN \qquad\qquad \text{(Eq. 09)}$$

$$TiC + (x/2)N_2 \rightarrow TiC_{1-x}N + xC \qquad\qquad \text{(Eq. 10)}$$

$$TiC_x + (y/2)N_2 \rightarrow TiC_xN_y \qquad\qquad \text{(Eq. 11)}$$

$$Ti + xC + (1-\text{x})/2N_2 = xTiC + (1-x)TiN = Ti(C_xN_{1-x})$$
$$\text{(Eq. 12)}$$
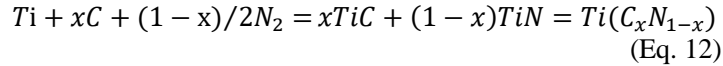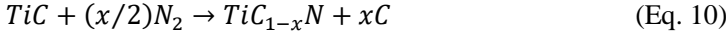
Boron from TiB_2 and the silicon from the SiCN network preferably reacts with iron as follows.

$$Fe + \frac{1}{2}B \rightarrow Fe_2B \qquad\qquad \text{(Eq. 13)}$$

$$xFe + Si \rightarrow Fe_xSi \qquad\qquad \text{(Eq.14)}$$

Based on the presented results it can be assumed that the TiB_2 particles decomposed under PAP at 1150 ° C, reacting with the elements from the SiCN network, iron and/or with the pyrolysis atmosphere, confirming the results obtained in the previous session/chapter with the filler $TiSi_2$ and reported elsewhere (SEIFERT et al., 2016).

To explain the differences found between PAP and CP the main assumption is that the chemical reactions and compositions change as a result from the use of highly reactive atmosphere, both chemically and physically, by means of the mechanisms promoted by nitrogen plasma atmosphere interactions when the sample acts as cathode during the pyrolysis process. Among the phenomena occurred during PAP it is listed the cathode bombardment from atomic nitrogen, ion and neutral species; cathode heating; sputtering effect, nitrogen adsorption and enhances diffusion of atomic nitrogen.

All these processes occur in an intermittent manner, simultaneously and out of thermodynamic equilibrium, being very difficult to isolate factors for analysis. The difficulty of explaining the physical and chemical phenomena that occur during plasma material treatment processes are so many that even processes that are well-known, as plasma nitriding, shows different conclusions and contradictions about the models to explain the nitriding phenomena in different studies in the literature ((LAMPE; EISENBERG; LAUDIEN, 1993), (HUDIS, 1973)(RIE, 1999) (MITTEMEIJER, 2013)).

Thus, even though it is well known that more investigation is

still necessary to explain the phenomena involved in the PAP process, it is believed, among the possible phenomena that occurred, significant contribution of the atomic nitrogen diffusion to the coating. This assumption is based on the fact that, in accordance with literature, the filler nitriding rate is limited by the diffusion of nitrogen species through the react layer((YU et al., 1995),(TORREY; BORDIA, 2007)) implying the low filler conversion during CP. Already, during PAP the presence of atomic nitrogen, which is much more reactive, enhances diffusion. It is acceptable that an enhance nitrogen diffusion due to ion bombardment (METIN; INAL, 1987) happens in PAP. As previous research had shown that even for low average ion bombardment energy (100 eV) occurs the enhancement of the interfacial diffusion up to 10^5 times over thermal values due to the presence of defects promoted by ion bombardment ETOUKHY (1980 apud (METIN; INAL, 1987)). Those punctual defects (vacancies, interstitial and/or substitutional atoms) in the specimen, promote a increasing diffusion between the elements.

A representative scheme show on how the filler conversion, during pyrolysis, can take place is show in Figure 58. Where in the first case (1) the active filler can react with the matrix, in this case SiCN, and/or pyrolysis product and occurs incomplete filler conversion. In the second case (2) the filler reacts with the reactive gas from atmosphere (N_2) and/or with the matrix and pyrolysis products, having an increase in the filler conversion. In the third case (3) is represented the plasma pyrolysis, where the filler react with reactive species from atmosphere, specially, the atomic nitrogen, and/or with the matrix and pyrolysis product. In this case the conversion can be almost complete, or even complete, depending on the system: filler, precursor, temperature and time.

Figure 58: Scheme showing three possibilities (1, 2 and 3) of how the filler conversion occurs.
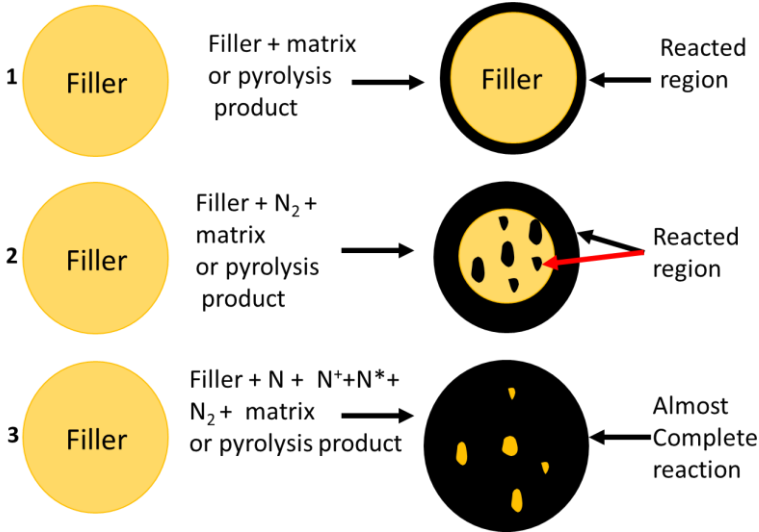
Source: Elaborated by the author

In addition, this hypothesis can be strengthened using thermodynamic concepts. Although, the DC glow discharge atmosphere is far away from the equilibrium conditions (SICARDI SCHIFINO et al., 2004)(LIEBERMAN; LICHTENBERG, 2005)), the thermodynamic analysis is the first consideration in materials processing to give general guidelines for the expected reactions and equilibrium composition of species at different temperatures ((TAYLOR; PIRZADA; MANRIQUE, 1994). Thus, it is still possible to use the thermodynamics law to predict that the system will always prefer to stay in the lowest level of energy, in accordance with Equation 15,

$$\Delta G_f^\circ = \Delta H_f^\circ - T\Delta S_f^\circ \qquad \text{(Eq. 15)}$$

Where, ΔG_f° is the standard Gibbs free energy of formation, ΔH°_f is the enthalpy change and ΔS°_f is the entropy change.

The standard Gibbs free energy of formation for an open system, for which matter can be exchanged with the surroundings, as is the case where reactivity species are introduced to the sample, can be represented by the equation 16, where the chemical potential specifies how much ΔG° changes as various substances j are added to the system.

$$\Delta G_f^{\circ} = \left(\Delta H_f^{\circ} - T\Delta S_f^{\circ}\right) + \sum_{j=1} \mu_j \, dn_j \qquad \text{(Eq. 16)}$$

Furthermore, the chemical potential of any chemical species B, in a mixture of two components for example, is related to the chemical potential of any specie A, by the Gibbs-Duhem equation (Eq. 17), where $\sum_{j=1} \mu_j \, dn_j = 0$.

$$d\mu_B = -\frac{n_A}{n_B} d\mu_A \qquad dn_j \qquad \text{(Eq. 17)}$$

The Gibbs-Duhem relation implies in which chemical potentials in a multicomponent system can vary in relation to each other. Thus, when the species promoted by the plasma atmosphere (especially atomic nitrogen) are introduced to the PDC specimen, the chemical potential of the system changes, compared with the traditional process, where there is only N_2 gas.

In addition the highly energetic nitrogen is an energy source to the system, therefore to decrease the free energy of the system, in accordance with the thermodynamics law represented in Eq 18, nitrogen will preferably react with titanium. Thus boron "gets free", generating a chemical potential gradient that is the driving force for chemical diffusion of iron from substrate to the coating, aiming at forming Fe_2B between iron and boron(DAVID. R. GASKELL, 2012).

$$\left|\Delta G_{f(TiN)}^{\circ} + \Delta G_{f(Ti(C,N))}^{\circ} + \Delta G_{f(TiC)}^{\circ} + \Delta G_{f(Fe_2B)}^{\circ}\right| > \left|\Delta G_{f(TiB_2)}^{\circ}\right|$$
$$\text{(Eq. 18)}$$

Previous results, Session 5.3.3 (SEIFERT et al., 2016) showed that for the bulk composition of HTT1800/TiSi$_2$, after PAP process at 1150 °C, 2h holding time, there is high amount of elemental Si as a result of the partial conversion of TiSi$_2$ in Ti(C,N). Since in this case it was a "bulk", there was no element to react with Si. However, when the PDC composite is on a substrate, diffusion between substrate and coating occurs, and the system will find the lower energy level stating the hypothesis that once the element boron gets free, the diffusion of iron from the substrate to the coating occurs. Furthermore, as already mentioned, the diffusion in that case is enhanced additionally due to the ion bombardment(ELTOUKHY; GREENE, 1980), in plasma assisted process, which improves the diffusion kinetics.

Using the software Thermocalc, the respective Gibbs free

energy of formation for mentioned phases was calculated and is shown in Figure 59 and Figure 60. It is in accordance with thermodynamic data available in the literature (JAIN et al., 2010; JUNG et al., 1999; KWON; KANG, 2012; ZAITSEV; ZAITSEVA; KODENTSOV, 2003), fulfilling the Eq. 18.

Figure 59: Calculated Gibbs free energy of formation for the indicated Titanium based phases as a function of Temperature.
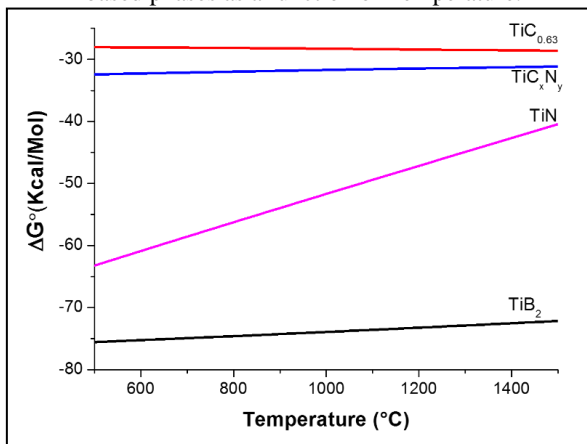
Source: Elaborated by the author

Figure 60: Calculated Gibbs free energy of formation for the indicated iron based phases as a function of Temperature.
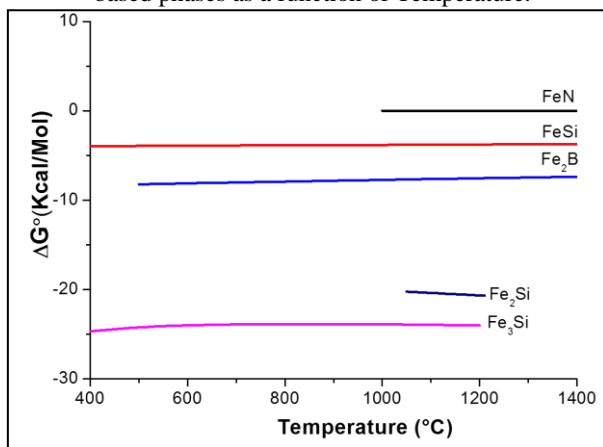
Source: Elaborated by the author

Based on previous results, it is believed that the presence of reactive species, promoted by the plasma atmosphere, accelerates the reaction kinetics resulting in higher reaction rates (LIEBERMAN; LICHTENBERG, 2005). This implies in the increase of the overall system activity, providing the required energy to overcome the energy barrier of reaction, in accordance with the formation free energies involved, and promoting the formation of new phases to the respective reactions between the elements in the system (Ti, C, N, Si, B and Fe).

Temperature Influence under PAP

To better understand the phase transformations and microstructural changes occurring during the plasma assisted pyrolysis process, as a function of temperature, it was performed PAP under the temperatures 900 °C, as already mentioned, and 1075 °C too. The SEM images, BSE signal, are shown in Figure 61. Didactically it is shown again the SEM image of the samples after 1000 °C and 1150 °C to simplify the comparison.

Figure 61: Micrography of the samples after PAP, at different temperatures.
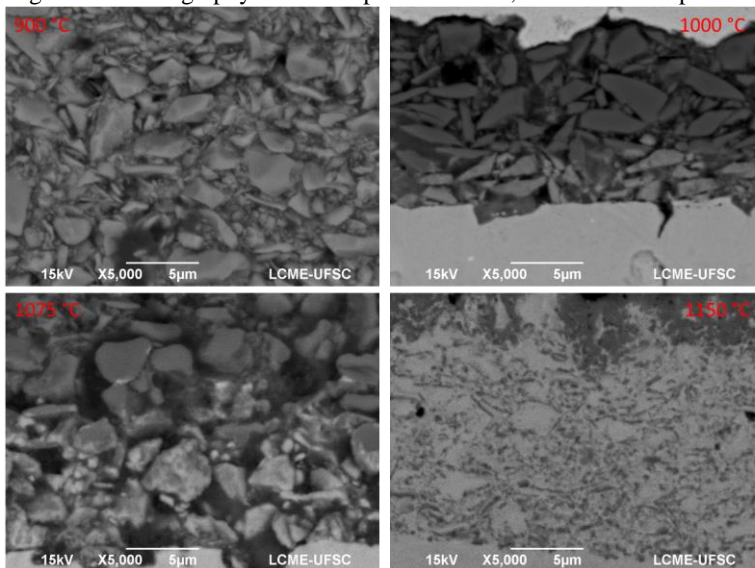
Source: Elaborated by the author

It is observed that the substantial microstructural change occurs at the pyrolysis at 1150 °C. Up to temperature of 1075 °C it is still

possible to identify the unreacted TiB_2 particles.

To follow the phase formation during plasma assisted pyrolysis, it were also performed XRD at 1075 °C, as shown in Figure 62.

Figure 62: XRD pattern of the samples after 1075°C. ($\circ$TiB$_2$,$\bullet$ TiC$_x$N$_y$, *Ti$_6$C$_{3.76}$, Φ TiN, $\blacklozenge$Fe$_2$B, $\Diamond$Fe$_3$Si, $\triangle$Fe)
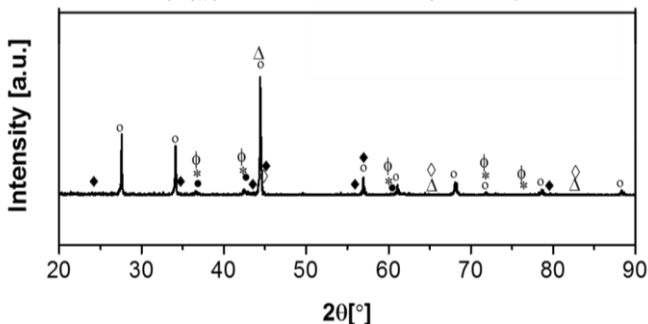
Source: Elaborated by the author

At 1075 °C, besides the phases detected at 1000 °C is also detected a small amount (1.1 %) (Rwp 3.53, GOF=0.45) of TiN, according to Rietveld Refinement. Table 17 summarizes the detected crystalline phases after PAP at different temperatures under flowing nitrogen. As the temperature increases to 1150 °C it is detected the presence of different solid solutions, as expected, since the solid solutions are favored to form at high temperature due to the system entropy increases (ANTHONY R. WEST, 1987).

Table 17: Detected crystalline phase after PAP at different temperatures

T (° C)	Detected phases
900	TiB$_2$
1000	TiB$_2$, Fe$_3$Si , Fe, Fe$_2$B, Ti$_6$C$_{3.76}$, TiC$_x$N$_y$
1075	TiB$_2$, Fe$_3$Si, Fe, Fe$_2$B, Ti$_6$C$_{3.76}$, TiC$_x$N$_y$, TiN
1150	TiC$_x$N$_x$, TiN, C$_{0.858}$(BN)$_{0.571}$, Fe$_3$Si, FeN$_{0.0897}$, Fe$_3$B$_{0.25}$Si$_{0.75}$, Fe$_{1.34}$Si$_{0.66}$, FeB$_{0.5}$N$_{0.5.}$

Source: Elaborated by the author

The EDS elemental mapping of iron, titanium and molybdenum at 900 °C, 1075 °C and at 1150 ° C (again, to compare) after PAP

process is shown in Figure 63. Analyzing the elements distribution it is possible to verify the decomposition of TiB_2 and iron and molybdenum diffusing from substrate to the coating, while temperature increases.

Figure 63: Elemental distribution of Ti, Fe and Mo after PAP at 900 °C, 1075 °C and 1150°C.
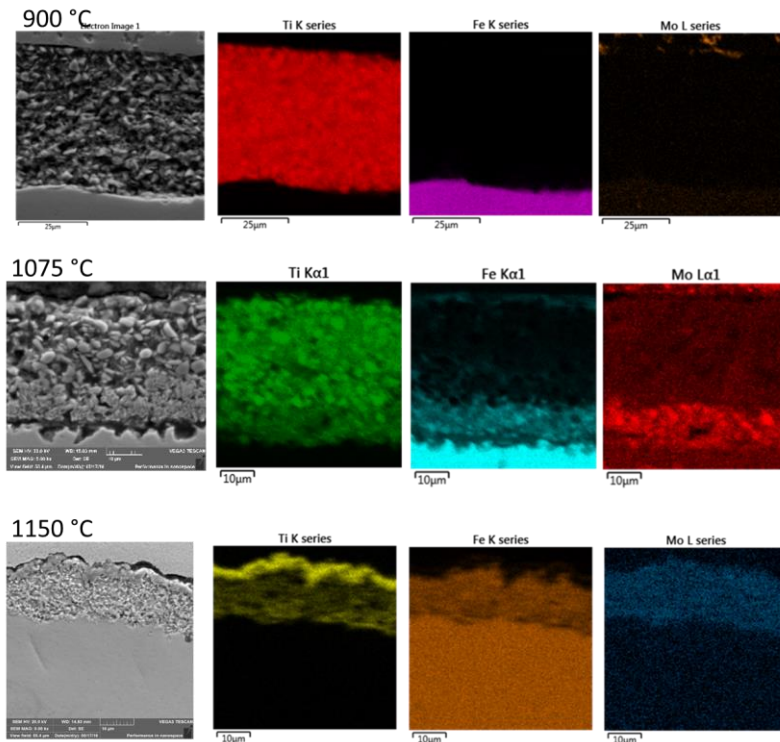
Source: Elaborated by the author

In order to highlight the influence of diffusion phenomenon it were also performed glow-discharge optical emission spectroscopy for the samples after PAP (900, 1000, 1075 and 1150 °C). The results are presented in a qualitative form, this means that it is possible to know the behavior of such element at the coating and substrate, but not the amount of each one. The elements were not quantified due to the lack of elemental standard to quantify all the elements involved in the studied system. It is worth highlighting that the analyzed system involves many elements: Ti, B, C, Si and N from the initial coating composition; Fe, C, Ni and Mo from the substrate. The atmosphere offers species based on

N_2. The handling and the reactor offer oxygen to the system, and even some impurities. Besides elements as Fe, Ni and Cr from the cathode. In the end, the complex system is based on at least nine elements.

To have information about the behavior of them and complement the results, especially EDS analysis, the GDOES curves are shown in Figure 64. Each graphic indicates the PAP temperature and the average thickness measured by SEM image. It is also important to highlight that the scale of each graphic are different due to the difference in the coating thicknesses and results provided by the characterization. For each sample it was used enough time to be sure that the substrate was reached. For example, the graphic of the sample pyrolyzed at 1075 °C shows the graphic scale up to 80μm, whereas the other samples shows the scale around 30 μm.

Figure 64: Profile of GDOES for the elements, Ti, C, Si, Fe, B, N, Mo, Ni and O, at different pyrolysis temperature, PAP-C.
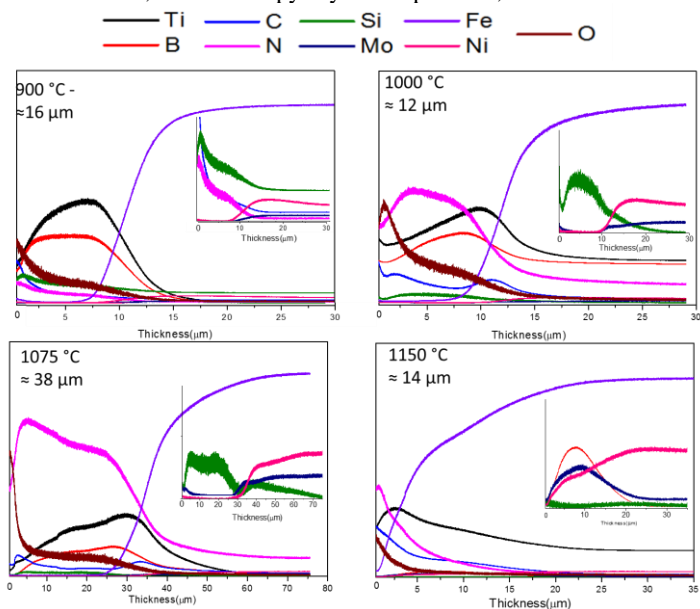
Source: Elaborated by the author

The results provided by GDOES evidence the diffusion phenomenon. Increasing temperature it is clear the behavior of iron, molybdenum and nickel, diffusing from substrate to coating. At 1150 °C the amount of Fe and Mo in the coating are considerable, in accordance

with the elemental mapping from EDS. In the same matter the B and C, which are small elements and can readily diffuse by meandering in the interstices, are diffusing. At 1000 °C and 1075 °C there is an evident concentration of B and C close to the interface coating/substrate, and increasing the temperature for 1150 °C they are diffusing to the substrate. Titanium is also diffusing to the substrate. At the temperature of 1000 °C the Ti is basically concentrated at the coating, and at 1150 °C there is also Ti in the substrate, close to the interface. Also confirming the EDS results.

These results show that atoms from coating have migrated to the metal substrate, and atoms have migrated from the substrate to the coating. Which is reasonable, since it has been known that the chemical gradient is a driving force for diffusion, whereas atoms tend to migrate from regions of higher concentration to regions of lower concentration. This means, diffusion is driven by decrease in Gibbs free energy or chemical potential difference, in accordance with the Fick´s Law (Eq. 19).

$$\frac{\partial C}{\partial t} = \frac{\partial}{\partial x}\left(D\frac{\partial C}{\partial x}\right), \qquad\qquad \text{(Eq. 19)}$$

Where C is concentration, D is the diffusion coefficient, t is time and x is the position.

The diffusion within the crystal lattice occurs mainly by either interstitial or substitutional (vacancy) mechanisms; Details about these phenomena will be not discussed here, and can be found elsewhere(MEHRER, 2007), however the diffusion is greatly affected by the motion/nature of all the atomic species and temperature. Particularly the rate and diffusion coefficient are significantly affected by temperature, generally following the Arrhenius equation (Eq. 20). At higher temperatures, the diffusion coefficient is greater because the atoms and molecules have more thermal motion.

$$D = D_0 e^{-(Q/KT)}, \qquad\qquad \text{(Eq. 20)}$$

Where D_0 is a temperature independent pre-exponential constant (m^2/s), Q is the activation energy for diffusion (J/mol), R is the gas constant (8.31 J/mol-K) and T is the absolute temperature (K).

5.4.3 Influence of plasma process parameters

One of the goals of this research, in the first approach, was to investigate the influence of some process parameters on the filler conversion. It was chosen to investigate the influence of the plasma switched on time (Ton) and voltage. The main purpose was to verify how these parameters could influence the filler conversion, specifically the amount of formed phases. Therefore, it was performed pyrolysis changing these parameters at 1000 °C. It was chosen to use this temperature considering the temperature in which the reactions should starts.

The SEM micrograph of the samples varying Ton (70, 100, 130 and 150 µs), is shown in Figure 65. Observing the SEM images is not possible to identify substantial differences in the coating. The unreacted filler is clearly visible in all the samples, and also the diffusion elements from substrate to coating is evident, forming a diffusion layer (light color) at the substrate/coating interface. The coating thickness and the used Ton for each sample are indicated in the images.

Figure 65: SEM images(transversal section), with BSE signal, of the samples after PAP at 1000 °C for the Ton 70, 100,130 and 150 µs.
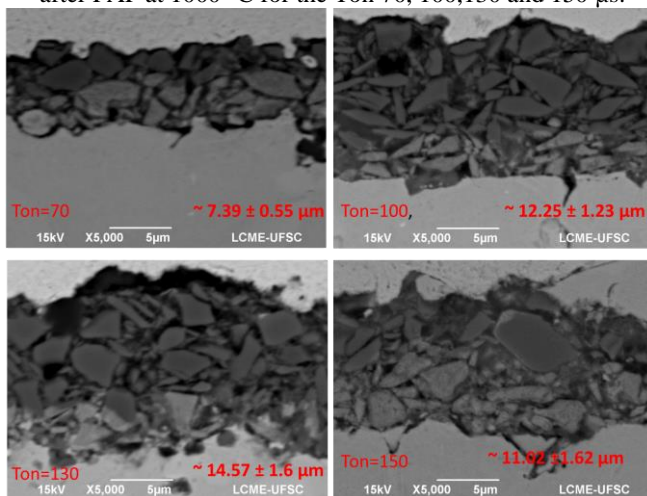
Source: Elaborated by the author

Figure 66 shows the FEG-SEM image of the surface, top view, of those samples. Analyzing the surface of the samples it is clear the plasma effect by those small "agglomeration", shown in detail in Figure 67. Increasing the plasma switched on time there is a visible increase in

their number, as expected since it is imply in the sample being bombarding by reactive species for longer.

Figure 66: FEG-SEM image, with BSE signal, of the top view samples after PAP at 1000 °C for the Ton 70, 100, 130 and 150 μs.
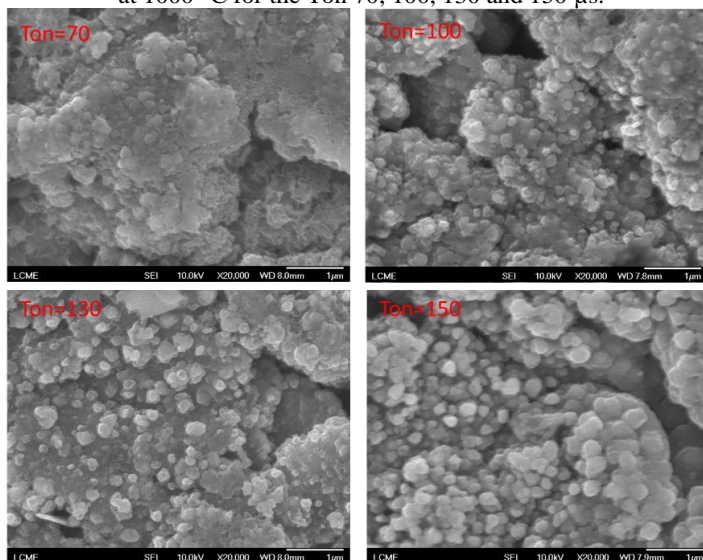
Source: Elaborated by the author

Figure 67:FEG-SEM image of the surface sample after PAP at 1000 °C for the Ton 70, indicating the sputtering effect and the TiB_2 filler.
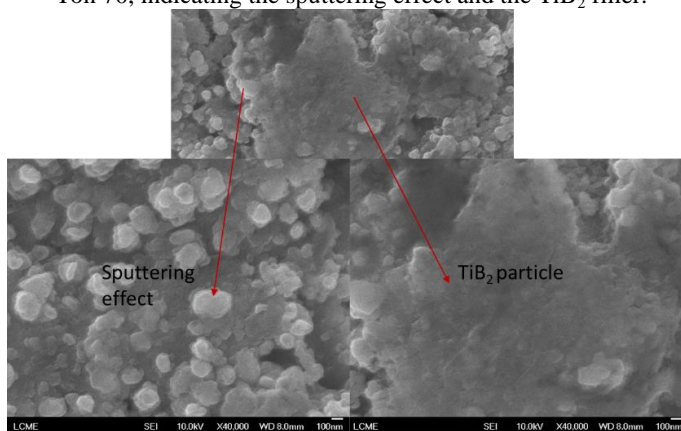
Source: Elaborated by the author

Iron distribution of the top view of the sample with Ton=100 μs, is shown in Figure 68. Those agglomerates are regions with enhanced iron and nitrogen concentration, compared with other regions, as confirmed by the punctual EDS analysis shown in the right side.

Figure 68: Elemental distribution of Iron and the EDS analysis of the region indicated by arrow, of the sample after PAP, at 1000 °C, Ton=100 μs.
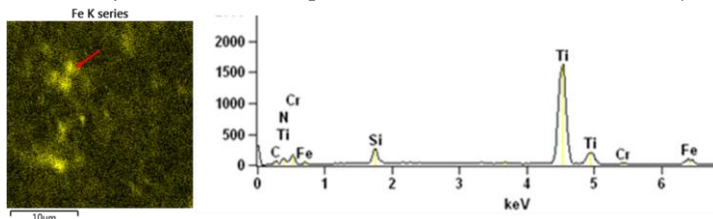
Source: Elaborated by the author

The XRD pattern of the samples pyrolyzed with different Ton are shown in Figure 69. It were identified the same phases for all the samples and no evident differences could be detected analyzing only the peaks. The Rietveld Refinement was then used to try to verify some difference in the formed phase.

Figure 69: XRD pattern of the samples after PAP, at 1000°C, and different Ton.
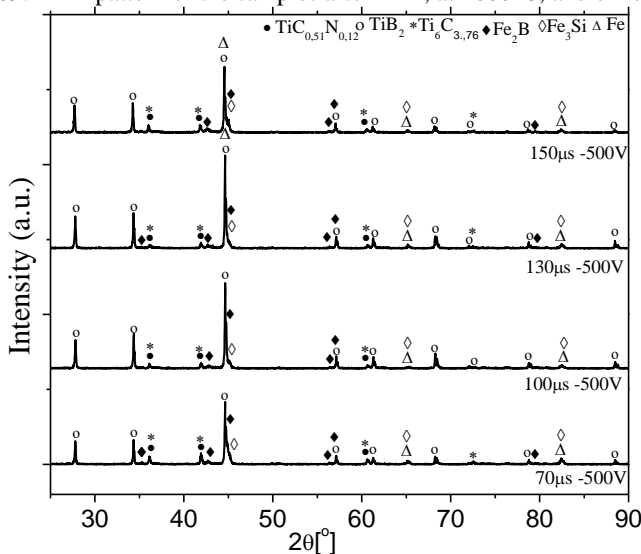
Source: Elaborated by the author

It was analyzed the amount of each phase for the different Ton (70, 100, 130 and 150 μs). However it was not found any direct relationship between Ton and formed phases. It means, no relation as for example, increasing the Ton promote an increase in the phase TiC_xN_y, as it was expected. Then, it was investigated if there was some trend related to the coating thickness. As shown in Figure 70, where is presented the amount of each phase, the coating thickness and the investigated Ton for each sample. It is possible to note that increasing the coating thickness, even in few microns, increased the amount of TiB_2. There is also some trend for the phase Fe_2B and $Ti_6C_{3.76}$. The amount of formed phase TiC_xN_y for the sample 1 and 4 are too small (less than 1%) that due to the scale it is not visualized in the graphic. It is important to mention that for such small amount of phase it is very doubtful the calculated amount, since the error promoted by the refinement is bigger than it. Another point is that the peaks overlap, making it difficult to distinguish between then. For example, there are authors that do not even distinguish the phases TiN and TiC from the TiC_xN_y solid solution, in such temperature, (SEIBOLD; GREIL, 1993) due to the peaks appear to be so close that it is not easy to be exactly distinguished. Anyway, in our study based on fact that the Refinement method is mathematical, following the same pattern for all the samples it were selected the results which shows best values in the mathematical simulation and the graphical representation. The R_{wp} and GOF for each sample is shown in Table 18.

Figure 70: Relative amount of phases (Mole %) in according with coating thicknesses and Ton.
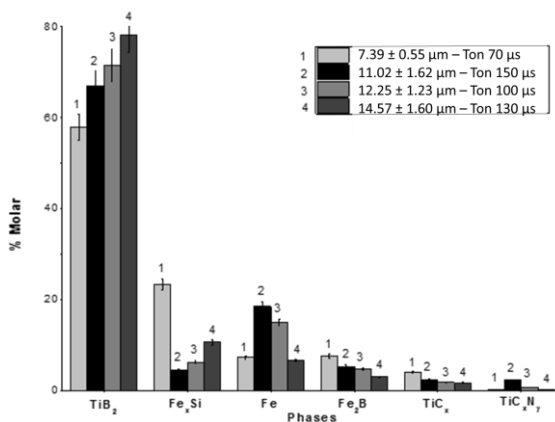
Source: Elaborated by the author

Table 18: Rwp and GOF obtained in the Rietveld Refinement.

Sample	Rwp	Gof
1- Ton=70 µs	3.20	0.41
3-Ton=100 µs	3.98	0.52
4-Ton=130 µs	4.31	0.56
2-Ton=150 µs	3.84	0.49

Source: Elaborated by the author

As those results are influenced by many aspects such as the x-ray penetration volume, the diffusion phenomenon and the changed Ton, it is not possible to compare these results or to verify the influence of each one itself, however it seems that the thickness has great influence on these results. Trying to support it, it were added the phases based on iron (Fe_xSi, Fe, Fe_2B) and titanium ($Ti_6C_{3.76}$, TC_xN_y). Figure 71 represents the amount for this sum. In the legend is indicated the Ton and the coating thickness. It is noted that increasing the coating thickness there is an increasing in the TiB_2 amount and a decrease in iron based phases. The amount of phases based on TiC_x and TC_xN_y are similar, less then 5 Mole %, for all the samples.

Figure 71: Relative amount of the TiB_2 and the phases added for each Ton and thickness
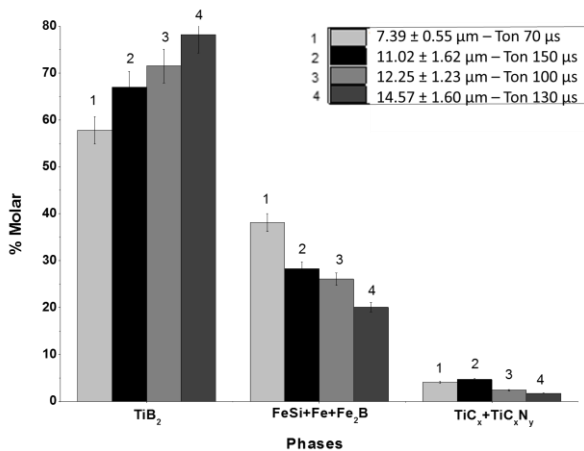
Source: Elaborated by the author

To verify the hypothesis of the thickness influences on the

formed phases amount, it is shown the results for two samples, processed in the same PAP conditions, using Ton 150 µs, and very similar thicknesses. Figure 72 shows this results. It seems that the process and the Rietveld refinement have reproducibility. To confirm the refinement quality it is shown in Figure 73 the measured (experimental) XRD pattern of the sample after PAP(1000 °C, Ton 150 µs), the patterns from each identified phase, and the Rietveld simulation (simulated). The R_{wp} and GOF of the sample 1 were 3.84 and 0.49, respectively; and for the sample 2 R_{wp} 3.37, GOF=0.43.

Figure 72: Relative amount (Mole %) of phases for the samples pyrolyzed with Ton=150µs.
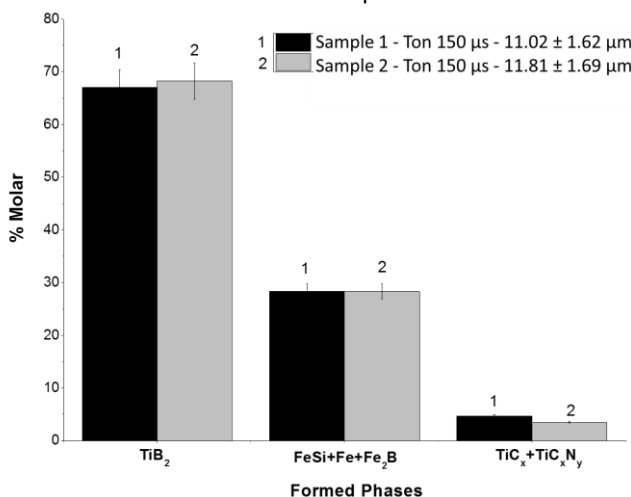
Source: Elaborated by the author

Figure 73: XRD (experimental) of the sample after PAP, 1000 °C, Ton=150μs, and the Rietveld simulation with the pattern of each phase.

Source: Elaborated by the author
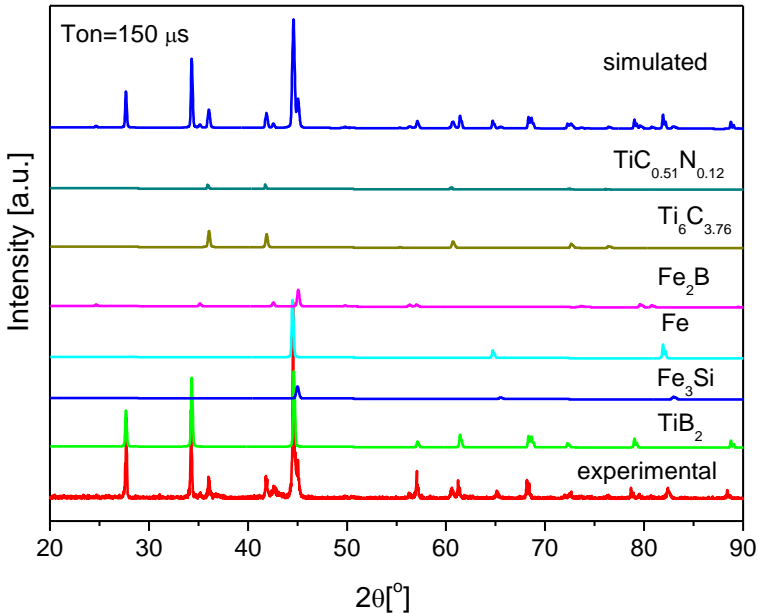
Likewise the results obtained when Ton was changed, the samples processed with different voltage (400 V, 500 V and 600V) had shown no significant difference in the microstructure. The XRD pattern (Figure 74) shows almost the identical behaviour, except by the fact that increasing the coating thickness, and also the voltage, there is a decrease in the peak referent to the Fe_3Si phase. As shown by the XRD pattern zoom of the samples in Figure 75.

For the sample with Voltage of 600V and thickness of 21.75 ± 0.76 μm thes phase Fe_3Si is not detected.

Again, it seems that the thickness is substantially influencing the results. Even though it is not possible to affirm it, since there was also the Voltage change, it apparently makes sense that the thickness increase makes the reaction difficult, meaning that more time is necessary for iron to diffuse into the coating to react with silicon.

Figure 74: XRD pattern of the samples after PAP, at 1000°C, for different Voltages.
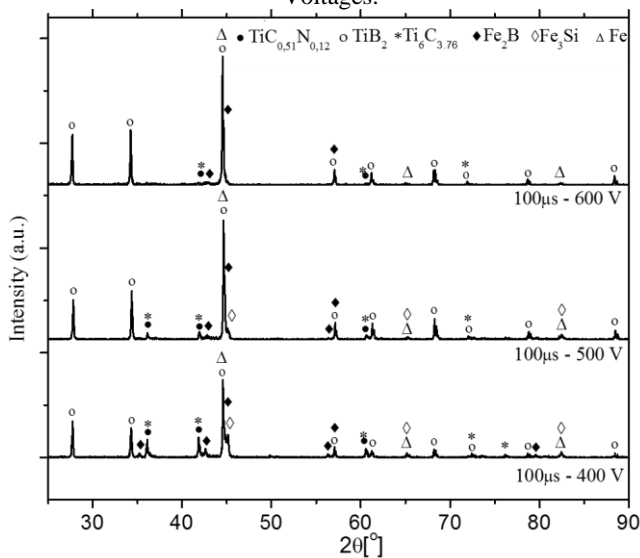
Source: Elaborated by the author

Figure 75: XRD pattern of the samples after PAP, at 1000°C, and different Voltages, showing the peak related to the phase Fe_3Si and the thickness coating.
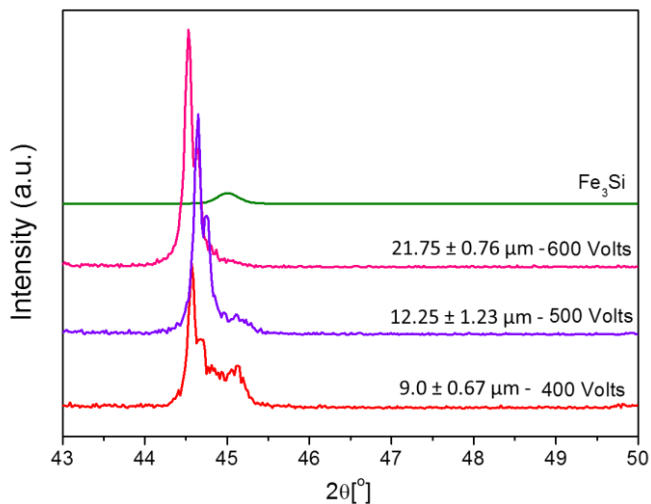
Source: Elaborated by the author

5.4.4   Substrate differences after PAP

After PAP under different temperatures, it was identified some difference in the sintered substrate microstructure, as expected since the sintered substrates were thermal treated again during the pyrolysis. However, since the focus of this research was not the substrate, even it being an important topic, only general remarks about the main difference between them close to the interface were done. The microstructures of the sintered substrate, after PAP at different temperatures, are shown in Figure 76. There is a substantial difference close to the interface substrate/coating for the samples pyrolyzed at 1000 °C and 1075 °C. It is mentioned that this different region is observed even without etching the sample.

Figure 76: Micrograph of the sintered substrate (etching with 2% Nital) after PAP, at different temperatures. SE signal.
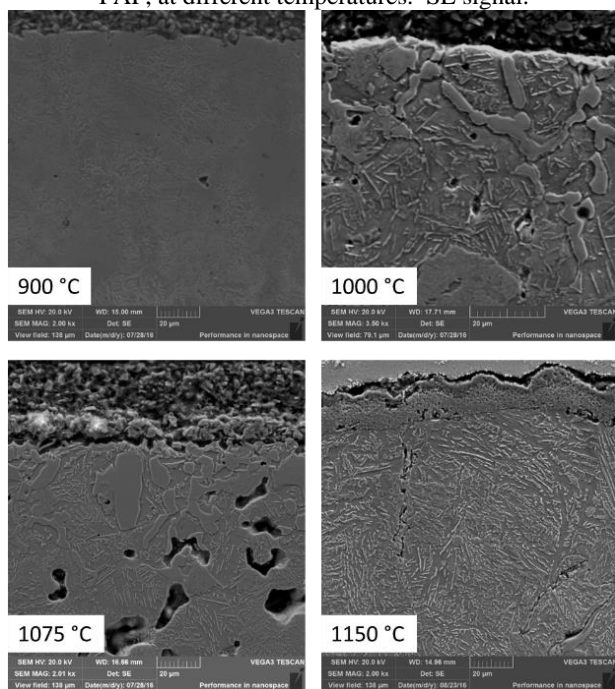
Source: Elaborated by the author

The backscattered SEM image for the sample after PAP at 1075 °C is shown in Figure 77. EDS analysis, line scan and punctual analysis, were performed to verify the composition differences. The region where were performed the line scan and the punctual analysis are represented by the red line and red spot, respectively. The EDS line scan results are shown in the right side of the Figure 77, and the EDS spectrum of the spot is shown in Figure 78.

Figure 77: Micrograph of the sintered substrate (etching with 2% Nital) after PAP, at 1075 °C (BSE signal), and the line scan results.
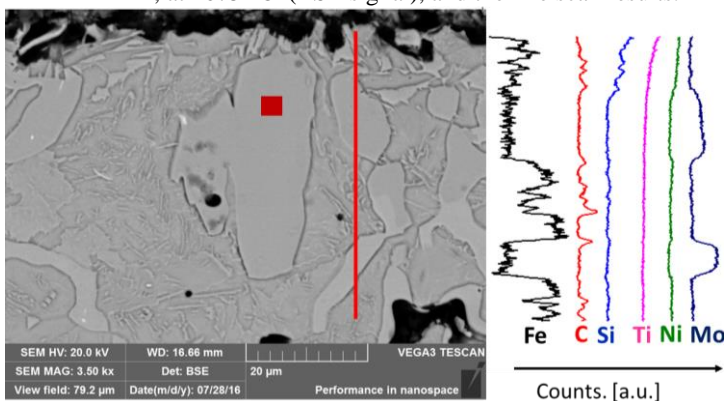
Source: Elaborated by the author

Figure 78: EDS spectrum of the region indicated by the red spot of the sample after PAP at 1075 °C.
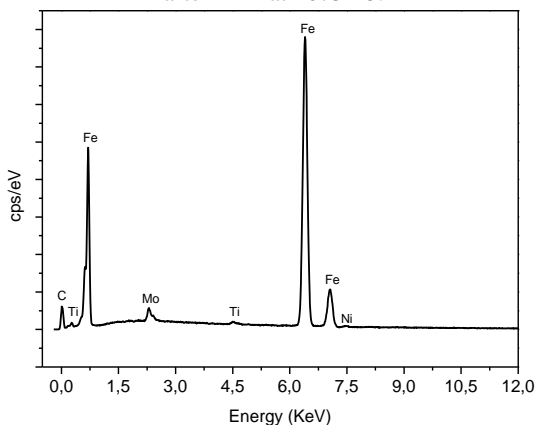
Source: Elaborated by the author

It is observed that the main difference is that those regions close to the interface are rich in molybdenum as already shown in the previous results by the elemental mapping from the cross section of the sample pyrolyzed at 1000 °C (Figure 44). It is also possible to confirm by the line scan, as already shown by the GDOES results, that titanium and silicon are diffusing from coating to the substrate, forming a diffusion zone at the interface coating/substrate.

It were verified the micro hardness of those formed phases. Figure 79 shows the indentations after the micro hardness measurement.

Figure 79: Micrograph of the sample after PAP, 1000 °C, showing the indentations where were performed the micro hardness measurement.
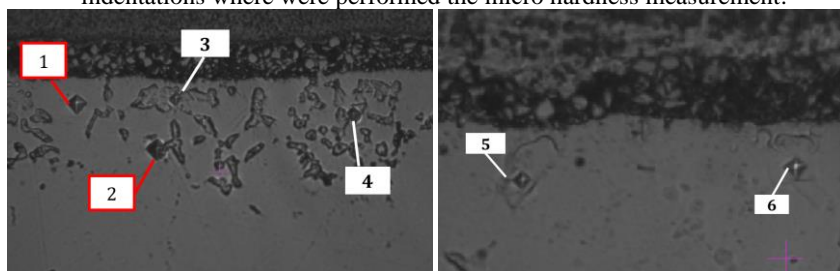
Source: Elaborated by the author

At the image of the left side are indicated four indentations, represented by the numbers, where the micro hardness were performed. The indentations 1 and 2, were performed in regions that do not show the region rich in molybdenum, but close to them, the harness of these points are 278 and 240 HV, respectively. Such values are in accordance with the sintered substrate hardness measured after sintering (before the pyrolysis thermal treatment). The indentations 3 and 4, where the phase rich in molybdenum was formed, show hardness of 533 and 411 HV, respectively. Even that these values show higher hardness, it is known that the substrate matrix could be also influencing such values, since it is not possible to affirm the depth of such phase. The results of the sample, where those regions are prominent, in the right side evidence this hypothesis. The indentations 5 and 6 had shown the hardness of 1183 and 639 HV, respectively; emphasizing that this phase is harder than the substrate matrix.

In the literature it is known that in the system of Mo-Fe-C forms complex carbides $(FeMo)_6C$ and $M_{23}C_6$ $(Fe_{21}Mo_2C6,)$ and Mo_2C.

Another possibility for the formation of such harder phase, could be due to the diffusion of boron at the interface substrate/coating. Boron in such system tends to form borocarbides $M_{23}(C,B)6$ and $M_3(C,B)$(DUARTE et al., 2014). However only based on the composition and hardness obtained it is not possible to identify the formed phase and more investigation is necessary, starting by one detailed investigation in the ternary diagram of those elements.

6.   SUMMARY OF RESULTS AND CONCLUSIONS

Several important accomplishments have been achieved in this research. First, the scope of this work was to develop the plasma assisted pyrolysis process of coatings, based on a polyorganosilazane as a ceramic precursor and fillers, on sintered steel, which was obtained successfully.

The results demonstrated that the use of DC cold plasma environment during pyrolysis of PDC coating promote an increase in the active filler conversion to the respective phases, such nitrides, carbides, and carbonitrides in lower temperature, compared to conventional pyrolysis whereas no significant filler conversion occurs. The enhancement of the filler conversions promote PDC coating and bulk with higher densification, since the shrinkage of the precursor is compensated and the formation of porosity is limited. By the choice of the system: precursor, active filler and plasma assisted pyrolysis process parameters it is possible to have materials, specially coatings, with tailored properties and compositions. Another important result is that the optimized processing route, including type of filler, amount, and pyrolysis parameters, enable the application of PDC coating into sintered substrate.

Below is presented a summary of the main results obtained in each phase of this thesis:

Phase 1

It was possible to apply PDC coating on sintered steel substrate, using inert fillers (BN, Si_3N_4, ZrO_2) and glasses. However, the final coatings still present some problems, such as cracks and porosity.
Comparing the samples after conventional pyrolysis and PAP, the sample after PAP seems to be denser. Indicating that the PAP process can promote PDC coating with optimized properties, even when inert fillers are used.

Phase 2

The results done with the bulk sample demonstrated that:
The used polyorganosilazane HTTS revealed no depolymerization or additional decomposition reactions after treatment in plasma environment. The ceramic yield as well as the elemental composition was not influenced adversely in comparison to conventional pyrolysis in a furnace under flowing nitrogen at 1000 °C,

but it was found differences in the structure of the resulting amorphous SiCN network. While the X-ray diffraction patterns revealed the expected formation of β-SiC environments beside a graphite structure during conventional pyrolysis, the diffraction patterns of the samples treated in the plasma atmosphere, anode and cathode, suggested the formation of Si_2CN_4 nanocrystallites.

Among the active filler, Ti, B and $TiSi_2$ the last one was choose for continuous the PAP investigation in this phase.

The pyrolysis behavior of the sample based on HTTS and $TiSi_2$ particle filler revealed also a strong dependency on the pyrolysis conditions. While during CP and PAP-A the $TiSi_2$ filler particles were insufficiently converted to Ti(C,N) and elemental Si in the temperature range of 900 to 1150 °C, the treatment in cathode configuration led to a strongly enhances filler conversion to the respective nitrides and carbonitrides.

The results demonstrated that nitridation reactions of the initially formed elemental Si yielded $α-Si_3N_4$ and $β-Si_3N_4$ already at a comparatively low temperature of 1150 °C. Therefore, the samples treated with PAP in cathode configuration are denser (porosity value smaller than 2 %) compared to the composites derived by conventional pyrolysis and PAP in anode, where the porosity range from 20 to 30%.

It is assumed that the densification is influenced by several processes which occur during treatment in cathode configuration, promoting an increased filler conversion. Among the processes occurred it is believed a strong influence from the presence of atomic nitrogen reacting with the sample.

The results demonstrated that the process of plasma assisted pyrolysis in cathode configuration is a feasible method to enhance the filler conversion in a nitrogen atmosphere and to generate PDC composite materials.

Phase 3

In this phase, the type and amount of filler and precursor, as well as the coating thickness and pyrolysis parameters were optimized to process coating, without cracks and delamination, on sintered substrate. It was found the amount precursor of 30 Vol % and 70 Vol% of the fillers $TiSi_2$ and TiB_2, as a composition to have the desired coatings.

The results after PAP and conventional pyrolysis of the coating on sintered steel substrates demonstrated:

The pyrolysis of coating based on precursor with TiB_2 as active filler proofed the increased filler conversion under PAP, in comparison with conventional pyrolysis. The pyrolysis behavior of the sample revealed a strong dependency on the pyrolysis environment atmosphere. At 1150 °C, during PAP, the active filler reacted with reactive species from atmosphere, specially the atomic nitrogen, and/or with the matrix and pyrolysis product, forming phases as TiC_xN_y, $C_{0.858}$ $(BN)_{0.571}$, TiN and also solid solutions as well as intermetallic phases based on iron. On the other hand, during CP the TiB_2 filler particles were insufficiently converted, forming only a small amount of TiN and most of the phase is composed of the remained TiB_2.

The pyrolysis behavior of the samples also revealed a strong dependency on the temperature and diffusion phenomenon. Increasing the temperature, occurs an increasing in the elements diffusion between coating and substrate. The elements diffusion influence greatly the formed phases.

The influence of the plasma parameters, Ton and Voltage, were not understood, due to the substantial influence of the coating thicknesses. It seems that the difference between the coating thicknesses affected greatly the obtained results, and further investigations are necessary.

Visually, the influence of the sputtering effect could be detected on the top view of the coating samples. Increasing Ton there is an increasing in the agglomerates from the sputtering.

The microstructures of the sintered substrate, after PAP at different temperatures, also showed difference. Specifically, there is a substantial difference close to the interface substrate/coating for the samples pyrolyzed at 1000 °C and 1075 °C, whereas a phase rich in molybdenum was formed. More characterization are necessary to identify this phase.

7.   FUTURE WORK

A research of more practical reactive filler powders is crucial for compensate better the coating shrinkage

To conduct a systematic study about the influence of the plasma environment on the filler conversion. For example, a study about the species presented in the plasma atmosphere, by the use of optical emission spectroscopy (OES) technique.

A study about the plasma process parameters (Ton, voltage, pressure) on the filler conversion is recommended. For this study, coatings with the same thickness are necessary.

A careful investigation about the pyrolysis of the HTTS precursor under plasma atmosphere conditions is necessary.

Further, a deeper analysis of the thermodynamics and kinetics of the phase evolution during PAP is needed, and a study about the influence of the PAP on the sintered substrate microstructure is necessary. Specifically, further investigations about the formed phase, rich in molybdenum, close do the interface substrate/coating.

To perform the mechanical characterization of the coatings, including hardness measurement, and specially the investigation of the adhesion between substrate and coating, by techiques as tape tests and scratch testing.

Additional precursor-filler combinations should be tested under PAP process.

8.   REFERENCES

ALDINGER, F.; WEINMANN, M.; BILL, J. Precursor-derived Si-B-C-N ceramics. **Pure and Applied Chemistry**. v. 70, n. 2, p. 439–448, 1998.

ALLAHVERDI, M.; CANNON, W. R.; DANFORTH, S. C. Processing and Properties of Blackglas^{TM}-Nextel^{TM} 312 (BN) Composites Incorporating Fillers. **Journal of the American Ceramic Society**, v. 83, n. 12, p. 2929–2937, dez. 2000.

ANTHONY R. WEST. **Solid State Chemistry and Its Applications**. [s.l.] John Wiley & Sons, 1987.

BARROSO, G. S.; KRENKEL, W.; MOTZ, G. Low thermal conductivity coating system for application up to 1000°C by simple PDC processing with active and passive fillers. **Journal of the European Ceramic Society**, v. 35, n. 12, p. 3339–3348, 2015.

BENDO, T. et al. The effect of Mo on the characteristics of a plasma nitrided layer of sintered iron. **Applied Surface Science**, v. 363, p. 29–36, 2016.

BRUNATTO, S. F. . et al. Sintering and Surface Texturing: Direct Current-Coupled Plasma-Assisted Parts Manufacturing. In: CRC PRESS - TAYLOR & FRANCIS GROUP (Ed.). . **Encyclopedia of Iron, Steel, and Their Alloys**. 1. ed. New York: [s.n.]. p. 3194–3207, 2016.

BUDTZ-JØRGENSEN, C. V.; BØTTIGER, J.; KRINGHØJ, P. Energetic ion bombardment of the grounded anode in pulsed DC-glow discharges. **Surface and Coatings Technology**, v. 137, n. 1, p. 104–110, 2001.

CGEE. **Materiais avançados no Brasil 2010-2022.**Brasília, Centro de Gestão e Estudos Estratégicos, , 2010.

CHAPMAN, B. Glow Discharge Processes: Sputtering and Plasma Etching. New York: John Wiley & Sons, 1980.

CHAWLA, N.; DENG, X. Microstructure and mechanical behavior of porous sintered steels. **Materials Science and Engineering A**, v. 390,

n. 1-2, p. 98–112, 2005.

COLOMBO, P. et al. Polymer-derived ceramics: 40 Years of research and innovation in advanced ceramics. **Journal of the American Ceramic Society**, v. 93, n. 7, p. 1805–1837, 2010.

CÓRDOBA, J. M. et al. Synthesis of titanium carbonitride phases by reactive milling of the elemental mixed powders. **Journal of the American Ceramic Society**, v. 88, n. 7, p. 1760–1764, 2005.

DAVID. R. GASKELL. Introduction to the Thermodynamics of Materials,. 5. ed. New York, 2012.

DE LIMA, J. C. et al. Modeling the amorphous structure of mechanically alloyed Ti50Ni25Cu25 using anomalous wide-angle x-ray scattering and reverse Monte Carlo simulation. **Physica B: Condensed Matter**, v. 424, p. 60–68, 2013.

DUARTE, M. J. et al. Crystallization, phase evolution and corrosion of Fe-based metallic glasses: An atomic-scale structural and chemical characterization study. **Acta Materialia**, v. 71, p. 20–30, 2014.

ELTOUKHY, A. H.; GREENE, J. E. Diffusion enhancement due to low-energy ion bombardment during sputter etching and deposition. **Journal of Applied Physics**, v. 51, n. 8, p. 4444–4452, 1980.

ERIC J. MITTEMEIJER; SCARDI, P. (EDS.). **Diffraction analysis of the microstructure of materials**. [s.l.] Springer, 2004.

ERNY, T. et al. Microstructure Development of Oxycarbide Composites during Active-Filler-Controlled Polymer Pyrolysis**. Journal of the American Ceramic Society**. v.76, n. 1, p.2017-213, 1993.

FLORES, O. et al. Selective cross-linking of oligosilazanes to tailored meltable polysilazanes for the processing of ceramic SiCN fibres. **Journal of Materials Chemistry A**, v. 1, n. 48, p. 15406–15415, 2013.

FRANCIS, A. et al. Crystallization behavior and controlling mechanism of iron-containing Si-C-N ceramics. **Inorganic Chemistry**, v. 48, n. 21, p. 10078–10083, 2009.

GONÇALVES, P. DA C. Dry sliding behavior of filled PDC coatings applied onto surface modified sintered steel. [s.l.] Federal University of Santa Catarina, 2016.

GREIL, P. Active-Filler-Controlles Pyrolysis of Preceramic PolymersJournal of the American Ceramic Society, 1995a.

GREIL, P. Active-Filler-Controlled Pyrolysis of Preceramic Polymers. **Journal of the American Ceramic Society**, v. 78, n. 4, p. 835–848, abr. 1995b.

GREIL, P. Near Net Shape Manufacturing of Polymer Derived Ceramics. **Journal of the European Ceramic Society**, v. 18, n. 13, p. 1905–1914, nov. 1998.

GREIL, P. Polymer Derived Engineering Ceramics. **Advanced Engineering Materials**, v. 2, n. 6, p. 339–348, 2000.

GREIL, P. Pyrolysis of Active and Passive Filler-loaded Preceramic Polymers. **Handbook of Advanced Ceramics: Materials, Applications, Processing and Properties**, v. 1-2, p. 369–390, 2003.

GREIL, P. Advancements in polymer-filler derived ceramics. **Journal of the Korean Ceramic Society**, v. 49, n. 4, p. 279–286, 2012.
GREIL, P.; SEIBOLD, M. Modelling of dimensional changes during polymer-ceramic conversion for bulk component fabrication. **Journal of Materials Science**, v. 27, n. 4, p. 1053–1060, 1992.

GÜNTHNER, M. et al. Advanced coatings on the basis of Si(C)N precursors for protection of steel against oxidation. **Journal of the European Ceramic Society**, v. 29, n. 10, p. 2061–2068, 2009.

GÜNTHNER, M. et al. High performance environmental barrier coatings, Part I: Passive filler loaded SiCN system for steel. **Journal of the European Ceramic Society**, 2011.

HÖGANÄS. Höganäs Handbook for sintered components. In: [s.l.] Höganäs, 1999. p. 270.

HUDIS, M. Study of ion-nitriding. **Journal of Applied Physics**, v. 44, n. 4, p. 1489–1496, 1973.

JACOBSON, N. S.; OPILA, E. J.; LEE, K. N. Oxidation and Corrosion of Ceramics. **Ceramics Science and Technology**, v. 5, p. 301–309, 2001.

JAIN, A. et al. Determination of the thermodynamic stability of TiB2. **Journal of Alloys and Compounds**, v. 491, n. 1-2, p. 747–752, 2010.

JUNG, I. et al. A STUDY OF THE FORMATION OF Ti (CN) SOLID. **Acta Metallurgica**, v. 47, n. 11, p. 3241–3245, 1999.

JUSTUS, T. D. D. Aplicação e caracterização de revestimento pdc resistente a oxidação em aço sinterizado. [s.l.] Universidade Federal de Santa Catarina, 2016.

KARAKUSCU, A. Synthesis and Characterization of Luminescent Nanostructured SiOC. **Thin Films**. n. January, p. 171, 2010.

KLEIN, A. N. et al. DC Plasma Technology Applied to Powder Metallurgy: an Overview. **Plasma Science and Technology**, v. 15, n. 1, p. 70–81, 2013.

KNIESS, C. T.; CARDOSO DE LIMA, J.; PRATES, P. B. The quantification of crystalline phases in materials: Applications of Rietveld method. **Sintering - Methods and Products**, p. 293–316, 2005.

KNITTLE, E. et al. High-pressure synthesis, characterization, and equation of state of cubic C-BN solid solutions. **Physical Review B**, v. 51, n. 18, p. 12149–12156, 1995.

KOKOTT, S.; MOTZ, G. Cross-Linking via Electron Beam Treatment of a Tailored Polysilazane (ABSE) for Processing of Ceramic SiCN-Fibers. **Soft Materials**, v. 4, n. 2-4, p. 165–174, 2007.

KROKE, E. et al. Silazane derived ceramics and related materials. **Materials Science and Engineering: R: Reports**, v. 26, n. 4–6, p. 97–199, 2000.

KRUGER, C. R.; ROCHOW, E. C. Polyorganosilazano. **J. Polymer Sci**, v. 2, p. 3179–3189, 1964.

KWON, H.; KANG, S. Stability domain of Ti(CN) in Ti–TiC–TiN. **Materials Letters**, v. 68, p. 426–428, 2012.

LAMPE, T.; EISENBERG, S.; LAUDIEN, G. Compound Layer Formation During Plasma Nitriding and Plasma Nitrocarburising. **Surface Engineering**, v. 9, n. 1, p. 69–76, 1 jan. 1993.

LEVI, G.; KAPLAN, W. D.; BAMBERGER, M. Structure refinement of titanium carbonitride (TiCN). **Materials Letters**, v. 35, n. June, p. 344–350, 1998.

LIEBERMAN, M. A.; LICHTENBERG, A. J. Chemical Reactions and Equilibrium. In: **Principles of Plasma Discharges and Materials Processing**. [s.l.] John Wiley & Sons, Inc., 2005. p. 207–233.

LUGMAIR, C. et al. Plasma Nitriding of Titanium and Titanium Alloys. **Proceedings of the 10th World Conference on Titanium**, p. 929–934, 2004.

MACKENZIE, K. J. . et al. Nitridation of silicon powder studied by XRD, 29Si MAS NMR and surface analysis techniques. **Journal of the European Ceramic Society**, v. 19, n. 16, p. 2731–2737, 1999.

MALISKA, A. M. et al. The influence of ion energy bombardment on the surface porosity of plasma sintered iron. **Materials Science and Engineering A**, v. 352, n. 1-2, p. 273–278, 2003.

MASON, R. S.; PICHILINGI, M. Sputtering in a glow discharge ion source - pressure dependence: Theory and experiment. **Journal of Physics D: Applied Physics**, v. 27, p. 2363, 1994.

MEHRER, H. Diffusion in Solids: Fundamentals, Methods, Materials, Diffusion-Controlled Processes. [s.l.] Springer, 2007.

MERA, G. et al. Ceramic Nanocomposites from Tailor-Made Preceramic Polymers. **Nanomaterials**, v. 5, n. 2, p. 468–540, 2015.

METIN, E.; INAL, O. T. Formation and growth of iron nitrides during ion-nitriding. **Journal of Materials Science**, v. 22, n. 8, p. 2783–2788, 1987.

138

MITTEMEIJER, E. J. Fundamentals of Nitriding and Nitrocarburizing. In: DOSSET, J.; TOTTEN, G. E. (Eds.). **ASM Handbook,**. Stuttgart: ASM Internation, 2013. v. 4.

MOCAER, D. et al. Si-C-N ceramics with a high microstructural stability elaborated from the pyrolysis of new polycarbosilazane precursors - Part V Oxidation kinetics of model filaments. **Journal of Materials Science**, v. 28, n. 11, p. 3059–3068, 1993.

MONTHIOUX, M.; DELVERDIER, O. Thermal Behavior of (Organosilicon) Polymer-Derived Ceramics. V: Main Facts and Trends. **Journal of the European Ceramic Society**, v. 16, n. 7, p. 721–737, 1996.

MOTZ, G. et al. **EPI12006145**, 2012.

MUCALO, M. R.; MILESTONE, N. B. Preparation of ceramic coatings from pre-ceramic precursors - Part II SiC on metal substrates. **Journal of Materials Science**, v. 29, n. 22, p. 5934–5946, 1994.

OKAMURA, K.; SEGUCHI, T. Application of radiation curing in the preparation of polycarbosilane-derived SiC fibers. **Journal of Inorganic and Organometallic Polymers**, v. 2, n. 1, p. 171–179, 1992.

PAVANATI, H. C. et al. Comparative Study of Porosity and Pores Morphology of Unalloyed Iron Sintered in Furnace and Plasma Reactor. **Materials Research.** v. 10, n. 1, p. 87–93, 2007.

RANGARAJAN, S.; ASWATH, P. B. Role of precursor chemistry on synthesis of Si-O-C and Si-O-C-N ceramics by polymer pyrolysis. **Journal of Materials Science**, v. 46, n. 7, p. 2201–2211, 2011.

RIE, K.-T. Recent advances in plasma diffusion processes. **Surface and Coatings Technology**, v. 112, p. 56–62, 1999.

RIE, K.-T.; LAMPE, T. Thermochemical surface treatment of titanium and titanium alloy Ti-6Al-4V by low energy nitrogen ion bombardment. **Materials Science and Engineering**, v. 69, n. 2, p. 473–481, 1985.

RIEDEL, R. et al. Silicon-Based Polymer-Derived Ceramics: Synthesis Properties and Applications- A Review. **Journal of Ceramic Society of**

Japan. v. 114, n. 6, p. 425–444, 2006.

ROGER, J.; MAILLÉ, L.; DOURGES, M. A. Isothermal nitridation kinetics of TiSi2 powders. **Journal of Solid State Chemistry**, v. 212, p. 134–140, 2014.

SAMBASIVAN, S.; PETUSKEY, W. T. Phase chemistry in the Ti-Si-N system: Thermochemical review with phase stability diagrams. **Journal of Materials Research**, v. 9, n. 09, p. 2362–2369, 1994.

SCHÜTZ, A. et al. Characterisation of novel precursor-derived ceramic coatings with glass filler particles on steel substrates. **Surface and Coatings Technology**, v. 207, p. 319–327, 2012.

SEIBOLD, M.; GREIL, P. Thermodynamics and Microstructural Development of Ceramic Composite Formation by Active Filler-controlled Pyrolysis (AFCOP). **Joural of the European Ceramic Socie O**, v. 11, n. March 1992, p. 105 –113, 1993.

SEIFERT, M. et al. Multiphase ceramic composites derived by reaction of Nb and SiCN precursor. **Journal of the European Ceramic Society**, v. 34, n. 8, p. 1913–1921, 2014.

SEIFERT, M. et al. A novel approach to develop composite ceramics based on active filler loaded precursor employing plasma assisted pyrolysis. **Materials and Design**, v. 89, p. 893–900, 2016.

SHAH, S. R.; RAJ, R. Mechanical properties of a fully dense polymer derived ceramic made by a novel pressure casting process. **Acta Materialia**, v. 50, n. 16, p. 4093–4103, 2002.

SICARDI SCHIFINO, A. C. et al. On the thermodynamic origin of energy principles in plasma physics. **Physica A: Statistical Mechanics and its Applications**, v. 334, n. 1-2, p. 201–221, 2004.

STÖRMER, H.; KLEEBE, H. J.; ZIEGLER, G. Metastable SiCN glass matrices studied by energy-filtered electron diffraction pattern analysis. **Journal of Non-Crystalline Solids**, v. 353, n. 30-31, p. 2867–2877, 2007.

SUGIMOTO, M. et al. Reaction mechanisms of silicon carbide fiber

synthesis by heat treatment of polycarbosilane fibers cured by radiation: I, Evolved Gas Analysis.**Journal of the American Ceramic Society**, 1995.

TAYLOR, P. R.; PIRZADA, S. A.; MANRIQUE, M. Thermodynamic predictions for material processing in a plasma reactor using solid oxide feed materials. **Metallurgical and Materials Transactions B**, v. 25, n. 5, p. 713–720, 1994.

TOBY, B. H. R factors in Rietveld analysis: How good is good enough? **Powder Diffraction**, v. 21, n. 01, p. 67–70, 2006.

TORREY, J. D.; BORDIA, R. K. Phase and microstructural evolution in polymer-derived composite system and coatings. **Journal of Materials Research**, v. 22. p. 1959-1966, 2007.

TORREY, J. D.; BORDIA, R. K. Processing of polymer-derived ceramic composite coatings on steel. **Journal of the American Ceramic Society**, v. 91, n. 1, p. 41–45, 2008.

TRASS, S. et al. Structural characterisation of silicon carbonitride ceramics derived from polymeric precursors. **Journal of the European Ceramic Society**, v. 20, n. 2, p. 215–225, 2000.

TRASSL, S. et al. Characterization of the Free-Carbon Phase in Si-C-N Ceramics: Part II, Comparison of Different Polysilazane Precursors. **Journal of the American Ceramic Society**, v. 85, n. 5, p. 1268–1274, 2002.

WANG, K. et al. High performance environmental barrier coatings, Part II: Active filler loaded SiOC system for superalloys. **Journal of the European Ceramic Society**, v. 31, n. 15, p. 3011–3020, 2011.

XIONG, S. et al. Size and shape dependent Gibbs free energy and phase stability of titanium and zirconium nanoparticles. **Materials Chemistry and Physics**, v. 120, n. 2-3, p. 446–451, 2010.

YU, S. H. et al. Pyrolysis of Titanium-Metal-Filled Poly(siloxane) Preceramic Polymers: Effect of Atmosphere on Pyrolysis Product Chemistry. **Journal of the American Ceramic Society**, v. 78, n. 7, p. 1818–1824, jul. 1995.

ZAITSEV, A.; ZAITSEVA, N.; KODENTSOV, A. Thermodynamic properties and phase equilibria in the iron–boron system. Transition of the Fe–B melt into the amorphous state. **Journal of Materials Chemistry**, v. 13, n. 4, p. 943–950, 2003.

ZIEGLER, G. et al. Synthesis , microstructure and properties of SiCN ceramics prepared from tailored polymers. **Materials, chemistry and physics**. v. 61, p. 55–63, 1999.